NASA SP-3038

HANDBOOK OF THE PHYSICAL PROPERTIES OF THE PLANET MARS

NATIONAL AERONAUTICS AND SPACE ADMINISTRATION

NASA SP-3030

HANDBOOK OF THE PHYSICAL PROPERTIES OF THE PLANET

MARS

by
C.M. Michaux

Prepared under contract for NASA
by Douglas Aircraft Company, Inc.
Santa Monica, California

Scientific and Technical Information Division
OFFICE OF TECHNOLOGY UTILIZATION 1967
NATIONAL AERONAUTICS AND SPACE ADMINISTRATION
Washington, D.C.

For Sale by the Superintendent of Documents,
U.S. Government Printing Office, Washington, D. C. 20402
Price 70 cents
Library of Congress Catalog Card Number 66-61839

Foreword

THE SPACE SCIENCE BOARD of the National Academy of Sciences has recommended that emphasis be placed on planetary exploration, with primary attention given to Mars. This planet has long held the interest of scientists looking for evidence of life elsewhere in the Solar System. Since the time when Percival Lowell hypothesized the possibility of life on Mars, observed phenomena, such as the highly debated existence of systems of canals and the yearly wave of darkening, have been interpreted as indications of life of some form on the planet.

Of all the planets, Mars is one of the two most accessible for study and exploration. It has a thin atmosphere through which surface features can be seen by telescope. Although Mars has been observed from the Earth at every possible opportunity since the turn of the century, many of the observed phenomena have yet to be explained. Exploration of the planet with spacecraft may be the only means of unraveling its mysteries.

This volume is an attempt to summarize our knowledge of Mars through the spring of 1966, based both on observational and theoretical studies. The theoretical studies attempt to explain the observational data but also include studies of a hypothetical planet having the same boundary conditions as Mars. The material was prepared in the Space Sciences Department of the Douglas Aircraft Company, Missile and Space Sciences Division, under contract with the National Aeronautics and Space Administration.

ORAN W. NICKS, *Director*
Lunar and Planetary Programs

Acknowledgments

IN PREPARING THIS HANDBOOK, valuable assistance has been provided by E. Ehrhardt, F. F. Fish, H. A. Hyatt, L. R. Koenig, F. W. Murray, E. V. Petersen, S. T. Rollins, V. Sirounian, and P. E. Wasko of the Douglas Aircraft Co., Inc.

Review of various portions of this material was performed by the late Dirk Brouwer (Yale University Observatory), Gerard De Vaucouleurs (University of Texas, McDonald Observatory), and Albert G. Wilson (The Rand Corp., Santa Monica, Calif.). Their comments and suggestions are appreciated.

Contents

		Page
1	ORBIT	1
2	CONFIGURATIONS AND SEASONS	7
3	MASS	11
4	DIAMETER AND SHAPE	15
5	ROTATION: AXIS AND PERIOD	27
6	SURFACE GRAVITY	37
7	MEAN DENSITY	41
8	INTERNAL STRUCTURE	43
9	ELECTROMAGNETIC AND PARTICLE FIELDS	51
10	SURFACE TEMPERATURE	53
11	OPTICAL PARAMETERS	63
12	ATMOSPHERIC COMPOSITION	73
13	ATMOSPHERIC STRUCTURE	85
14	ATMOSPHERIC CIRCULATION	97
15	CLOUDS	99
16	BLUE HAZE	105
17	SURFACE FEATURES	111
18	LIFE	133
19	SATELLITES	139
REFERENCES		147
GLOSSARY		163

1

Orbit

IN COMMON WITH ALL PLANETS in the solar system, Mars, as seen from the north pole of the ecliptic, revolves around the Sun in a counterclockwise direction. Its orbital plane is slightly inclined (at an angle of 1°51′) to the orbital plane of Earth. Mars' path around the Sun is decidedly more elliptical (eccentricity, $e=0.093$) than Earth's nearly circular orbit. Figure 1–1 somewhat exaggerates this eccentricity for the sake of visual clarity (refs. 1 and 2).

MEAN ORBITAL ELEMENTS AND SECULAR VARIATIONS

Because the orbital paths of planets are affected by the attractions of other planets, they are not truly elliptical. The actual (perturbed) motion of a planet may be represented by osculating elements, that correspond to instantaneous position and velocity vectors for any time relative to an epoch (starting point for comparison purposes). Expressed as functions of time, these osculating elements contain both secular terms (the progressively changing part) and periodic terms. Mean elements, obtained by ignoring the periodic terms, cannot be used for precise calculation of a planet's position, but have the merit of demonstrating the progressive changes in the orbit.

Table 1–1 presents the mean orbital elements of Mars in the period 1960–66, at epochs separated by 400 days, as given in the corresponding volumes of *The American Ephemeris and Nautical Almanac* (ref. 1). These values and all currently published ephemerides of Mars are based upon the classical work of Newcomb (refs. 3 and 4) on the elements of the four inner planets and tables of their motions and are supplemented by corrections prepared by Ross (ref. 5).

Secular variation formulas which start from the Fundamental Epoch 1900 are given in table 1–2. These equations make possible calculation of mean elements for any later date. In each formula shown, mean solar distance is a constant, in accordance with the

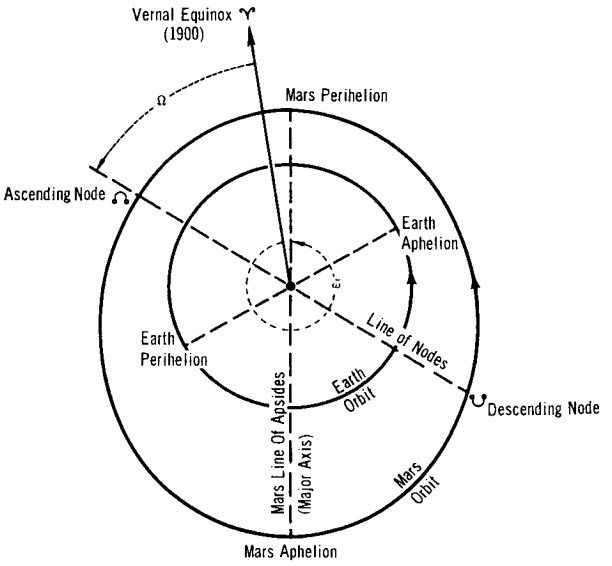

FIGURE 1-1.—Orbits of Mars and Earth (Values: refs. 1 and 2).

Constant	Mars	Earth
Mean solar distance, a, astronomical unit	1.5236915	1.000000
Mean motion, n, deg/sidereal day	0.52403295	0.985609
Eccentricity of orbit, e	.09331290	.016750
Inclination of orbit to ecliptic, i, deg	1.850334	.000000
Longitude of ascending node, Ω, deg	48.786442	.....
Longitude of perihelion, $\bar{\omega}$, deg	334.218203	101.21971
Solar distance at perihelion, astronomical unit	1.381426	.983276
Solar distance at aphelion, astronomical unit	1.665954	1.0166

Laplace-Poisson theorem of celestial mechanics on the invariability of semimajor axes. Mean sidereal motion is very nearly constant. Although orbital eccentricity and inclination are dependent upon time in response to the influence of the other planets, these factors vary quite slowly. The longitudes of ascending node and perihelion vary rather rapidly with time. The larger part of the contribution in time (T and T^2) arises from the constantly changing reference system of mean equinox and ecliptic. Newcomb intended that these mean elements represent merely a mean reference orbit as a basis for deriving the actual orbit by the theory of general perturbations.

The mean distance, a, in an unperturbed orbit or in an osculating orbit, is related to the mean motion, η, by Kepler's third law, $\eta^2 a^3 = k^2 (1+m)$, where m is the ratio of the mass of the planet to the Sun, and k is the Gaussian constant of gravitation. If η and

TABLE 1-1.—*Mean Orbital Elements for Mars, 1960 to 1967*

[Mean elements are taken from *The American Ephemeris and Nautical Almanac* and referred to the mean equinox and ecliptic of date.]

Epoch		Mean distance from Sun, a, astronomical units	Mean motion, η, deg/ ephemeris day	Eccentricity of orbit, e	Inclination of orbit to ecliptic, i, deg	Ascending node longitude, Ω, deg	Perihelion longitude, $\bar{\omega}$, deg
Gregorian date	Julian date						
1960—Sept. 23	2437200.5	1.523691	0.524033	0.093369	1.84993	49.25464	335.33609
1961—Oct. 28	2437600.5	1.523691	.524033	.093370	1.84992	49.26308	335.35625
1962—Dec. 2	2438000.5	1.523691	.524033	.093371	1.84991	49.27153	335.37641
1964—Jan. 6	2438400.5	1.523691	.524033	.093372	1.84991	49.27997	335.39657
1965—Feb. 9	2438800.5	1.523691	.524033	.093373	1.84990	49.28841	335.41673
1966—Mar. 16	2439200.5	1.523691	.524033	.093374	1.84989	49.29686	335.43689
1967—Apr. 20	2439600.5	1.523691	.524033	.093375	1.84989	49.30530	335.45705

TABLE 1–2.—*Secular Variations of Mean Orbital Elements for Mars*

Element	Value in 1900	Formula for secular variation
Mean distance from Sun, a	1.5236915 astronomical units	Constant
Mean motion, η	0°.52403295	$+0°.0000000001\ T$
Eccentricity of orbit, e	0.09331290	$+0.000092064\ T-0.000000077\ T^2$
Inclination of orbit to ecliptic, i	1.850334 deg/ephemeris day	$-0°.000676\ T+0°.000013\ T^2$
Longitude of ascending node, Ω	48°.786442	$+0°.771007\ T-0°.000001\ T^2-0°.000005\ T^3$
Perihelion longitude, $\bar{\omega}$	334°.218203	$+1°.840790\ T+0°.000130\ T^2-0°.000001\ T^3$

1. Fundamental Epoch is 1900 January 0.5 ephemeris time (12^h E.T.), or 1900 January 0.0 (0^h E.T., prior to 1925) or Julian date (J.D.) 2415020.0.

2. Elements are referred to the mean equinox and ecliptic of date.

3. Unit of time is the Julian century of 36525 ephemeris days. Symbol T denotes the time interval in Julian centuries since start of Epoch, thus

$$T = \frac{\text{J.D.} - 2415020.0}{36525}$$

4. Formulas are those adopted by the current edition of *The American Ephemeris and Nautical Almanac*, expressed here in decimals.

a are mean elements, the relation becomes $\eta^2 a^3 = k^2 (1+m)(1+\delta)$, where δ is a small quantity that arises from neglect of the periodic terms in the definition of the mean elements. Mars orbital constants derived from the mean elements for 1960 are given in table 1–3, as taken from Kirby's survey of the orbital and physical data for Mars (ref. 6).

NEW THEORY OF THE MOTION OF MARS

At present, no official ephemeris accurately predicts the position of Mars. Soon after the appearance of Newcomb's tables for Mars, it was noticed that the observed positions of the planet increasingly diverged from its predicted positions. Clemence and Scott (ref. 7) were dissatisfied not only with Newcomb's orbit but also with Ross' improved empirical corrections. Clemence decided to construct a new theory of the motion of Mars, which would include all the second-order perturbations (neglected by Newcomb) related especially to the effects of Earth and Jupiter and, to a lesser extent, to the effects of Venus and Saturn. Some third-order terms were also included.

Clemence's first-order theory appeared in 1949 and was followed in 1961 by the completed second-order theory (refs. 8 and

TABLE 1–3.—*Derived*[a] *Orbital Constants for Mars*

[After ref. 6]

Orbital time intervals

	Earth sidereal years	Earth tropical years	Earth ephemeris days
Mars sidereal year	1.88082	1.88089	686.980
Mean synodic period	2.13531	2.13539	779.935

Distances from the Sun

	Astronomical unit	Kilometer $\times 10^6$	Miles $\times 10^6$
Mean distance	1.523691	227.9424	141.637
Distance at perihelion	1.381426	206.6600	128.412
Distance at aphelion	1.665954	249.2247	154.861

Orbital velocity

	Kilometer/second	Miles/second
Mean orbital velocity	24.13	14.99

[a] Derived from mean orbital elements, epoch 1960 January 0.5 ephemeris time, or Julian date (J.D.) 2436934.0.

9). Provisional ephemerides calculated by Duncombe (ref. 10) and Duncombe and Clemence (ref. 11) were compared with observations made as much as a hundred years apart. This check proved, without doubt, not only the validity of the general theory but also its great accuracy. Comprehensive comparison with all reliable (meridian-circle) observations is in progress at the U. S. Naval Observatory as of this writing, under the direction of Duncombe. Satisfactory proof of the precision of the theory has been provided by P. Herget who used the Naval Ordnance Research Calculator to perform a numerical, step-by-step integration of the orbit of Mars over a 35-year period (1919 to 1954). Finding no more than 0.04 second of arc as the difference in the calculated and the observed orbital longitudes of Mars, Herget affirmed new standards of accuracy. The agreement in orbital latitude was even better, as 0″.008 was found to be the greatest difference. It is hoped that, in a few years, the constants employed in the new formulas will have been confirmed sufficiently to permit publication of a reliable ephemeris for Mars.

Clemence suggested and introduced two improvements to Newcomb's theories of planetary observations: (1) the use of ephemeris time, which corrects for the effects of deceleration and irregularities in Earth's rate of rotation; and (2) the relativistic correction to the motion of the perihelion, which cannot be considered negligible for Mars. While the excess for the advance of the Mars perihelion, unexplained by Newton's gravitation theory, was predicted as 1″.35 by relativity theory, it was observed as $1''.5 \pm 0''.04$ by Clemence (quoted in ref. 12).

2

Configurations and Seasons

OPPOSITIONS

OPPOSITIONS (and superior conjunctions) of Mars with respect to Earth occur at an average interval of 780 days, the mean synodic period of revolution of the two planets. Because of the eccentricity of the Martian orbit, however, the actual synodic period can differ from the mean period by as much as 20 days. For the same reason, the distance between Mars and Earth at opposition is not constant, but varies by a factor of nearly 2 in the 15-to-17-year cycle of successive oppositions around the Martian orbit. The 15 oppositions between 1950 and 1980 are shown in figure 2–1, demonstrating the variation in opposition distances and the alternating periods of the cycles. Oppositions near the Mars perihelion are termed favorable. The most favorable, the perihelic opposition, occurs once each cycle normally in August or September, when Mars is closest to Earth, at a distance of approximately 35 million miles or 0.38 astronomical unit. They offer the optimum opportunity for the astronomer-physicist to study Mars closely. The most recent perihelic opposition took place in September 1956; and the next such event will be in August 1971, when Mars will again be only 0.38 astronomical unit from Earth. The previous perihelic oppositions occurring in 1862, 1877, 1892, 1909, 1924, and 1939 stand out as landmarks in Martian studies. The least favorable, the aphelic opposition, occurs near aphelion in either February or March, when Mars is approximately 0.67 astronomical unit from Earth.

The distance between Mars and Earth at opposition is seldom the minimum distance achieved during oppositional approach because of the eccentricity of their orbits. Although the difference between these distances is always very small, the difference between the date of opposition and the date of closest approach can be as much as 10 days. For accurate calculations of times of opposition and conjunction, a small correction should be included for the effect of light-time. This amounts to about plus 7 minutes for Earth-Mars oppositions and minus 24 minutes for their superior

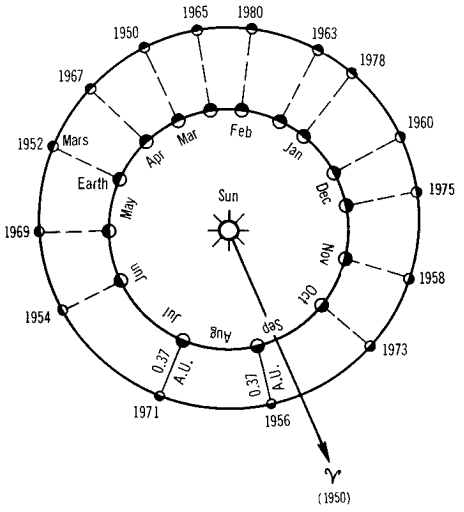

FIGURE 2–1.—Oppositions of Mars, 1950 to 1980.

conjunctions, according to reference 13. Table 2–1 which lists pertinent data of all Mars approaches from 1901 through 1980 was constructed by graphic and inverse interpolation from the planet's heliocentric longitudes and radii vectors as given in the *Planetary Coordinates* volumes issued by the British Nautical Almanac Office for the years after 1800 (refs. 14, 15, and 16). Additional information was taken from the appropriate annual volumes of *The American Ephemeris and Nautical Almanac,* from calculations by Heath (ref. 17) for oppositions of 1956 through 1999, and by Meeus (ref. 18) for oppositions of 1960 through 1980. Earth-Mars distances are in kilometers, miles, and in astronomical units. The apparent diameters 2σ of Mars were calculated from the simple relationship $2\sigma = 9''.36/\Delta$, where $9''.36$ is the angular diameter in seconds of arc at 1 astronomical unit (American Ephemeris value), and Δ is the distance in astronomical units.

MARTIAN SEASONS

Because the tilt of the rotation axis of Mars upon its orbit is nearly the same (25°) as for Earth (23°.5), Mars experiences distinct seasons comparable to those of Earth. Because the celestial orientation of its axis is different, the location of the Martian solstices and equinoxes is displaced in heliocentric longitude η with respect to those of Earth. This displacement is $\Delta\eta = 87°$ ahead of Earth; it varies quite slowly with centuries as a direct effect of the unequal precessions of the axes of the two

TABLE 2–1.—*Mars Opposition and Closest Approach Data, 1901 to 1980*

Year	Opposition date	Closest approach data				Maximum angular diam, sec of arc
		Date	Distance			
			Astronomical units	km × 10^6	miles × 10^6	
1901	Feb. 22	Feb. 23	0.6774	101.34	62.97	13.8
1903	Mar. 29	Apr. 2	.6380	95.44	59.31	14.7
1905	May 8	May 16	.5366	80.27	49.88	17.4
1907	July 6	July 13	.4076	60.98	37.89	22.9
1909[a]	Sept. 24	Sept. 18	.3895	58.27	36.21	24.0
1911	Nov. 25	Nov. 17	.5112	76.47	47.52	18.3
1914	Jan. 5	Jan. 1	.6224	93.11	57.86	15.0
1916	Feb. 9	Feb. 9	.6748	100.95	62.73	13.9
1918	Mar. 15	Mar. 18	.6613	98.93	61.47	14.1
1920	Apr. 21	Apr. 28	.5831	87.23	54.20	16.0
1922	June 10	June 18	.4560	68.22	42.39	20.5
1924[a]	Aug. 23	Aug. 22	.3729	55.79	34.66	25.1
1926	Nov. 4	Oct. 27	.4588	68.64	42.65	20.4
1928	Dec. 21	Dec. 15	.5850	87.52	54.38	16.0
1931	Jan. 27	Jan. 26	.6622	99.06	61.56	14.1
1933	Mar. 1	Mar. 4	.6746	100.92	62.71	13.9
1935	Apr. 6	Apr. 12	.6210	92.90	57.73	15.0
1937	May 19	May 28	.5085	76.07	47.27	18.4
1939[a]	July 23	July 28	.3879	58.03	36.06	24.1
1941	Oct. 10	Oct. 3	.4105	61.41	38.16	22.8
1943	Dec. 5	Nov. 29	.5395	80.71	50.15	17.3
1946	Jan. 13	Jan. 10	.6394	95.65	59.44	14.6
1948	Feb. 17	Feb. 18	.6776	101.37	62.99	13.8
1950	Mar. 23	Mar. 27	.6497	97.19	60.39	14.4
1952	Apr. 30	May 8	.5583	83.52	51.90	16.8
1954	June 24	July 2	.4278	64.00	39.77	21.9
1956[a]	Sept. 10	Sept. 7	.3781	56.56	35.15	24.7
1958	Nov. 16	Nov. 8	.4877	72.96	45.34	19.2
1960	Dec. 30	Dec. 25	.6068	90.78	56.41	15.4
1963	Feb. 4	Feb. 3	.6704	100.29	62.32	14.0
1965	Mar. 9	Mar. 12	.6685	100.01	62.14	14.0
1967	Apr. 15	Apr. 21	.6012	89.94	55.89	15.6
1969	May 31	June 9	.4796	71.75	44.58	19.5
1971[a]	Aug. 10	Aug. 12	.3757	56.20	34.92	24.9
1973	Oct. 25	Oct. 17	.4360	65.22	40.53	21.4
1975	Dec. 15	Dec. 8	.5655	84.60	52.57	16.2
1978	Jan. 22	Jan. 19	.6532	97.72	60.72	14.3
1980	Feb. 25	Feb. 26	.6773	101.32	62.96	13.8

[a] Perihelic opposition.

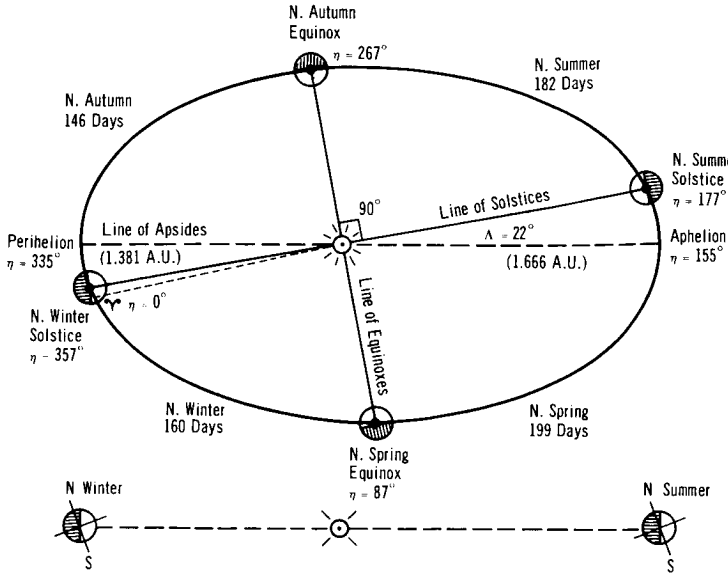

FIGURE 2–2.—The Martian seasons.

TABLE 2–2.—*The Martian Seasons*

Heliocentric longitude, deg	Northern Hemisphere	Southern Hemisphere	Duration	
			Terrestrial days (24h)	Martian days (24h37m)
87 to 177	Spring	Autumn	199 } 381	194 } 371
177 to 267	Summer	Winter	182 }	177 }
267 to 357	Autumn	Spring	146 } 306	142 } 298
357 to 87	Winter	Summer	160 }	156 }
87 to 87	Year		687	670

planets. Figure 2–2 and the accompanying table 2–2 show the positions of the four seasonal points and the durations of the seasons. The latter are seen to be appreciably unequal, in contrast to those of Earth, as a result again of the marked eccentricity of the orbit of Mars. The Martian seasons are, of course, about twice as long as seasons on Earth, since the Martian year is almost double the terrestrial year.

3

Mass

THE MASS OF MARS can be determined by two methods: (1) a complex analysis of the perturbations Mars causes in the orbits of other major or minor planets, or (2) a direct analysis, using Kepler's third law on the orbital elements of the Martian satellites.

The perturbations method is the older, more cumbersome general technique, which was necessarily used before the discovery of the Martian satellites. When applied to the perturbations of neighboring planets, this method produced a wide range of mass values for Mars. When applied to minor planets, especially Eros, however, the perturbations method was capable of greater refinement and yielded values in much better agreement with those determined by the more accurate satellite method.

The satellite method is unquestionably simpler and more direct. However, since the mass of Mars is derived from the scale of the orbits of the satellites and therefore from the measured angular distances of the satellites from the center of the planet, the result may be affected by systematic errors. Soon after discovering the satellites Phobos and Deimos, Hall (ref. 19) measured their mean distances and periods of revolution with great precision. Using these data, he arrived at a value for the mass of Mars, which is still accepted by most astronomers, and used in *The American Ephemeris and Nautical Almanac*.

Hall's value was adopted by Newcomb in preparing his tables of orbital elements (ref. 3). A more broadly based value was proposed by Van Den Bosch (ref. 20), using a weighted average of 27 values for the mass of Mars, as determined by the satellite method during the period from 1877 to 1917. Later, Clemence and Brouwer (refs. 21 and 22) confirmed this average value and narrowed its uncertainty, using a similar process but including additional data. It is the value recommended here. It should be noted, however, that Clemence (ref. 23) advocated a slightly larger mass at the International Astronomical Union (I.A.U.) meeting of August 1964. Analysis of the Mariner IV trajectory

TABLE 3-1.—*Determination of the Mass of Mars*

Author	Relative mass		Absolute mass, $g \times 10^{26}$	Method
	Sun = 1 (reciprocal)	Earth = 1		
Hall[a] (ref. 19)	3 093 500	0.10747	6.4296	Both satellites' orbits
Leveau (ref. 24)	≤ 3 648 000	.9114	5.4523	Vesta perturbations
Leveau (ref. 25)	3 601 280	.9232	5.5230	Vesta perturbations
Van Den Bosch (ref. 20)	3 088 000 (±5000)	.10766	6.4411 (±0.0040)	Weighted mean, 27 determinations, satellite orbits
De Sitter (ref. 26)	3 085 000 (±5000)	.10777	6.4473 (±0.0040)	Mean, several determinations from satellites
Rabe (ref. 27)	3 110 000 (±7700)	.10690	6.3955 (±0.0026)	Eros perturbations
Urey (ref. 28)	3 079 000 (±5700)	.10798	6.4599 (±0.0035)	Deimos orbit
Brouwer and Clemence[b] (ref. 22)	3 088 000 (±3000)	.10766	6.4411 (±0.0066)	Both satellites' orbits
Makemson, Baker, Westrom (ref. 29)	3 090 000 (±10 000)	.10759	6.4369 (±0.0020)	Mean, satellite determinations
Clemence (ref. 23)	3 050 000	.10900	6.5213	Mean, satellite determinations
Jet Propulsion Laboratory	3 098 500	.10730	6.4192	Mariner IV trajectory

[a] Values adopted by *The American Ephemeris and Nautical Almanac*, 1895 to 1967.

[b] Recommended value.

TABLE 3–2.—*Comparison of Masses*

Body	Absolute mass, g	Relative mass	
		Sun=1 (reciprocal)	Earth=1
Sun	1.989×10^{33}	1	332 464
Earth (alone)	5.9826×10^{27}	332 464	1
Mars	6.441×10^{26}	3 088 000	0.10766
Moon	7.3527×10^{25}	27 051 300	0.01229
Phobos, Deimos	Negligible	Negligible	Negligible

near Mars indicates that the mass of Mars is slightly smaller than Clemence and Brouwer's or Van Den Bosch's value, and is fairly close to the value adopted by *The American Ephemeris and Nautical Almanac.*

Table 3–1 presents the results of various determinations of the mass of Mars in terms of absolute mass, as a reciprocal of the mass of the Sun, and in direct comparison with the mass of Earth. Table 3–2 uses the Brouwer and Clemence (ref. 22) value for the mass of Mars in comparing masses of the Sun, Earth, Mars, the Moon, and the satellites of Mars.

4

Diameter and Shape

THE EXACT DIMENSIONS AND SHAPE of Mars are perhaps the least exactly known of all the fundamental physical characteristics of the planet. Numerous micrometric measurements have been taken at the telescope since Huygens' time (1659), and more rigorous modern microphotometric tracings have been made of photographs of the disk by Camichel (refs. 30 and 31). Nonetheless, the true value of the equatorial diameter is accepted even today as lying somewhere between 6725 and 6825 kilometers. These approximate limits result from a recent critical examination by De Vaucouleurs (ref. 32) of the most reliable observations of the past 100 years.

METHODS OF MEASURING DIAMETER

DIRECT VISUAL MEASUREMENT.—The visual method of direct measurement of the disk's diameter makes use of either the single-image wire micrometer, also known as a filar micrometer, or the double-image micrometer. The latter may refer either to the outdated heliometer or to the more modern birefringent micrometer. With the single-image micrometer, two wires are set tangentially to opposite limbs of the disk, and their separation is measured by a precision screw. With the double-image micrometer, an identical image of the disk is moved into tangential contact on opposite limbs, and the displacement is measured by a precision screw.

DIRECT PHOTOGRAPHIC MEASUREMENT.—The photographic method of direct measurement makes use of large-scale photographs. A wire micrometer may be used to make tangential settings at the limb of the photographic image, or a microphotometer can obtain tracings of luminance (brightness) diametrically across the disk by scanning the plate with a tiny spot of light.

INDIRECT MEASUREMENT.—The indirect method makes use of a wire micrometer to measure the apparent positions or paths of surface markings on the disk. This may be done visually; however, the use of photographs is preferred. A physical ephemeris

of Mars is used to determine the location (areographic latitude) of the center of the disk and the direction (angle with celestial north) of its axis of rotation. If timed measurements are made of the apparent path of selected surface markings as rotation carries them across the disk, the known rotation rate determines their angular positions. The major axis also may be determined for the ellipses described by selected surface markings, preferably along the equator.

SYSTEMATIC ERRORS IN MEASUREMENT

Numerous difficulties hinder the determination of a planetary diameter from Earth. The sources of error can be atmospheric, optical, instrumental, or even subjective. An unsteady telescopic image can result from air turbulence and erratic clock-drive, or a distorted image with indefinite edges can be caused by diffraction, chromatism, eye astigmatism, and irradiation. The corrections applied may also be highly arbitrary; for instance, the irradiation correction is often taken as a constant. Thus, the accuracy of measurements suffers greatly from this combination of poorly understood systematic errors. Furthermore, the correct interpretation of measurements must take into account the particular conditions or phenomena involved in measuring a planetary body at great distances. The astronomical position of the planet, or specifically, its phase angle, may make the illuminated portion noncircular. Allowances must also be made for sky background luminance, distinguishing between nighttime, twilight, and daytime observations, which for Mars correspond to near-opposition, near-quadrature, and small-elongation configurations with Earth. The physical nature of the exterior of the body, its surface, and its atmosphere may together produce a nonuniform luminance. The surface brightness of the disk is also affected by the wavelength of observation, especially for Mars. (See fig. 4–1.)

Micrometric measurements of photographed disks have other important systematic errors, as shown by Van De Kamp (refs. 33 and 34) and Reuyl (ref. 35). The photographed diameter increases with density of the image (photographic irradiation) and with increasing atmospheric turbulence (reduced visibility). Measurements are often corrected inadequately by assuming a constant error, c. Van De Kamp recommends making a plot of c as a function of density. Images should be reduced to some standard density representing normal exposure before applying any correction. The wavelength (or color filter) used in securing

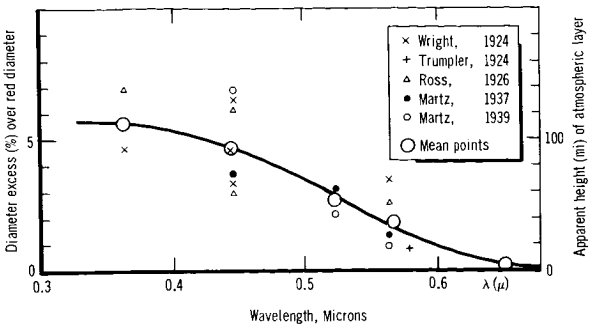

FIGURE 4–1.—Wright's phenomenon. (After ref. 39.)

the image must always be specified when quoting photographic diameters. Perhaps the best micrometric measurements on photographs are those of Trumpler (ref. 36) during the perihelic opposition of 1924.

WRIGHT'S EFFECT

A systematic color survey of Mars by photography undertaken by Wright (ref. 37) led him to discover that the size of the images varied with the color of the filter used. The variation was greatest, approximately 3 percent, between ultraviolet and infrared images. Ross (ref. 38) even found a difference as great as 6 percent. Trumpler found the yellow image to be larger than the red image by a mean value of 0.86 percent. This wavelength dependence of the observed diameter of Mars, since called Wright's phenomenon or Wright's effect, has received different explanations, none of which is entirely satisfactory.

Wright immediately attributed the phenomenon, by analogy with Earth, to atmospheric scattering which increases with shorter wavelengths. From the ultraviolet to the yellow to the red and infrared, a rapid shrinking of the image takes place, as shown in figure 4–1 which was plotted from the data of De Vaucouleurs (ref. 39). Both Wright and Trumpler suggested that this rapid shrinking seemed to mark the transition from the disk of Mars seen with its surrounding atmosphere, or at least part of it, to the disk representing the solid surface alone. The depth of the visible atmosphere of Mars was estimated by Wright to be approximately 100 kilometers in the blue-violet, by Trumpler as 84 kilometers in the yellow, and 55 kilometers in the red along the equator. However, this explanation was disputed at the time on theoretical grounds by Menzel (ref. 40), Fessenkov (ref. 41), and later by Barabashov and Semejkin (ref. 42), who cited the tenuous

Martian atmosphere and the great height at which scattering was being considered. A layer of dust suspended very high was then assumed to be a more likely cause.

Ross (ref. 38) suggested instrumental or photographic sources of error. Barabashov and Timoshenko (ref. 43), using increasing exposures, ascertained later that the diameter in the blue did not change, but that the diameter in the red changed markedly, throwing some suspicion on Wright's and Ross' original measurements, although Wright's phenomenon is definitely real. Besides the photographic exposure effect, another important phenomenon was shown to coexist by Barabashov and Timoshenko, and by Sharonov (ref. 44). This phenomenon consists of limb darkening in the red and limb brightening in the blue, which causes essentially smaller red and infrared images, whereas blue ones tend to appear larger; however, this illusion is only a partial explanation of Wright's effect. A true atmospheric layer effect must definitely be present, because the ultraviolet images are large, compared to red ones. It is difficult to say whether the red image actually defines the solid globe of Mars, but, so far, it can be assumed to be for a first approximation of the true diameter. The excess in diameter of the ultraviolet image over the red image generally is assumed to include the so-called violet layer, a hypothetical atmospheric region presumably containing aerosols to account for its optical effects.

LIMB EFFECTS

Any planet with an atmospheric envelope produces disk images of nonuniform brightness or luminance, even if allowance is made for local surface or atmospheric features of varying reflectivity. The Martian disk shows decided limb darkening at the longer wavelengths ($\lambda > 0.5\ \mu$), and limb brightening at the shorter wavelengths ($\lambda < 0.5\ \mu$). This is illustrated in figure 4–2, which is based on the study by Barabashov and Timoshenko in photographic photometry of Mars. The explanation must lie in a combination of absorption and scattering within the Martian atmosphere.

Limb darkening reduces all diameter measurements made with micrometers, especially those made with the double-image micrometer. By measuring the polar diameter in the daytime to eliminate irradiation, Müller (ref. 45) obtained a value of only 9″.00 with a double-image micrometer; See (ref. 46) obtained a value of 9″.22 with a filar micrometer, as compared with Camichel's value of 9″.30 (table 4–1). In any case, in filar measurements the irradiation of the disk compensates in part for limb darkening.

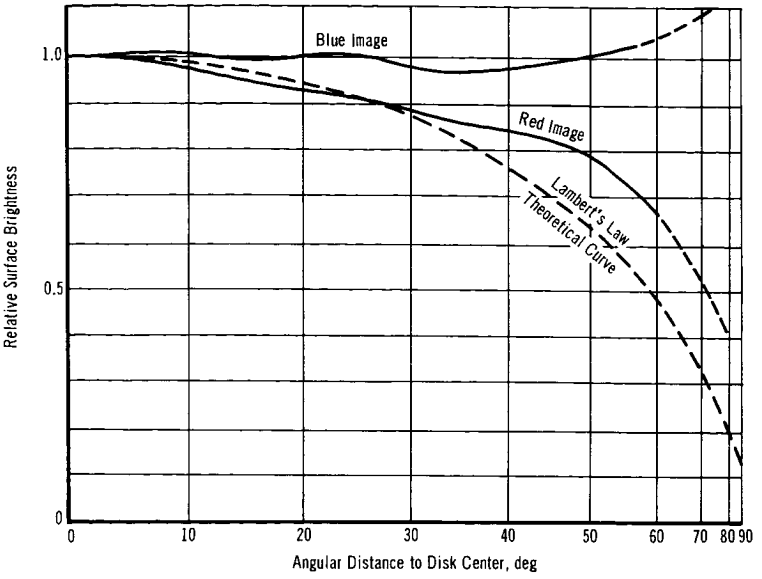

FIGURE 4–2.—Variation of surface brightness across Mars' disk. (After ref. 43.)

DIAMETER OF MARS, WITHOUT AN ATMOSPHERE

Diameters of Mars measured in ordinary or yellow light undoubtedly include a significant fraction contributed by the atmospheric envelope; that is, the densest layers. Schemes to eliminate this envelope from measurements were devised and applied by Wirtz (ref. 47) and Wright (ref. 48). Their method consisted of timing the angular positions of selected surface markings rotating across the disk and using the known period of rotation for the reduction. In another indirect method, proposed and used by Trumpler (ref. 36) and later refined by Camichel (refs. 30 and 31), one observes on photographs the elliptical paths described by known markings, preferably near the equator, and derives the major axis of the ellipses. If the areographic coordinates of the markings or other needed constants are not known accurately, corrections can be determined from the residuals between observed and ephemeris-predicted values by a least-squares solution with many equations of condition. Trumpler used this elaborate correcting technique. The direct micrometric method, applied to red images only, was also tried by Trumpler, but it is less certain that the diameter so derived refers to the solid surface alone, because of the effect of limb darkening.

TABLE 4–1.—*Apparent Diameters of Globe of Mars at Unit Distance*

[Ref. 32]

Method	Observer; years observed	Apparent equator diam, d_1', sec	Apparent polar diam, d_1'', sec	Weight
Visual. Filar micrometer in daytime, from cusps diam.	Campbell 1894 to 1895	.....	9.254	1
	See 1901	.....	9.22	1
Visual. Double-image micrometer, in daytime.	Müller 1937 to 1938	.....	9.00	½
Photographs in red light. Micrometer.	Trumpler 1924	9.33	9.24	1
Visual. Positions of surface markings.	Wirtz 1909	9.122	.....	½
Photographs. Ellipses of surface markings.	Trumpler 1924	9.178	9.074	1
	Camichel 1941	9.48	.....	1
	Camichel 1943	9.40	.....	1
	Camichel 1946	9.20	.....	1
	Camichel 1948	9.26	.....	1
	Camichel 1950	9.23	[a](9.30)	1
	Camichel 1954	9.466	.....	1
Simple mean		9.275	9.18	.....
Weighted mean		9.285	9.20	.....

[a] By North Polar Cap—very questionable value.

SUMMARY OF DIAMETER DETERMINATIONS

Tables 4–2 and 4–3 list results of various determinations of the apparent polar and equatorial diameters of the Martian disk, as well as apparent optical flattening. Table 4–4 represents De Vaucouleurs' summary and evaluation of the most reliable observations to date by all methods. His weighted means for diameters at 1 astronomical unit are the apparent equatorial diameter, $d_1'=9''.415$, and the apparent polar diameter, $d_1'=9''.315$. These

TABLE 4–2.—*Apparent Polar Diameter of Mars, Disk at Unit Distance*

[Ref. 32]

Conditions	Method	Observer; years observed	Polar diam, d_1'', sec
Visual at night.....	Heliometer, value corr. by constant.	Hartwig 1877 to 1878	9.300
		Hartwig 1879 to 1880	9.511
		Hartwig 1890 to 1909	9.318
	Heliometer, cusps diam.	Schur 1896 to 1899	9.35
	Filar micrometer.	Wirtz 1906 to 1909	9.634
	Filar micrometer, cusps diam.	Rabe 1914 to 1916	9.439
		Rabe 1926 to 1927	9.433
Photo, yellow light....	Micrometer on photographs.	Wright 1924	9.17
		Trumpler 1924	9.28
		Trumpler 1924	9.32
	Micrometer on photographs, cusps.	Van de Kamp 1924	9.26
		Van de Kamp 1924 to 1927	9.48
		Reuyl 1934 to 1939	9.44
	Microphotometer on photographs.	Camichel 1941 to 1950	9.22
Visual at night.....	Double-image micrometer.	Müller 1948	9.29
		Dollfus 1954 to 1958	9.31

angular diameters correspond to linear diameters of $2R_1'=6828$ kilometers and $2R_1'=6756$ kilometers, respectively. These diameters pertain to the disk of Mars in yellow light. Because of atmospheric optical effects, they are not representative of the actual solid-body dimensions, differing from them by what may be a considerable amount.

Table 4–1 presents values proposed for the diameter of the globe alone, as evaluated by De Vaucouleurs (ref. 32). He emphasizes

TABLE 4–3.—*Apparent Equatorial Diameter at Unit Distance and Apparent Optical Flattening of Mars, Disk Near Opposition*

[Ref. 32]

Method	Observer; years observed	Equatorial diam, d_1', sec	Optical flattening, f_o
Heliometer	Hartwig 1879	9.445	0.0086
	Hartwig 1890 to 1909	9.41	.0096
Filar micrometer	Campbell 1892	9.638	.0016
	Barnard 1894	9.701	.0087
	Douglass 1894	9.419	.0066
	Young 1894	9.765	.0017
Heliometer	Schur 1896	9.524	.0215
	Schur 1899	9.563	.0187
Filar micrometer	Wirtz 1903 to 1909	9.674	.0095
Micrometer on photographs, yellow	Trumpler 1924	9.41	.0094
	Camichel 1941	9.48	.016
	Camichel 1943	9.35	.012
	Camichel 1946	9.30	.013
	Camichel 1948	9.24	.004
	Camichel 1950	9.29	.012
Double-image micrometer	Müller 1948	9.43	.015
	Dollfus 1954	9.395	.0118
	Dollfus 1956	9.47	.0117
	Dollfus 1958	9.43	.0116
	Focas 1961	9.29	.0116

TABLE 4–4.—*Best Determinations of Apparent Equatorial and Polar Diameters of Mars*

[Ref. 32]

Author	Year of observation	Number of nights	Diam, sec	Probable error, sec	Weight
Best polar diameter determinations, d_1''					
Müller	1948	4	9.29	±.04	½
Schur	1896 to 1899	7	9.35	.02	½
Hartwig	1890 to 1909	15	9.32	.02	1
Dollfus	1954 to 1958	6	9.31	.03	1
Double image			9.305	±.02	2
Photographic			9.32	±.02	2
Weighted mean			9.315	±.010	.....
Best equatorial diameter determinations, d_1'					
Douglass	1894	10	9.42	.....	½
Hartwig	1879	12	9.445	.....	½
Hartwig	1890 to 1909	15	9.41	.....	1
Müller	1948	4	9.43	.....	½
Trumpler	1924	14	9.41	.....	1
Camichel	1941 to 1950	7	9.33	.....	½
Dollfus	1954 to 1958	6	9.435	.....	1
Weighted mean			9.415	±0.02	.....

the determinations of Camichel at the six successive oppositions of Mars from 1941 to 1954. The mean of the equatorial values is 9″.28, which corresponds to a linear diameter of 6723 kilometers. The mean of the polar values is 9″.18 in table 4–1. Three polar values were derived by micrometric determinations on the faint daytime disk, near superior conjunction, when the Martian atmosphere may become invisible through the brighter terrestrial atmospheric light. The diameter of the globe must be less than the diameter in yellow light, 9″.415, or 6828 kilometers at the equator. De Vaucouleurs states that the true equatorial diameter of Mars must therefore be between 6723 and 6828 kilometers. He adopts provisionally a rounded figure of 6750 kilometers, with ±20 kilometers probable error. For the polar diameter, he provisionally proposes 6700 kilometers, with ±20 kilometers probable error.

Radio observations of the recent spacecraft occultation by Mars, during the Mariner IV mission, gave data for a new computation of Mars' equatorial radius. By timing Mariner's immersion and emersion and knowing the spacecraft's trajectory, JPL in 1965 estimated that the equatorial diameter of Mars lies in the range

of 6777 to 6803 kilometers (corresponding mean radius would be 3395 kilometers).

SHAPE

The shape of a planet can be approximated by an oblate ellipsoid of revolution generated by rotation of an ellipse about its minor axis, or better, an oblate spheroid, which is a surface of higher order produced by rotational distortion of an initial sphere composed of homogeneous concentric layers. The polar flattening, f, or oblateness, is defined in terms of ellipticity, which is the ratio of the difference between equatorial and polar radii to the equatorial radius, thus: $f=(R_{eq}-R_{po})/R_{eq}$. This should not be confused with the eccentricity, e, of the meridian ellipse, which is expressed as $e=\sqrt{R_{eq}^2-R_{po}^2/R_{eq}}$.

The shape of Earth has been determined by astronomical, dynamic, gravitational, and geodetic methods; the results are concordant. For Mars, the telescopic image yields a flattening value of the disk (optical flattening), while the satellite orbits yield a flattening value of the gravitational equipotential surface (dynamical flattening). These two values differ widely, the optical being approximately twice the dynamical.

DYNAMICAL FLATTENING

An astronomically observed value for dynamical flattening, f_d, can be deduced for a planet from the period of precession, ψ, of the orbit of a close satellite, as perturbed by the oblateness of the planet:

$$\psi=\frac{a^2}{R^2}\cdot\frac{p}{f_d-\frac{1}{2}\phi}$$

where

a semimajor axis of the satellite orbit
p period of revolution of the satellite
R radius of the planet
ϕ ratio of centrifugal force to gravity at the equator.

In turn, $\phi=3\pi/G\bar{\rho}P^2$, where G is the universal gravitational constant, $\bar{\rho}$ is the planet's mean density, and P is the planet's period of rotation.

For Mars, its satellites (especially Phobos) are close enough so that perturbations caused by the attraction of the Sun can be neglected. Struve (ref. 49) and Woolard (ref. 50), using data

related to Phobos, obtained f_d=0.00521 and f_d=0.005215, respectively. The calculation was recently updated by De Vaucouleurs (ref. 32), using a mean diameter d_1=9″.30, to give: f_d=0.00525.

OPTICAL FLATTENING

For Mars, true or geometric flattening, $f_g=(R_{eq}-R_{po})/R_{eq}$, is as uncertain as are the values of the radii. Apparent or optical flattening, $f_o=(R'-R'')/R'$, derived from diameter measurements of the disk, depends on the wavelength.

The optical flattening in yellow light is f_o=0.0105, corresponding to a diameter difference, $d'_1-d''_1$=0″.100, in angular measure at 1 astronomical unit, or $R'_1-R''_1$=36 kilometers in linear measure. This value is double that of the dynamical flattening calculated from the motions of the satellites, f_d=0.00525. The latter amounts to a linear radius difference, $R'_c-R''_c$=18 kilometers. Thus, it is probable that $f_d<f_g<f_o$.

The major discrepancy between optical and dynamical flattening, which is the source of these uncertainties, is poorly understood. The most logical explanation would seem to be that the yellow disk is defined by the top of a dust-laden convective layer (troposphere), which is higher at the equator than at the pole by some 18 kilometers. This excess seems to be corroborated by estimates of the thickness of the layer obtained as a difference between apparent radius in yellow light and radius of the globe. Specifically, at the equator there exists thickness, z', equal to ½(9″.415 − 9″.27), or 0″.072, corresponding to 52 kilometers and at the pole, z'', equal to ½ (9″.313 − ″.22), or 0″.048, corresponding to 35-kilometer thickness of the atmospheric layer visible in yellow. This produces a 17-kilometer equatorial bulge. Such altitudes for the top of this denser layer seem consistent with estimates of altitude of some yellow clouds projecting over limb or terminator. (See ch. 15.) Dollfus (ref. 51) estimated the average measured thickness of the atmosphere as approximately 30 kilometers.

This interpretation, however, does not agree with Trumpler's flattening values (ref. 36) obtained from globe diameters in red light or those obtained by the indirect method. These difficulties notwithstanding, the diameters in yellow are rather well established, including an atmospheric layer of uncertain height. Therefore, it seems safe to conclude, with De Vaucouleurs, that the true diameters of Mars are in the range, 6723 kilometers $\leq 2R_{eq} \leq$6828 kilometers, and the difference between diameters is in the range 36 kilometers $\leq (2R_{eq}-2R_{po}) \leq$72 kilometers.

5

Rotation: Axis and Period

AXIS OF ROTATION

THE EQUATOR OF MARS is inclined to its orbit by an angle very similar to that of Earth; the Martian "obliquity of the ecliptic" is about 25°, as compared to 23°.5 for Earth. There is still some uncertainty as to the exact value of this equatorial tilt, as can be seen from the data given by De Vaucouleurs (ref. 52) and summarized in table 5–1. His critical examination of all values previously determined, with a view to producing an accurate, modern map of Mars based on a revised, homogeneous physical ephemeris by Meiller (ref. 53), led him to adopt the value I=24°.936, which differs by 1° from the value I=23°.984, used in the current issue of *The American Ephemeris and Nautical Almanac* for its physical ephemeris of Mars.

PRECESSION OF MARS' EQUINOXES

These values for the inclination, or equivalently, the values for the celestial coordinates of the North Pole of Mars (α_0, δ_0) refer to the epoch 1905.0, chosen for convenience. They are not rigorously fixed in time because of a very slow precessional motion of the Martian line of equinoxes caused by the attraction of the Sun upon the equatorial bulge of Mars. The rate of this solar precession was calculated as 7".07 per Julian year by Struve (ref. 54), and as 7".08 by Lowell (ref. 55) which is much slower than Earth's rate of 50".2 per year for its luni-solar precession. The period of this precession for Mars, therefore, is about 183 050 years, whereas the Earth's line of equinoxes completes one revolution in about 25 725 years.

Adopting these rates of precession, the position of the Martian North Pole (right ascension α and declination δ) as used by De Vaucouleurs (ref. 52) and the physical ephemeris revised by Meiller (ref. 53) is given by the following formulas, for any year other than epoch t_0=1905.0 (within a timespan of about 100 yr for accuracy):

TABLE 5–1.—*Celestial Coordinates of Mars North Pole (1905) and Inclination of Equator to Orbital Plane*

[After ref. 52]

Method	Observer; years observed	α_0, deg	δ_0, deg	Inclination, deg
Position angles of polar caps	Schiaparelli 1877 to 1886	319.90	54.92	24.70
	Schiaparelli 1877 to 1886	319.6	54.2	25.1
	Lohse 1884 to 1894	317.18	54.35	23.96
	Cerulli 1896 to 1898	318.63	54.07	24.75
	Lowell 1901 to 1905	316.05	54.52	23.37
	Wirtz 1903 to 1909	312.71	53.90	21.99
	Lowell and Lampland 1901 to 1907	315.50	54.32	23.16
	Lowell 1901 to 1909	315.8	54.4	23.3
	Lowell 1901 to 1911	316.61	53.95	23.98
	Slipher 1909 to 1911	315.5	54.0	23.5
	Widorn 1909 to 1926	317.0	53.5	.....
Longitudes of surface markings	Ashbrook 1877 to 1952	319.2	55.8	.....
Latitudes of surface markings	Pickering 1914 to 1922	315.03	51.77	24.93
Coordinates of surface markings	Trumpler 1924	315.77	54.63	.....
Paths of selected surface markings	Camichel 1941 to 1950	316.48	52.78	24.80
Poles of satellite orbits	Burton (Phobos) 1877 to 1926	317.33	52.66	25.25
	Burton (Deimos) 1877 to 1926	315.92	53.23	25.15

$$\alpha_0\ (t) = 316^\circ.55 + 0^\circ.00675\ (t - 1905.0)$$
$$\delta_0\ (t) = \ 52^\circ.85 + 0^\circ.00346\ (t - 1905.0)$$

The current physical ephemeris, which is based on Lowell's (ref. 56) North Pole position (α_0, δ_0), adopted in 1909 by the Nautical Almanac Office, uses the formulas:

$$\alpha_0\ (t) = 317^\circ.5 + 0.00652\ (t - 1905.0)$$
$$\delta_0\ (t) = \ 54^\circ.5 + 0.00350\ (t - 1905.0)$$

Thus, the Martian North Pole is situated some 35° away from the North Star of Earth. It is directed toward a point on the geocentric celestial sphere some 10° from the star Deneb (the Martian "Polaris").

Methods of determining the direction of the axis are generally based on one of these three techniques:

(1) Determination of the center of a polar cap, allowing for its eccentric displacement from the true areographic pole.

(2) Determination of the axis of ellipses described by the rotation of selected surface markings near the equator, such as Juventae Fons, using a physical ephemeris and numerous graphs or least-squares equations for accurately positioning the observed points.

(3) Determination of the pole of the nearly equatorial orbits of the Martian satellites, especially the orbit of Phobos.

NEW RATE OF PRECESSION OF MARS' EQUINOXES

Calculations of the rate of precession of the equinoxes depend on the mechanical ellipticity, H, of the planet. This quantity is defined as the ratio: $H = (C - A)/C$, where C is the polar moment of inertia (around the rotation axis) and A is an equatorial moment of inertia. For Mars the value of H is still unknown and can be only approximated, as it depends upon the undetermined internal density distribution of the planet. Lowell (ref. 55) arrived at a value of $H = 0.004935$ by a crude interpolation assuming that the density distribution for Mars lies between that of Earth (important core) and that of a homogeneous planet, and selecting it close to homogeneity. The rate of precession which Lowell derived, 7″.08 (from such a value of H), as well as Struve's earlier value of 7″.07 (ref. 54), together with the assumption of hydrostatic equilibrium, is therefore somewhat arbitrary and questionable.

Recently, Fish (ref. 57) proposed a much more likely value for the precessional rate, based on modern geophysical considerations and the assumption that strengths (departures from hydrostatic equilibrium) are equal for Mars and Earth. His value is

7″.35±0″.20, if the inclination of equator to orbit is taken as I=25°.20. If De Vaucouleurs' inclination, I=24°.94, is used, the precessional rate is nearly the same (7″.34). This revised precessional rate would change slightly the values of both physical ephemerides mentioned.

PERIOD OF ROTATION

The period of rotation, P, of Mars is one of the most readily measurable of planetary constants because the solid surface of Mars is visible most of the time. Observations for many years of the rotation of surface markings have established a highly accurate value of the rotation period to within 0.02 second. Measurements of areographic longitudes of markings on old drawings dating as far back as 1659, and later on photographs, as well as the timing of transits of conspicuous markings across the central meridian of Mars have been combined to greatest advantage by Wislicenus (ref. 58), Bakhuyzen (ref. 59), and Ashbrook (ref. 60) to obtain the precise values quoted in table 5–2.

The value for rotational period which seems most reliable is the one derived critically by Ashbrook. He excluded all material from old drawings for the sake of accuracy, and depended primarily upon the timed meridian transits from 1877 to 1952. His value of P=24^{h}37^{m}22^s.6689±0^s.0026 (m.e.) in ephemeris time (or P=24^{h}37^{m}22^s.6679 in universal time) has been adopted by *The American Ephemeris and Nautical Almanac* starting from epoch 1960 January 0.0 and has since been adopted by the revised *Physical Ephemeris of Mars 1877–1967*, prepared by Meiller (ref. 53) for the Mars map project initiated by De Vaucouleurs.

The period of rotation quoted is the sidereal period, and is referred to the Martian vernal equinox; that is, the ascending node of the orbit of Mars on its equator. This is slightly different from the actual or true period because of the slow regression of the Martian line of equinoxes. The true period has heretofore been taken as 0.0012 second longer, at the precession rate of 7″.07 per year. The Martian day is only about 37 minutes longer than the terrestrial day, or roughly 1.03 times the Earth day.

CENTRAL MERIDIAN AND AREOGRAPHIC LONGITUDES

Areographic longitudes are measured from 0° to 360° in a direction opposite to the rotation of Mars; that is, clockwise as viewed from above its north pole, or eastward on the geocentric celestial sphere. The zero meridian, or longitude 0°, is defined by an adopted

TABLE 5-2.—*Determination of Sidereal Rotation Period of Mars*

[Ref. 52]

Author	Sidereal rotation period, P			Mean error, sec	Method and remarks
	hr	min	sec		
Wislicenus...	24	37	22.655	±0.013	Combination of 33 estimates from drawings between 1659 and 1881; mean error recomputed by Ashbrook. True rotation period, mean solar time.
Bakhuyzen..	24	37	22.66	±0.0132	Same as Wislicenus, but much more critical discussion. True rotation period, mean solar time.
Ashbrook....	24	37	22.672	±0.018	Same with old drawings 1659 to 1881, of Syrtis Major; as a check. Sidereal rotation period, ephemeris time (mean solar time over 1659 to 1881).
Ashbrook....	24	37	22.6689	±0.0026	Combination of best central meridian transits, 1879 to 1952, of 16 markings. Sidereal rotation period, ephemeris time. Period is 0.0010 shorter in mean solar time, over interval 1879 to 1952. True rotation period is 0.0012 shorter than sidereal period.

position for the axis of rotation (α_0, δ_0) and an adopted value for the longitude of the central meridian at a specified epoch (ω_0, t_0). The central meridian is the meridian passing through the central point of the geometrical disk of the planet. In 1909, the British Nautical Almanac Office assigned to this zero point the reference longitude ω_0=344°.41 for the chosen epoch, t_0=2418322.0 Julian date, or January 15, 1909, at Greenwich mean noon (or again, 15.0 Greenwich mean astronomical time, or Jan. 15.5 universal time). In the same year Lowell's 1905 value for the position of the axis was adopted by the nautical almanac, and has been used ever since. The precession rate is taken into account according to the formulas mentioned earlier for Lowell's coordinates. The reference longitude, ω_0, was assigned a value consistent with the earlier ephemeris of Crommelin (refs. 61, 62, and 63) for 1899 to 1905. Once these reference values are adopted, the longitude of the central meridian

at any later date is determined by the number of degrees through which the planet has rotated in the interim. The longitude of a surface marking can be determined easily by noting its precise transit time across the central meridian.

Before 1909, areographic longitudes were reckoned with respect to a specific surface marking on Mars, chosen as the zero of longitude. Schiaparelli (ref. 64) and Marth (ref. 65) thus introduced as origin of longitudes the Fastigium Aryn, the forked division at the center of Sinus Meridiani, a prominent and stable dark feature located on the equator of Mars. This areographic system, however natural it may have seemed, had to be abandoned. Too much confusion was introduced by observers who applied arbitrary corrections to the elements and physical ephemerides of Marth or Crommelin, instead of keeping to a uniform ephemeris. The recently revised ephemeris of Mars for oppositions 1877–1967 was computed to remedy the inconsistencies in reported positions of Martian stations (refs. 66 and 67). In the currently used ephemeris system, the longitude of Fastigium Aryn is near 357°, instead of zero.

The adoption of a highly accurate rotation period is essential in the modern system of reckoning Martian longitudes, as introduced by the 1909 British nautical almanac (ref. 68), because the origin is not defined by any specified surface marking. To this purpose, it is important to note that in 1960 the period of rotation adopted by *The American Ephemeris and Nautical Almanac* from 1909 to 1959 was changed from $24^h37^m22^s.6542$ to the revised value, $24^h37^m22^s.6679$ (in mean solar time). This slight increase of 0.0137 second makes it necessary to introduce a correction into all central meridian longitudes determined with the 1909–1959 ephemerides. The correction to apply varies linearly with time:

$$\Delta_1\omega_0' = -0^\circ.000058\ (\text{J.D.} - 2418322.0),$$

where date (J.D.) is Julian days, or

$$\Delta_1\omega_0' = -0^\circ.0212\ (t - 1909.04),$$

where time (t) is in years.

In the 50-year interval, this cumulative correction amounts to almost −1° in longitude. That is, a discontinuity exists of about −1° in the ephemeris values of ω between December 31, 1909, and January 1, 1960. There is an additional minor correction necessitated by the use of ephemeris time (E.T.), instead of mean solar time or universal time (U.T.). The correction is as follows:

$$\Delta_2\omega_0' = +0.00406\ (\Delta t - 9),$$

where Δt=E.T.–U.T. is in seconds.

ELEMENTS OF PHYSICAL EPHEMERIDES

A physical ephemeris is designed to furnish elements needed for observing and reducing the projected positions of surface markings on the apparent disk to their actual planetocentric coordinates. These elements, which are dependent on time, t, of observation, may be divided into three groupings for convenience:

PLANETOGRAPHIC ELEMENTS.—These elements determine exactly the orientation of the Mars disk in space, the position of its central point, and the amount of rotation of the globe, as follows:

(1) Position angle, p, of the central meridian; that is, the apparent angle between the rotation axis (projected onto the celestial sphere) and the celestial north.

(2) Areocentric latitude, D_E, of the center of the Earth's disk; that is, the declination of Earth referred to the equator of Mars.

(3) Areographic longitude, ω, of the central meridian, reckoned from some arbitrary meridian.

ILLUMINATION ELEMENTS.—These elements are as follows:

(1) Phase angle, α, of the planet; that is, the angle between the directions to Earth and the Sun, as seen from the planet.

(2) Ratio, k, of the illuminated area to the total area of the disk, regarded as circular.

(3) Angular amount, q, of the greatest defect of illumination, as seen from Earth.

(4) Position angle, Q, of the greatest defect of illumination.

(5) Stellar magnitude, m, of the planet.

ADDITIONAL ELEMENTS.—For convenience of calculations, the following elements may also be given:

(1) Apparent angular diameter, d, of the planet.

(2) Value of light-time, $k\Delta$; that is, the time required for light to travel from the planet to Earth.

(3) Areocentric longitude of the Sun, $\odot$, measured in the planet's orbit from the ascending node on its equator.

(4) Areocentric latitude, $D_\odot$, of the Sun's center; that is, its declination referred to the planet's equator.

(5) Areocentric right ascensions, A_E and $A_\odot$ of the centers of Earth and the Sun, respectively, measured in the plane of the planet's equator from its vernal equinox.

BASIS OF THE PHYSICAL EPHEMERIDES OF MARS

Physical ephemerides are based upon the fundamental ephemerides of the Sun and planets, supplemented by specific data.

For Mars, the first two elements, p and D_E, depend on the orbital elements of Earth and Mars, on the relative positions of both planets in their orbits, and on the direction of the axis of rotation of Mars; that is, the celestial coordinates α_0 and δ_0 of its north pole. The third element, ω, depends on the adopted value ω_0 of the central meridian at some arbitrary time or epoch t_0, and on the adopted value of the sidereal rotation period, P, of Mars. Figure 5–1 shows the planes and poles involved.

In the past 100 years, various ephemerides of Mars have been published and used for determining positions of markings. However, they were constructed with different values for the rotational constants (ω_0, t_0), P, and (α_0, δ_0). Table 5–3 lists the values adopted for these rotational constants in the various ephemerides of Mars since 1869, as presented by De Vaucouleurs (ref. 52);

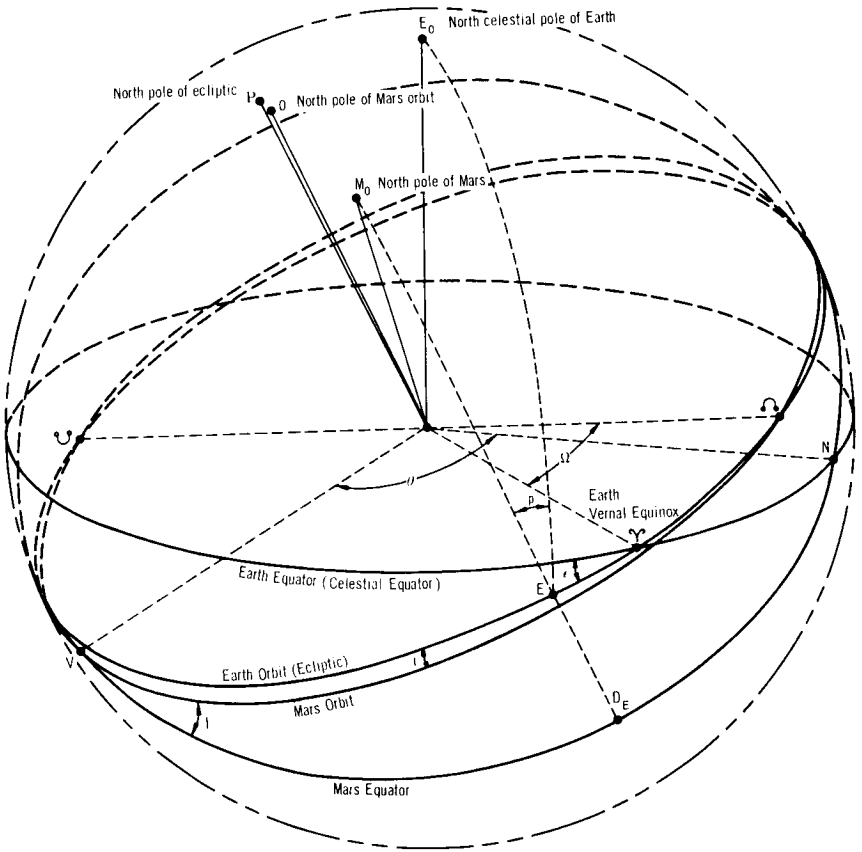

FIGURE 5–1.—Celestial sphere (with reference planes and poles—for physical ephemerides of Mars).

TABLE 5–3.—*Constants Used in Physical Ephemerides of Mars*

[After ref. 52]

Ephemeris		Celestial coordinates, North Pole, 1905.0		Sidereal rotation		Central meridian	
Period	Author	Right ascention, α_0 deg	Declination, δ_0 deg	Period,[a] 24^h37^m plus—	Rate, deg/day	Longitude, deg	Epoch, Julian date
1869 to 1877...	Marth	318.05	+50.35	22.63	350.8922384	(from Bessel, Oudemans)	
1879 to 1883...	Marth	318.11	+53.83	22.62	350.8922384	(from Schiaparelli)	
1886 to 1894...	Marth	318.29	+53.71	22.63	350.8921784	(from Schiaparelli)	
1896	Marth	317.29	+52.65	22.654	350.89202	(from Lowell)	
1899 to 1905...	Crommelin	317.29	+52.65	22.654	350.89202	(from Lowell)	
1909 to 1959...	Nautical almanac	317.5	+54.5	22.654	350.89202	344.41	2418322.0
1960	Nautical almanac	317.5	+54.5	22.6689	350.891962	344.41	2418322.0
1877 to 1965...	Revised ephemeris	316.55	+52.85	22.6689	350.891962	344.41	2418322.0

[a] Ephemeris time for Meiller's (1964) revised ephemeris; all others are mean solar time.

the rotation is also given for convenience as the angular rate of rotation: $R=360°/P$ (in degrees/day).

De Vaucouleurs proposed for systematic comparison purposes that the U.S. Naval Observatory's Nautical Almanac Office recompute a new physical ephemeris of Mars for all oppositions from 1877 to 1967 (for 60 days centered about each opposition). The result of this work has been to unify all zero points and correlate all available records of areographic positions by a uniform, homogeneous system. The new ephemeris by Meiller (ref. 53) is based on values of the constants slightly different from those of the current physical ephemeris of Mars contained in the 1966 volume of *The American Ephemeris and Nautical Almanac*. Also, the orbital positions of Mars used were based on Clemence's new theory (see ch. 1) and the time argument is ephemeris time.

6

Surface Gravity

THE SURFACE GRAVITY, g, on a planet is calculated to a first approximation from its mass and its radius at the given location, using the gravitational formula:

$$g=\frac{GM}{R^2}$$

where

M mass of the planet
R radius of the planet at the location
G universal gravitation constant, 6.67×10^{-8} dyne cm^2 g^{-2}

The formula applies to a nonrotating planet. When rotation is taken into account, a small correction, c, must be applied which is dependent upon the latitude and equal to the centrifugal acceleration directed away from the planet's axis of rotation; that is, $c=-R\omega^2\cos^2\phi$, where ω is the rate of rotation of the planet in radians per second, and ϕ is the latitude of the point of location.

Because a rotating planet is not a perfect sphere, the radius R must be considered a function of the latitude ϕ. If a planet's shape is that of an ellipsoid of revolution, the function in question is

$$R_\phi^2=\frac{(1-e^2)}{(1-e^2\cos^2\phi)}R_{eq}^2$$

where

R_{eq} equatorial radius
e eccentricity of the elliptical meridian
R_ϕ radius at latitude ϕ

The surface gravity of Mars as presented in table 6–1 has been calculated for every 10° of latitude from equator to pole. In the manner of Kirby (ref. 69), two extreme values for the equatorial radius R_{eq} have been selected, 3362 and 3414 kilometers. (See ch. 4.) The accepted value 0.00525 was used for dynamical flattening, f_d, in deriving the radius for each latitude. For the polar radius, R_{po}; for instance, $R_{po}=R_{eq}\ (1-f)=0.9948R_{eq}$. Other constants

TABLE 6–1.—*Surface Gravity of Mars at Various Latitudes*

Latitude, ϕ, deg	Values using minimum radii				Values using maximum radii			
	Radius, R, km	Uncorrected g, cm/sec^2	Correction, c, cm/sec^2	Corrected g, cm/sec^2	Radius, R, km	Uncorrected g, cm/sec^2	Correction, c, cm/sec^2	Corrected g, cm/sec^2
90	3344.5	384.08	—0.00	384.08	3396.2	372.47	—0.00	372.47
80	3345.0	383.96	— .05	383.91	3396.8	372.35	— .05	372.30
70	3346.5	383.61	— .20	383.41	3398.3	372.01	— .20	371.81
60	3348.9	383.08	— .42	382.66	3400.7	371.50	— .43	371.07
50	3351.7	382.43	— .70	381.74	3403.5	370.87	— .71	370.16
40	3354.7	381.74	— .99	380.75	3406.6	370.20	—1.00	369.92
30	3357.6	381.09	—1.27	379.82	3409.5	369.57	—1.28	368.28
20	3359.9	380.56	—1.49	379.07	3411.9	369.05	—1.51	367.54
10	3361.5	380.21	—1.64	378.58	3413.5	368.72	—1.66	367.06
0	3362.0	380.09	—1.69	378.40	3414.0	368.60	—1.72	366.89

employed were accepted values for mass, 6.4411×10^{26} grams, and rotation period, $24^h37^m22^s6689$. This rotation period is equivalent to an angular rate of rotation of 7.0882×10^{-5} radians per second. The uncertainty of R_{eq} results in a range of possible values for g amounting to ± 3.4 percent of the average value at any given latitude.

7

Mean Density

THE MEAN DENSITY OF MARS is of course dependent upon the mass and the volume of the planet. The chapters on mass and diameter and shape demonstrate, however, the degree to which these values are uncertain. It follows that mean density, $\bar{\rho}$, cannot yet be assigned a really accurate value. Using De Vaucouleurs' (ref. 32) lower and upper limits for the equatorial diameter ($6723 \leq 2R_{eq} \leq 6828$ km), and upper and lower limits for the mass from Clemence (ref. 23) and Rabe (ref. 27) ($6.5213 \times 10^{26} > M > 6.3929 \times 10^{26}$ g), corresponding limits are derived for the mean density of Mars:

$$3.85 < \bar{\rho} < 4.12 \text{ g/cm}^3$$

Using probable values for the equatorial diameter ($2R_{eq} \cong 6750$km) and for the mass (6.4411×10^{26} g), the derived probable value of the mean density of mass is $\bar{\rho} = 4.02$ g/cm^3. The calculation of mean density uses the simple formula:

$$\bar{\rho} = \frac{\text{Mass}}{\text{Volume}} = \frac{M}{4/3\,\pi \bar{R}^3}$$

where $\bar{R}$ is the mean radius defined by the expression $\bar{R}^3 = R_{eq}^3 (1 - f)$. R_{eq} is the equatorial radius and f is the true flattening. For these calculations, dynamical flattening, f_d, was used, with a value of 0.00525 taken from Woolard (ref. 50) as corrected by De Vaucouleurs.

8

Internal Structure

THE SIMILARITY IN THE MEAN DENSITIES of the terrestrial planets suggests a general parallelism in their internal constitutions. Our knowledge of the Earth's interior, coupled with the assumption of its similarity to the interior of Mars, has served as the basis for deriving models of the Martian interior.

INTERIOR OF THE EARTH

The rapid development of seismology and geochemistry early in this century enabled scientists to construct hypothetical models of the Earth's interior. Studies of compressional and shear seismic waves traveling through the interior provided proof of fundamental two-shell structure beneath the thin outer crust. This structure was held to consist of a dense central core surrounded by a less-dense mantle. Consideration of the variation with depth of seismic velocities, and of the moment of inertia, made possible reasonably accurate models of density-depth distributions. Geochemical evidence is less certain. The bulk-chemical composition of the two shells can be deduced speculatively, with the aid of certain assumptions about the behavior of materials under extreme pressure (on the order of a megabar) and high temperature (several thousand °C). This can be achieved by basing these assumptions upon extrapolations from experimentally established properties of materials at much lower pressures and temperatures.

There is a general agreement that the Earth's mantle is composed primarily of a mixture of iron and magnesium silicates, and that the pronounced steepening of the density gradient at depths of 200 to 900 kilometers is produced by pressure-induced phase changes of the silicates to a spinel structure. Ringwood (refs. 70, 71, and 72) provided experimental support of this idea. The composition of the core is uncertain. It is generally believed to consist of iron mixed with minor amounts of other elements such as nickel, cobalt, and silicon. Ramsey (ref. 73) proposed an unorthodox model in which the core and mantle are not chemically

differentiated. In this model, the core is composed of iron and magnesium silicates in which normal molecular and crystal binding have been broken by extreme pressure, and a dense metallic phase has been created.

INTERIOR OF MARS

Information pertaining to the interior of Mars is inferred from the few available planetary constants: the mass, the radii, or simply the mean radius, and the moment of inertia. The mass is fairly well known, but the radii (or mean radius) are not accurately known. The moment of inertia may be derived from the coefficient J_2 (the zonal harmonic gravitational potential coefficient), obtained through the motion of the satellites, assuming hydrostatic equilibrium in the interior. The basic assumptions underlying all models for the interior of Mars are: (1) analogy with Earth, both in structure and composition, and (2) hydrostatic equilibrium. Other assumptions made before constructing a model include: the number of layers, or discontinuities, the composition of each layer, and the equation of state for each composition.

As a result of the uncertainty of these assumptions, and of the radius, the moment of inertia and the mass, models of the interior of Mars are highly speculative. Many uncertainties should be resolved once seismic studies are made at the surface and areophysical measurements are obtained by orbiting vehicles.

CONSTRUCTION OF DENSITY MODELS

The general method for constructing a density model of the interior of a planet is to integrate the hydrostatic equation inward using an assumed equation of state. The integration is carried out for the hypothetical model using boundary conditions of radius, mass, and moment of inertia.

CLAIRAUT'S RATIO

An indication of the density distribution in the central part (core) of the planet is obtainable from consideration of the ratio between dynamical flattening f_d and the constant $\phi = R_{eq}^3 \omega^2/GM = 3\pi/G\bar{\rho}P^2$, where G is the universal gravitational constant, P the rotational period, and $\bar{\rho}$ the mean density of the planet. Two centuries ago, Clairaut (ref. 74) showed that the ratio f_d/ϕ equals 1.25 for a homogeneous planet, and 0.50 for a planet with its mass

almost totally concentrated in a small core. For Mars, the ratio is somewhere between 1.11 and 1.20, depending on whether 3418 or 3350 kilometers is taken for the equatorial radius R_{eq}. If the radius adopted by De Vaucouleurs (R_{eq}=3375 km) is used, the ratio f_d/ϕ is 1.16 which suggests that the interior of Mars is closer to homogeneity than the interior of Earth, where f_d/ϕ is 0.97. Therefore, no more than a small central core of heavy metals is expected for Mars.

The indicator ratio of Clairaut served as a valuable guide in selecting working hypotheses for the interior of Mars. The following paragraphs review the models representing the two conflicting theories of the interior of Mars, and also of Earth. One maintains that Mars contains less iron than Earth, the other that both planets have the same overall chemical composition.

DENSITY MODELS

Jeffreys (ref. 75) first proposed the following two models for Mars: (J.I) resembling the Earth with three layers, and (J.II) with only two layers, but no metal core. His calculations led him to prefer the first. Both models are represented in figure 8–1(A), with pertinent data. Ramsey (ref. 73), at Jeffreys' suggestion, undertook the investigation of the two-layered model on the grounds that a metallic phase of silicates can exist under extreme pressures. He suggested the model would consist of a core of silicates (olivine) in metallic state or phase and a mantle of the same silicates in the normal molecular state. Calculations to confirm this model were not completed. Ramsey's main idea was to explore the broader hypothesis that all four terrestrial planets were of the same basic composition. Bullen (ref. 76) modified Ramsey's Earth model for Mars (B.II) by using a quadratic r–p relation (instead of assuming adiabatic compression). He also found that a differentiated, iron-nickel model fitted Mars better (B.I). These two models are shown in figure 8–1(B). Through numerous calculations, Bullen found that the value adopted for the mean radius is critical. These models, mentioned here principally for their historical interest, have been given a most adequate treatment by Wildt (ref. 77). The following models are modern ones formulated by the opposing proponents.

MacDONALD'S MODELS

MacDonald (ref. 78) calculated numerous possible models by varying the structural assumptions and the planetary radius.

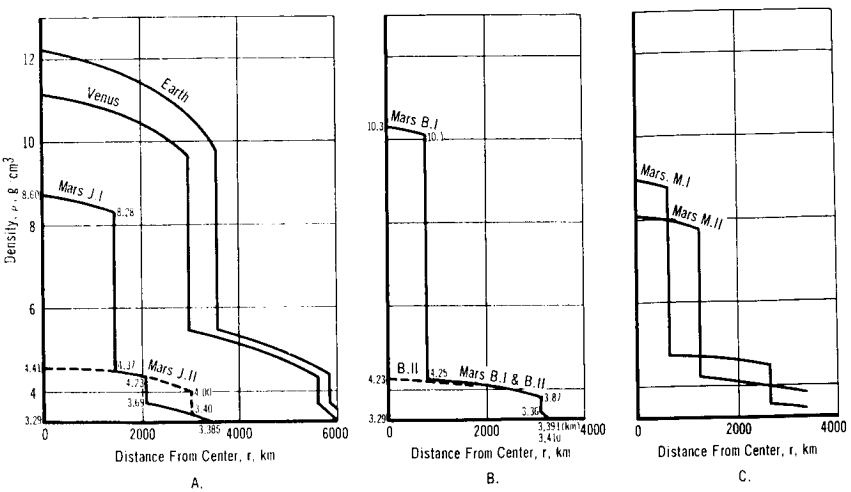

FIGURE 8–1.—Density models of Mars' interior.

He showed that core radius and surface density are critically dependent on the value of the hydrostatic flattening. His models have three layers, but the thicknesses vary greatly. Figure 8–1(C) illustrates two of the models, adopting a mean radius of 3345 kilometers, a flattening of 0.0050, and assuming either a phase transition in the mantle or no phase transition. The former assumption leads to a chemically distinct core of iron and silicon, amounting to only 1 percent of the total planetary mass. The latter assumption gives a core which is 9.3 percent of the total mass. By adopting a lower flattening value, 0.0047, the core would increase considerably, to 11.7 or 20 percent of total mass with or without phase transition, respectively. Surface densities appear to be quite high, on the order of 3.5 to 3.8 g/cm³. If a lower radius is adopted (3310 km), the surface densities are unduly large (about 3.8 to 4.0 g/cm³), pointing to the improbability of a near-homogeneous Mars according to these calculations. From examination of all his models, MacDonald concluded that a model with a small metallic core, containing 1 percent or less of the total mass, appears to be the most likely one for Mars.

LYTTLETON'S MODELS

Lyttleton (ref. 79) has supported Ramsey's hypothesis that Mars has no metallic core. He calculated two-layer models of composition and structure similar to the two outer layers of Earth. Thus, he assigned each model a mantle and outer shell, separated only by a phase discontinuity of the material, and as-

sumed a linear pressure-incompressibility law for each layer. He indicated that no liquid core was to be expected within Mars, such as had been previously postulated by Bullen. This would be true because pressures and temperatures should be definitely lower for Mars than for Earth at equal depths, even with similar proportions of radioactive elements. His undifferentiated "core" of silicates contained over half the total mass, 56 percent for a mean radius of Mars of 3396 kilometers and 65 percent for a mean radius of 3408 kilometers. Lyttleton does not specify a definite model of Mars because of the uncertainty of the observed radius and the suspected uncertainty of dynamical ellipticity and mass, which is as much as 2 percent for each.

OTHER DENSITY MODELS

Lamar (ref. 80) proposed a model for the internal structure of Mars based on the assumption that the actual shape of Mars is that determined from optical rather than dynamical flattening. In such a model, the equatorial bulge would be isostatically compensated by variations of the crust thickness.

It is pertinent to mention three recent papers by Jobert (ref. 81), Levin (ref. 82), and Kovach and Anderson (ref. 83) on the terrestrial planets which are considered as a group. These papers regard Mars as an important entity used for comparison with Earth or the Moon, since Mars seems to be intermediate in structure and, perhaps, in composition.

THERMAL MODELS

Various models of temperature distribution in the interior of Mars can be constructed by varying the following parameters: (1) distribution and amount of radioactive materials, and (2) initial thermal conditions. The major check for Earth models is the observed heat flow at the surface. This is equal to the product of the thermal conductivity and the temperature gradient, which are both measurable quantities. The radioactivity of Earth has usually been assumed to be that of chondritic meteorites containing the long-lived radioelements K^{40}, U^{235}, U^{238}, and Th^{232}. This assumption is considered highly doubtful today. A variety of initial thermal conditions are then used to try to reproduce the observed heat flow. Although the latter constraint has recently been measured fairly well for Earth, the calculated thermal models for Mars are tentative, because of uncertainties in the assumptions used.

Thermal models derived for other terrestrial planets by analogy with Earth are highly speculative, even more so than the density models. Nevertheless, the thermal models for Mars calculated by Kopal (refs. 84 and 85) and by MacDonald (ref. 78) should be briefly reviewed in anticipation of eventual measurements of surface heat flow. MacDonald calculated two different model types. One assumes uniform chondritic radioactivity throughout the planet and the other assumes only the mantle to be radioactive. The mantle comprises the outer two-thirds of the planet. (See fig. 8–2.) MacDonald's analysis led him to conclude that a level of radioactivity equal to that of chondrites is too high for Mars. Kopal was more concerned with testing the assumption of conduction as the main mechanism responsible for the heat flow and with exploring the expansion and stresses produced on the planet after billions of years of thermal history. Using only models of uniform chondritic radioactivity throughout, Kopal found that high temperatures (over 2000° K) would have prevailed during most of the past history of Mars. Also, the conductive temperature gradient assumed must exceed the adiabatic gradient of molten rocks, so that convective heat flow occurs.

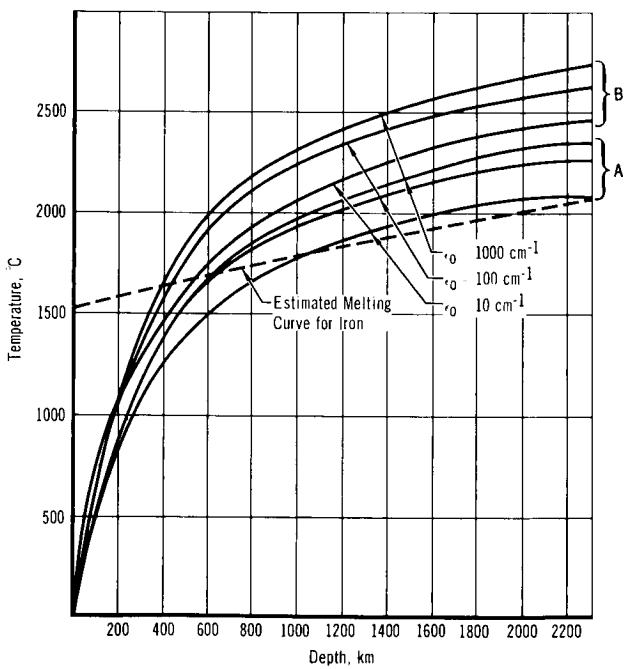

FIGURE 8–2.—Thermal models of Mars' interior: (*A*) Uniform radioactivity; (*B*) Radioactivity in mantle. (After ref. 78.)

MARINER IV IMPLICATIONS

Mariner IV findings indicate little or no magnetic field for Mars. According to a concept of the origin and maintenance of a planetary magnetic field, the planet must rotate and must possess a liquid, electrically conducting core. Since Mars has a rotation period (24.62 hr) nearly the same as that of Earth, the weaker magnetic field may indicate a different internal structure and/or chemical composition, and it is probable that Mars possesses no liquid, electrically conducting core. Consequently, Mars may have an apparent internal constitution closer to that of the Moon than to that of Earth.

9

Electromagnetic and Particle Fields

MAGNETIC FIELD

THE MAGNETIC FIELD SURROUNDING A PLANET is believed to be the consequence of convection currents in a liquid, conducting core. The core of Mars was estimated to be considerably smaller than that of Earth, and as a result, pre-Mariner estimates of the Martian magnetic field strength were generally lower than that of Earth.

Highly speculative results on the Martian magnetic field had been obtained by Singer (ref. 86) by making an analogy with Earth's magnetic dipole field. On the assumption that the magnetic moment M of a planet is roughly proportional to its volume V, he derived for Mars the value $M_M = 9.2 \times 10^{24}$ gauss-cm^3, or 15 percent that of Earth. (Singer used $M_E = 6.1 \times 10^{25}$ instead of the generally used 8.06×10^{25} gauss-cm^3.)

MARINER IV RESULTS.—The magnetometer on board Mariner IV detected no increase in magnetic field during encounter with Mars, although it was only 14 700 kilometers from the planet's center. From this observation and the value of solar wind pressure (0.5×10^{-8} dyne-cm^{-2}) given by the plasma probe also at encounter time, Smith et al. (ref. 87) derived an upper limit for the magnetic dipole moment of Mars. They assumed that the interaction with the solar wind in the case of Mars has geometrically similar effects to those observed for Earth. Using the equation:

$$M_M/M_E = (R_M/R_E)^3 \, (P_M/P_E)^{1/2}$$

where R is the radius and P the solar wind pressure, they obtained: $M_M \leq 10^{-4} \, M_E$. If allowance is made for the possibility that the Mars dipole axis was not parallel to the rotation axis, then: $M_M \leq 3 \times 10^{-4} \, M_E$. This latter value implies an equatorial surface magnetic field strength on Mars less than $\sim$100 gammas, or 10^{-3} gauss (since 1 gamma $= 10^{-5}$ gauss).

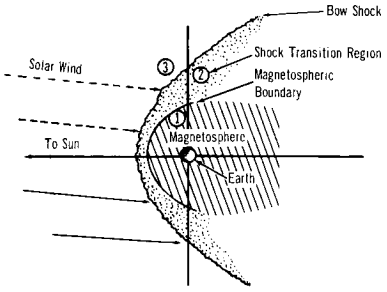

FIGURE 9–1.—Interaction of the solar wind with Earth's magnetosphere. (After ref. 89.)

RADIATION BELTS

According to Van Allen et al. (ref. 88), for a planet to have radiation belts similar to those of Earth, it is necessary that the planet possess (1) strong magnetization of its body and (2) sufficient exposure to the solar wind.

The impact of the hypersonic solar wind against the planet's magnetosphere results in a shock front (bow shock) at some distance outside the magnetopause. Bursts of electrons are characteristic of the interaction, and concentrate especially in the shock transition region. (Energies in the keV range have been detected in the Earth's transition region since 1963.) Such electron bursts in the three regions marked out (see fig. 9–1) provide the "signatures" of trapped radiation belts. The assumption was made that for Mars, there would be analogous radiation signatures if belts were present. Since all functioning particle detectors on board Mariner IV yielded negative results, it was inferred that no such belts existed around Mars, and by conclusion an insignificant magnetic field was confirmed. The detectors consisted of four trapped radiation detectors built by Van Allen et al., and a cosmic ray telescope consisting of three detectors placed by O'Gallagher and Simpson (ref. 89).

10

Surface Temperature

THEORETICAL TEMPERATURES

A ROUGH ESTIMATE of the temperature of the surface of a planet can be derived from its mean solar constant, S, with the reasonable assumption that the entire planet (solid globe and atmosphere) has reached a state of thermal equilibrium. According to Stefan's law, the rate of radiation, W, of a perfect radiator (blackbody), when integrated over all wavelengths, is proportional to the fourth power of the absolute temperature, T, of its surface: $W=\sigma T^4$, where σ is the Stefan-Boltzmann constant.

If the planetary reflectivity or albedo is A, then the rate of solar energy absorption is $S(1-A)$. The thermal equilibrium equation is therefore $S(1-A)=\sigma T^4$. This simple equation makes possible the determination of a theoretical surface temperature, T, for the planet, considered now to be a graybody.

For a planet in rapid rotation, the planetary emission occurs almost uniformly over the entire planet, but the solar radiation is intercepted over the cross-sectional area of the globe. Hence, the formula may be improved by inclusion of the factor ¼, producing for the average surface temperature of Mars:

$$T_{av}^4=\frac{S_M(1-A)}{4\sigma}$$

where S_M is the mean solar constant at Mars.

The planetary albedo, A, used should be the radiometric albedo A^*, defined as the albedo integrated over all wavelengths. (See ch. 11 for this value.)

The mean solar constant at a planet is inversely proportional to the square of the planet's mean distance from the Sun. From the known value of the solar constant of Earth, S_E, which is at unit distance (1 A.U.) by definition, the Martian solar constant is easily obtained:

$$S_M=\frac{S_E}{a_M^2}$$

where a_M is the mean solar distance of Mars in astronomical units. Table 10–1 presents the values of S_M, as derived from the various published values of S_E. Since there is a discrepancy of 4 to 5 percent in the latter, a corresponding uncertainty will be introduced in the derived temperatures. The table also depicts the variation of S_M resulting solely from the eccentricity of the Martian orbit. The actual solar flux received at Mars varies by as much as 37 percent between perihelic and aphelic positions. Only the mean value of S_M will be used.

Using the following values of the two uncertain constants

$S_M=0.857$ cal/cm²/min (from $S_E=1.99$ cal/cm²/min, Allen (ref. 90))

$A^*=0.295$ (radiometric albedo, De Vaucouleurs (ref. (32))

and the well-determined fundamental constant,

$$\sigma=8.127\times10^{-11}\ \text{cal/cm}^2/\text{deg}^4$$

the average (annual) surface temperature of Mars is

$$T_{av}=207.6^\circ\ \text{K}$$

The values published in the literature, namely 217° K by Kuiper (ref. 91) and 219° K by Ohring et al. (ref. 92), are slightly higher. They are based on the visual albedo $A=0.15$. The radiometric albedo, A^*, was only recently estimated by De Vaucouleurs.

The average temperature, T_{av}, as derived, may be safely considered the lowest limit of the actual T_{av} because the equation does not consider the atmosphere of Mars. Tenuous as it may be, the carbon dioxide (and water vapor) in the Martian atmosphere is expected to absorb some of the radiant energy and produce a weak greenhouse effect that would increase the calculated T_{av}, which

TABLE 10–1.—*Solar Constant at Mars*

[Ref. 6]

Observed terrestrial solar constant, cal/cm²/min	Computed value of solar constant[a] at Mars-Sun distance, cal/cm²/min			Author
	Aphelion	Mean	Perihelion	
1.896	0.683	0.817	0.994	Moon (1940).
1.94	.699	.836	1.02	List (1951).
1.946	.701	.838	1.02	Aldrich, Hoover (1954).
1.97	.710	.849	1.03	Allen (1955).
2.00±0.004	.721	.861	1.05	Johnson (1954).
2.05	.739	.883	1.07	Stair, Johnson (1956).

[a] Based upon aphelion, mean, and perihelion distances listed in table 1–3.

refers to an airless planet. An upper limit of the average temperature can be obtained by calculating, using a more sophisticated method, the surface temperature that would result from a maximum greenhouse effect model. Ohring, Tang, and DeSanto (ref. 92) made such calculations, using a radiative absorption method by Elsasser (ref. 93) and radiation tables by Elsasser and Culbertson (ref. 94) for a Martian greenhouse model that was based upon a surface pressure of p_0=85 millibars, the presence of 4 percent carbon dioxide, 10^{-2} cm precipitable water vapor, and 0.15 cm-atm ozone. The heat balance equation used was of the form:

$$W=I_M\,(1-A),$$

where I_M is the average incoming solar radiation flux per day and W is the outgoing flux (longwave radiation) at the top of the atmosphere per day.

Using the commonly accepted values, S_E=2.00 cal/cm^2/min and A=0.15 (visual albedo), these authors obtained $T_{av}^{max}=233°$ K for the estimated maximum possible value of the average surface temperature of Mars. Compared with their value, $T_{av}^{min}=219°$ K, a maximum greenhouse effect would increase the Martian surface temperature by only 14° C (for Earth, a similar estimation with A=0.35 yields 252° and 288° K as limits, indicating an average greenhouse effect of 36° C). Since it is now known to be 85 millibars, the greenhouse effect is probably much smaller.

An estimate of the maximum surface temperature of Mars, often seen in literature, again assumes the planet to be a spherical graybody, but in locked or synchronous rotation. In this mode, planetary emission does not occur over the entire planet and the following equation applies:

$$T_{max}^4=\frac{S_M\,(1-A)}{\sigma}$$

or

$$T_{max}^4=4T_{av}^4$$

With identical values of the three constants: T_{max}=293.6° K. (Kuiper gives 307° K, using A=0.15.) This maximum theoretical temperature corresponds to the temperature at the subsolar point, if Mars were airless, and in locked rotation. When tested with Earth, it appears that the theoretical T_{max} is a fairly good estimate of the maximum temperature observed.

Temperatures derived by these radiative equilibrium methods may be substantially different from the actual or true temperatures. It should be pointed out that: (1) only rotational extremes

have been used; (2) it is unlikely that Mars behaves as a graybody, even less as a blackbody (the temperatures calculated for a blackbody assumption would be about 5° to 10° lower); (3) the heat exchange between surface and interior was neglected; (4) the atmospheric absorption and transmission assumed by Ohring et al. may be unrealistic; and (5) the emissivity of the Martian surface is, of course, unknown (its effect is included with planetary albedo).

OBSERVED TEMPERATURES

Planck's law and energy curves can be used to give a temperature estimate from various observed regions of the spectrum. Although most planetary radiation is concentrated in the infrared, centimeter radio waves called "thermal radio waves" have also been used to measure temperature. This will be discussed as radio emission radiometry.

INFRARED RADIOMETRY

Coblentz and Lampland (refs. 95 through 98) at the Lowell Observatory and Pettit and Nicholson (ref. 99) at the Mount Wilson Observatory performed the first radiometric measurements on Mars. During the oppositions of 1922, 1924, and 1926, they employed a variety of techniques involving spectral filters and lunar comparisons to determine the temperature of Mars over a large number of points on the surface. New data available on the transmission of the atmosphere of Earth and the discovery of the selective emission by the surface of Mars between 8.5 and 9.5 microns led to the revision of some of the results of Coblentz and Lampland.

Coblentz drew a number of interesting conclusions regarding temperatures on the surface of Mars:

(1) The Southern Hemisphere is warmer than the Northern Hemisphere.

(2) Temperature rises rapidly with the advance of summer.

(3) The highest temperatures in the Southern Hemisphere, at least in temperate and frigid zones, occur not at solstices, but a month or so later (as on Earth).

(4) The morning is cooler than the evening under a clear sky.

Coblentz's initial work was continued and expanded under Lampland into a systematic program of measurements of the Martian surface temperatures. In 1952, Gifford undertook the

task of reducing and summarizing some 1300 measurements made between 1926 and 1943. The results were presented in a Lowell Observatory Report on planetary atmospheres (refs. 100 and 101). Later, Sinton and Strong (refs. 102 and 103) at Mount Palomar Observatory supplemented these data with some accurate drift curve data obtained especially on the summer side of the equator.

DAILY TEMPERATURE VARIATION.—Averages of radiometric measurements along the equator of Mars at opposition times (1926, 1928, and 1954) for morning-to-evening locations yielded the average daily variation curve given in figure 10–1. The lag of maximum temperature after local noon is about 1 hour. The temperature curve pertains to the actual surface of Mars, since the infrared radiometer measures the planetary surface emission. The curve for the air temperature just above the surface (some 2 meters above ground) must have less variation, and the time of maximum temperature will be even more retarded. This is true for similar curves for data taken in the Gobi Desert during June at heights of 0 and 2 meters. Milankovitch (ref. 104) calculated that a lag of 3 hours in the maximum temperature would occur for an airless rotating planet if it were a perfect conductor; if it were a perfect insulator, no temperature lag would occur.

The extreme variation in temperature for the equatorial regions of Mars is about 50° C, with the ground temperature above 0° C occurring at midday. This is a rigorous climate, but does not preclude the possibility of life on Mars.

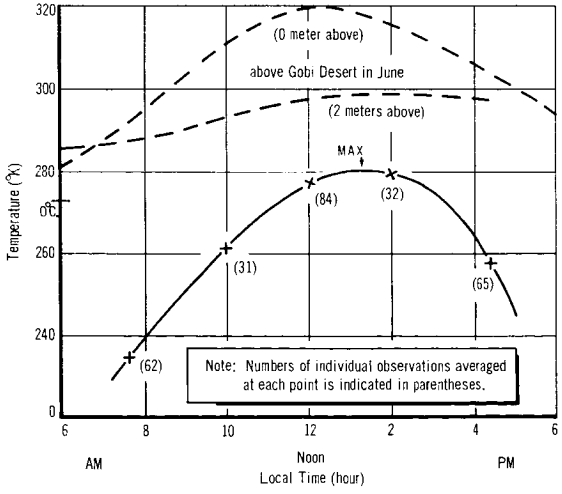

FIGURE 10–1.—Daily temperature variation—average near Martian equator. (After ref. 100.)

ANNUAL TEMPERATURE VARIATION.—Gifford displayed the average latitude distribution of temperature on Mars at the noon meridian for each of the four seasons by curves (fig. 10–2(A)) for latitude ranging from 60° N to 80° S.

Ohring et al. (ref. 92) have extrapolated these curves to the poles for computations of an annual average temperature as a function of latitude (fig. 10–2(B)). The four curves illustrate the annual march of summer and fall seasons particularly well. The winter curve lacked adequate data and the apparently abnormal spring curve was also based on too few observations, most

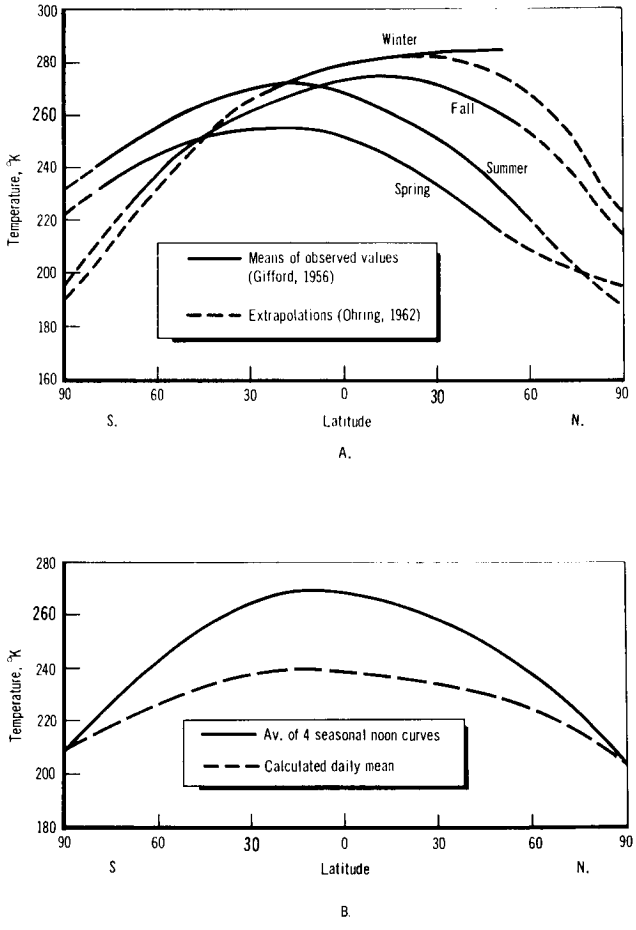

FIGURE 10–2.—Mars annual and seasonal surface temperature—latitudinal variation: (*A*) Variation along noon meridian, southern hemisphere seasons; (*B*) Annual temperatures (ref. 92).

of which happened to have been made in the Hellas region (assumed to be a high plateau).

SEASONAL TEMPERATURE DISTRIBUTION.—Gifford prepared the series of three isotherm maps for the Southern Hemisphere during summer, fall, and winter shown in figure 10–3. Insufficient data were available for a spring isotherm map. The summer isotherm map substantiates that of Hess (ref. 105). Certain isotherm configurations are identifiable with well-known surface markings. (The closed 290° K isotherm on the summer map is just over the dark area Mare Cimmerium. The closed 280° K isotherm on the fall map is over Syrtis Major.) Since the data represent averages over large areas, the use of these maps is more appropriate for atmospheric circuits than for topographical interpretations.

Conclusions by De Vaucouleurs (ref. 106) from the excellent, early radiometric work, are the following:

(1) The average annual temperature of Mars is 50° to 60° C lower than on Earth; its range with latitude is from about –20° to –30° C in tropical-equatorial regions to –70° or –80° C in polar regions.

(2) The average diurnal variation of temperature is about 50° C in equatorial regions. The maximum temperature occurs at 12:30 to 1 p.m., and the nocturnal minimum temperature occurs shortly before sunrise.

(3) The annual temperature variation is about 100° C or more in polar regions, about 50° C in temperate regions, and about 30° C in tropical regions.

(4) The dark areas in the tropical regions may be about 10° C warmer in daytime than the adjacent bright areas.

(5) The air above ground is possibly 20° or 30° C colder than the ground itself at noontime; but the difference diminishes rapidly with darkness, probably disappearing before sunrise.

RADIO-EMISSION RADIOMETRY

Two determinations of the radio-emission temperature of Mars have been made to confirm the results obtained by infrared radiometry. Mayer et al. (refs. 107 and 108) obtained a blackbody disk temperature of 218° ±76° K from observations during the 1956 opposition at a wavelength of 3.15 centimeters. During the 1958 opposition, Giordmaine et al. (ref. 109) claimed greater accuracy by means of a maser amplification technique; a temperature of 211°±20° K was obtained.

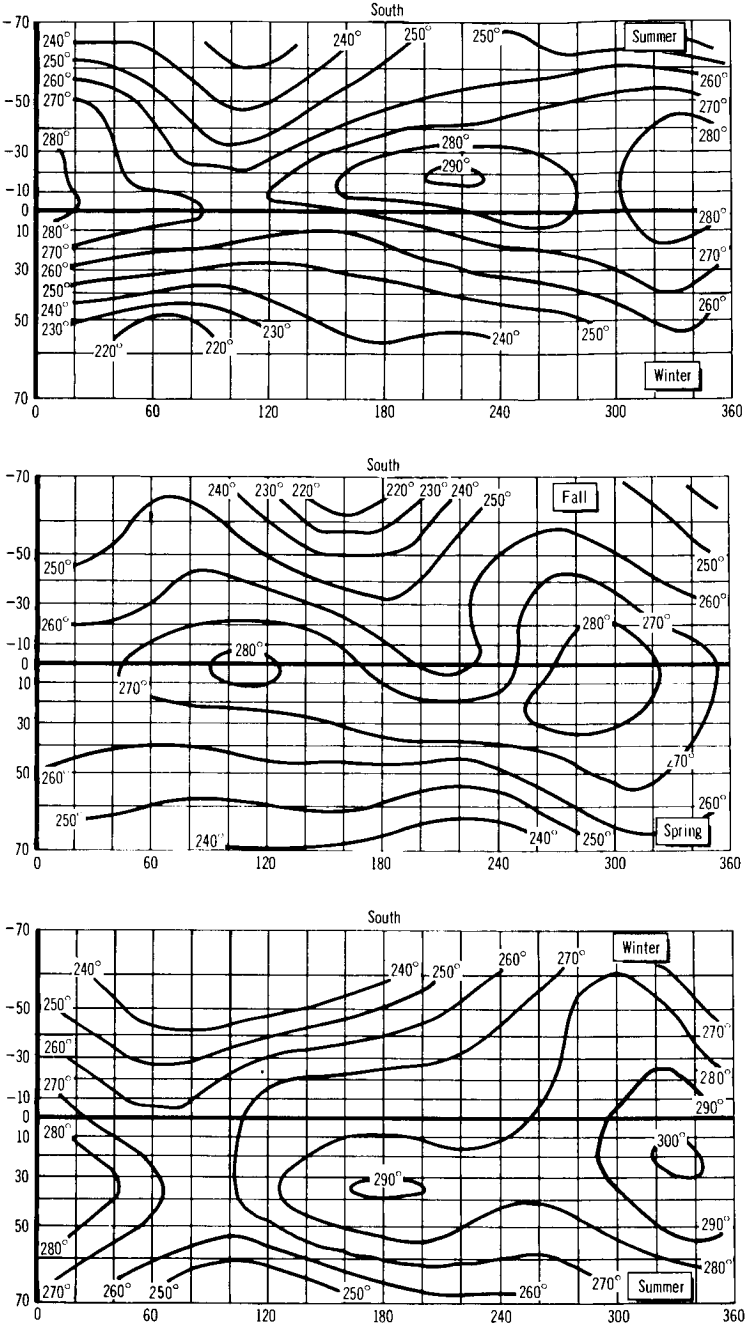

FIGURE 10 3.—Average Martian isotherms. (After ref. 100.)

Mayer argued that since the radio emission temperature is lower than the infrared temperature, the radio waves originate slightly below the surface of Mars. The radio waves approximate the average temperature over the whole surface of Mars, whereas the infrared temperature represents the average temperature over the sunlit surface. The radio-emission temperature is surprisingly close to the theoretically predicted graybody temperature. Table 10–2 summarizes the general results of measurements of Martian surface temperatures.

CLIMATOLOGY

To a certain extent, there is a climatological parallel between Mars and Earth which is a direct consequence of the nearly equal axial inclinations and periods of rotation of the two planets and their spatial proximity. The distinctly lower surface temperature of Mars is basically a result of the greater distance of Mars from the Sun, a distance about 1½ times that of Earth. Considering the planetary albedo, Mars has a mean effective insolation that is approximately half that of Earth.

The major climatological differences between Mars and Earth

TABLE 10–2.—*Temperature of the Surface of Mars*

Method	Observer	Average surface temperature, °K
Infrared	Coblentz and Lampland (refs. 95 through 98)	245
	Pettit and Nicholson (ref. 99)	260
	Sinton and Strong (ref. 103)	230
Radio	Mayer (refs. 107 and 108)	218±76
	Giordmaine et al. (ref. 109)	211±20

Summary of Information
[After ref. 110]

	°K
Maximum temperature at equator	~300
Mean amplitude of diurnal variation:	
Noon to sunset	~ 60
On Earth in desert	~ 30
Night side temperature cannot be measured but probably can be estimated at the equator	~200
Day side temperature at poles	~220
Mean temperature of day side	~260
Mean temperature of whole planet	~230

arise solely from the fact that Mars has practically no water in either a liquid or a vapor state to regulate its climate. More specifically, Mars has: (1) no oceans to act as a heat reservoir to store or release heat during the change of seasons; and (2) insignificant atmospheric water vapor (humidity) and clouds too sparse to produce any significant greenhouse effect.

Martian climatology is thus much simpler than that of Earth. Most of the ground-emitted infrared rays escape to space because carbon dioxide, which is practically the only heat absorber in the atmosphere of Mars, has large transparent regions in the infrared, with the result that perhaps 70 percent of the energy escapes. Therefore, Martian nights are extremely cold (around 200° K). The temperature changes closely follow the large extremes in insolation. Because of the very small greenhouse effect, the outgoing infrared radiation must necessarily decrease from equator to pole instead of remaining almost constant with latitude as on Earth. A comparative study made recently by Mintz (ref. 111), based upon theory and observation, discusses the mean annual radiation budgets; namely, the quantities: $I(1-A)$, effective daily insolation; W, outgoing infrared emissions; and ΔQ, their difference, or net differential heating. For Mars, this last quantity remains very small.

11

Optical Parameters

ZÖLLNER (REF. 112) PUBLISHED the results of the first reliable photometric observations of Mars, but this subject remains a fertile area of research from both an observational and a theoretical point of view. The latest photometric data are presented here; however, revisions are expected as new data are obtained. For simplicity, definitions are omitted but they may be found in the glossary.

MAGNITUDE

VISUAL MAGNITUDE

The visual magnitudes of Mars, $V(1, 0)$, reduced to unit distances from Earth and Sun and to zero-phase angle, which are presented in table 11–1 are based on a reduction by Harris (ref. 113) of both past and present observations (refs. 114–120). The mean value of the reduced visual magnitudes of Mars derived from over a century of observations is −1.52.

SPECTRAL VARIATION OF MAGNITUDE

The variation with wavelength of Martian reduced magnitudes, m (1, 0), is exhibited in table 11–2 and figure 11–1. The values are based on Mount Stromlo Observatory spectrophotometric data of 1952 and 1954 by Woolley (refs. 121 and 122), Lowell Observatory (Flagstaff) photoelectric data of 1954 and 1958 by Johnson and Gardiner (ref. 119) and De Vaucouleurs (ref. 120), and McDonald Observatory photoelectric data of 1952 and 1954 by Hardie (quoted by ref. 113).

VISUAL PHASE CURVE

Observation of the planet Mars from Earth is limited to phase angles α smaller than 47°. In this range, the correction for variation in magnitude of the planet with phase angle is expressed by means of a linear phase law. The best determination of visual-phase coefficient a_v is +0.01486 magnitude per degree, obtained by

TABLE 11–1.—*Reduced Visual Magnitudes of Mars*

Method	Observer	Period of observation (opposition)	Reduced visual magnitude, $V(1, 0)$
Visual	Zöllner (ref. 112)	1864 to 1865	—1.59
	Müller (ref. 114)	1876 to 1877	—1.44
		1879 to 1880	—1.48
		1881 to 1882	—1.57
		1883 to 1884	—1.55
		1886	—1.51
		1888 to 1889	—1.52
Photovisual	King (refs. 115 and 116)	1916	—1.52
		1918	—1.51
		1920 to 1921	—1.45
		1922	—1.56
	Livländer (ref. 117)	1926	—1.7(?)
		1928	
		1930 to 1931	
Visual	Radlova (ref. 118)	1939	—1.38(?)
Photoelectric	Harris (ref. 113)	1952	—1.56
	Johnson and Gardiner (ref. 119)	1954	—1.51
	De Vaucouleurs (ref. 120)	1958	—1.56
Mean value			—1.52

Müller (refs. 114 and 123) on the basis of extensive observations from 1877 to 1889. Figure 11–2 represents the visual phase curve plotted from Müller's observations; the slope of this straight line gives the value of the phase coefficient. For phase angles greater than 47°, the phase law must be extrapolated. De Vaucouleurs (ref. 32) uses as a guide the Earth's phase law, as obtained by Danjon (ref. 124) from observations of earthshine upon the Moon. The resulting phase law for Mars is found to depart from linearity. Numerical integration over the range $\alpha=0°$ to 180° of the phase function $\phi(\alpha)$, representing best the phase law, can then yield a value for the phase integral $q=\int\phi(\alpha)$ sin a $d\alpha$ which is used in the calculation of Russell-Bond albedo.

SPECTRAL VARIATION OF PHASE COEFFICIENT

The phase coefficient is strongly dependent upon wavelength. Figure 11–3 represents variation of the phase coefficient a with respect to wavelength as determined from the Lowell Observatory photoelectric photometry and the Mount Stromlo photographic spectrophotometry.

TABLE 11–2.—*Reduced Monochromatic Magnitudes of Mars*

Years observed	Reduced magnitudes $m(1,0)$ at λe=3300Å through 4950Å							Author
	3300 Å U′	3700 Å U	4050 Å	4250 Å	4500 Å B	4550 Å	4950 Å	
1952	.....	.....	+0.53	+0.29	.....	—0.32	—0.72	Woolley (ref. 121)
1954	.....	.....	+.24	+.08	.....	—.53	—1.04	Woolley (ref. 122)
Mean[a]	.....	.....	+.40	+.19	.....	—.42	—.88	
1954	.....	+0.41	.....	.....	—0.17	.....	.....	Johnson and Gardiner (ref. 119)
1958	+0.39	+.495	.....	.....	—.235	.....	.....	De Vaucouleurs (ref. 120).
Mean[a]	.....	+.45	.....	.....	—.20	.....	.....	
1952 to 1954	.....	+.42	.....	.....	—.16	.....	.....	Hardie, quoted by Harris (ref. 113).

Years Observed	Reduced magnitudes $m(1,0)$ at λe=5430 Å through 8220 Å							Author
	5430 Å	5550 Å V	5980 Å	6360 Å	6900 Å R′	7000 Å R	8200 Å I	
1952	—1.24	.....	—1.86	—2.10	.....	.....	.....	Woolley (ref. 121)
1954	—1.50	.....	—1.88	—2.21	.....	.....	.....	Woolley (ref. 122)
Mean[a]	—1.37	.....	—1.87	—2.15	.....	.....	.....	
1954	.....	—1.49	.....	.....	.....	.....	.....	Johnson and Gardiner (ref. 119)
1958	.....	—1.56	.....	.....	—2.505	.....	.....	De Vaucouleurs (ref. 120)
Mean[a]	.....	—1.53	.....	.....	.....	.....	.....	
1952 to 1954	.....	—1.52	.....	.....	.....	—2.64	—3.02	Hardie, quoted by Harris (ref. 113).

[a] Mean values per De Vaucouleurs (ref. 120).

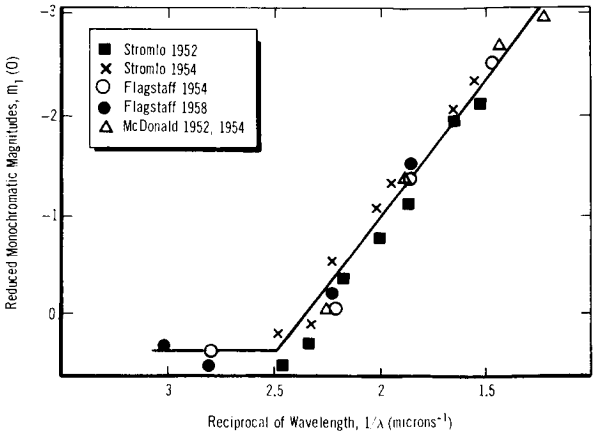

FIGURE 11-1.—Spectral variation of Mars' magnitude. (After ref. 32.)

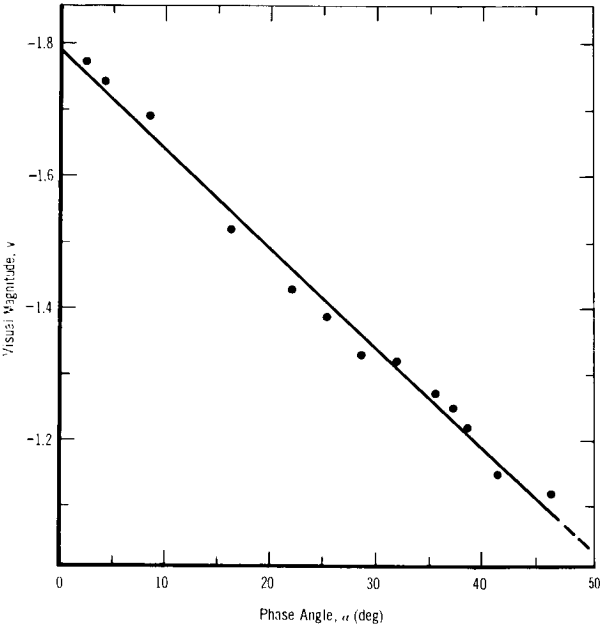

FIGURE 11-2.—Mean visual phase curve of Mars. (After ref. 114.)

LONGITUDINAL VARIATION OF MAGNITUDE

Variation in the visual brightness of Mars with rotational period was first established visually by Lau (ref. 125), and then photoelectrically by Guthnick and Prager (ref. 126), by Johnson and

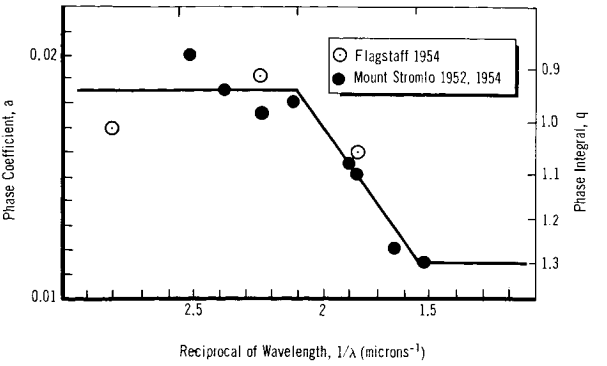

FIGURE 11–3.—Spectral variation of Mars' phase coefficient. (After ref. 32.)

Gardiner (ref. 119), and finally by De Vaucouleurs (refs. 120 and 127). Figure 11–4 represents this variation with longitude ω of the central meridian. The brightness of Mars at short and long wavelengths, however, is not significantly dependent upon longitude.

BOND ALBEDO

The visual Bond albedo A_v for Mars, based on an average value for visual phase integral q (fig. 11–3), is 0.159 at λ 5550 Å. Toward red (λ6360 Å), the Bond albedo reaches 0.30, and for blue-violet wavelengths drops to a relatively constant 0.05 (fig. 11–5). An unconfirmed, very high albedo of 0.2 in the near-ultraviolet (λ2740 Å) was obtained in 1958 by rocket (ref. 128). If proven, this may indicate some special upper atmosphere effect in ultraviolet.

A summary of monochromatic albedos recently calculated by Woolley, De Vaucouleurs, and Harris is presented in table 11–3. This summary is based upon the monochromatic magnitudes of Mars in table 11–2. Mars appears red and bright in the visible spectrum, and even brighter in the near-infrared. It is dark in the near-ultraviolet, which suggests strong absorption by aerosols or absorbing gases.

COLOR INDEX

Harris (ref. 113) derived mean color indices for Mars and compared them with the corresponding color indices for the Sun. (See table 11–4.) Harris' values for the color differences between

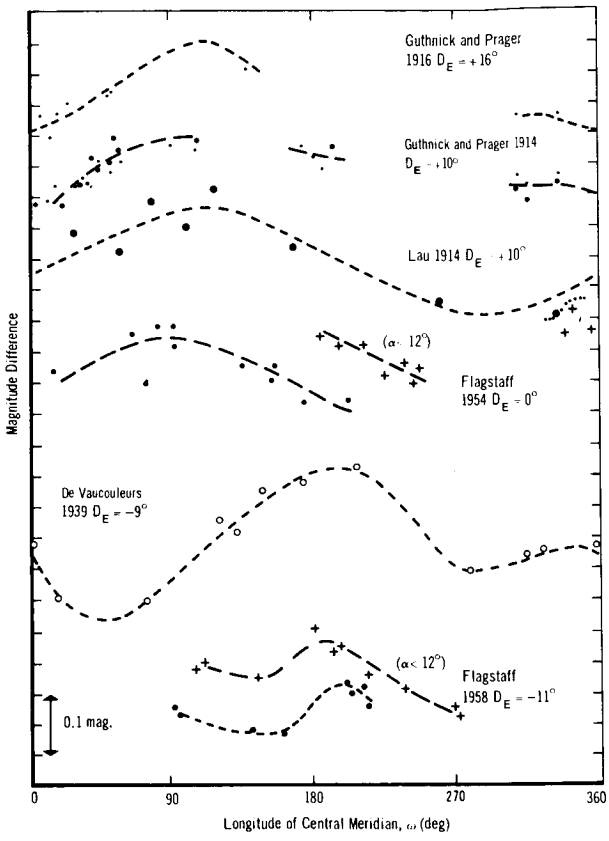

FIGURE 11-4.—Longitudinal variation of visual magnitude of Mars. (After ref. 32.)

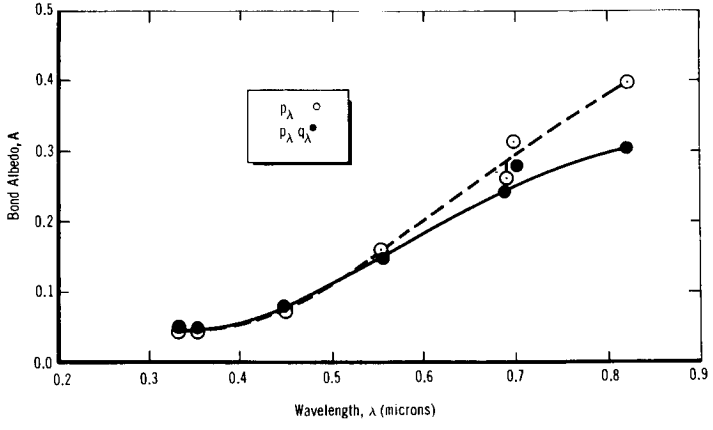

FIGURE 11-5.—Spectral variation of Mars' albedo. (After ref. 32.)

TABLE 11-3.—*Monochromatic Albedos and Phase Integrals of Mars*

Author	Values at various wavelengths														
	3300 U′	3550	3600 U	4050	4250	4500 B	4550	4945	5430	5550 V	5980	6360	6900 R′	7000 R	8200 I
Geometrical albedo, $p(\lambda)$															
Woolley (ref. 122)	.....	.....	.....	0.049	0.054	.....	0.081	0.097	0.131	.....	0.194	0.227	.....	.....	.....
De Vaucouleurs (ref. 120)	0.049	.....	0.0485	.....	.....	.....	.087	.....	.....	0.165	.....	.....	0.253	.....	.....
Harris (ref. 113)	.....	0.052	.....	.....	.....	0.080	.....	.....	.....	.154	.....	.....	.....	0.286	0.310
Phase integral, $q(\lambda)$															
Woolley	.....	.....	.....	0.95	0.99	.....	1.04	1.09	1.19	.....	1.25	1.31	.....	.....	.....
De Vaucouleurs	0.938	.....	0.938	.....	.....	.....	0.938	.....	.....	1.100	.....	.....	1.295	.....	.....
Harris	.....	.....	.....	.....	.....	.....	.....	.....	.....	1.04	.....	.....	.....	.....	.....
Bond albedo, $A(\lambda)$—$p(\lambda)\times q(\lambda)$															
Woolley	.....	.....	.....	0.047	0.053	0.084	.....	0.106	0.16	.....	0.24	0.30	.....	.....	.....
De Vaucouleurs	0.046	.....	0.046	.....	.....	.....	0.082	.....	.....	0.181	.....	.....	0.327	.....	.....
Harris	.....	.....	.....	.....	.....	.....	.....	.....	.....	.16	.....	.....	.....	.....	.....

TABLE 11-4.—*Mean Color Indices and Color Differences*
[After ref. 113]

Body	Mean color indices from differences between magnitudes			
	U-B	B-V	V-R	R-I
Mars	0.58	1.36	1.12	0.38
Sun	.14	.63	.45	.29

Color differences between Mars and the Sun for each wavelength region				
U	B	V	R	I
+1.17	+0.71	0.00	—0.67	—0.76

Mars and the Sun at each of the effective wavelengths for U, B, V, R, and I are also listed. In the conventional B–V index, the greater the value, the redder the body.

Variations in the Martian color index have been noted by Livländer (ref. 117) as dependent upon such factors as the following:

Solar Phase Angle.—Mars becomes redder with increasing phase angle α at the rate of 0.003 magnitude per degree, thus giving at quadrature (when $\alpha \sim 47°$) a color index greater by about 0.15 magnitude. To someone viewing Mars from a place in the solar system where the phase angle is much larger, it is expected that Mars would appear bluer because of scattering in its atmosphere.

Hemispheric Presentation.—The color index is increased by a maximum of 0.1 to 0.15 magnitude when the Southern Hemisphere of Mars is tilted toward Earth (perihelic opposition).

Surface Variations.—Surface variations, especially in the dark areas and polar caps, affect color index.

Atmospheric Variation.—Atmospheric variation of Mars caused by clouds and haze contributes to variation in the planet's color index.

RADIOMETRIC ALBEDO

Radiometric or integral spherical albedo, A^*, is an important parameter in meteorology because it determines the fraction $(1 - A^*)$ of the incident solar energy absorbed by the planet. However, determination of this parameter is complicated by the incompleteness of our knowledge of the photometric parameters of Mars, especially in the ultraviolet and infrared regions. De

Vaucouleurs (ref. 32) extrapolated the visual geometrical albedo p and the visual phase integral q into the ultraviolet and infrared regions to obtain p^* and q^*. His value for Mars' radiometric albedo A^* is 0.295; for its components p^* and q^*, 0.235, and 1.24, respectively. These values have been adopted generally.

12

Atmospheric Composition

SPECULATION ON THE COMPOSITION of the Martian atmosphere will continue until more direct experimental evidence is obtained. At the Earth's surface, the spectroscopist is limited to two types of investigations: (1) the study of Martian absorption bands (or the lack thereof) in the spectral windows of the terrestrial atmosphere, and (2) the comparison of the spectrum of the terrestrial atmosphere alone with that obtained by the superimposed effect of the Martian atmosphere. By combining this limited spectroscopic data with dynamical, cosmological, radiological, and photochemical considerations, certain conclusions have been drawn regarding the composition of the atmosphere of Mars, but with much uncertainty. The recent physical probing in situ of the Martian atmosphere by the Mariner IV demonstrates, for instance, the error in assigning nitrogen as the most abundant element in the atmosphere.

CARBON DIOXIDE

Carbon dioxide was repeatedly found by spectrography to be abundant in the Mars atmosphere; the amounts found were definitely higher than on Earth. Kuiper (ref. 91),[1] using the 1.6-micron band, calculated the Martian carbon dioxide mass/cm^2 to be nearly twice that of Earth. Recalculation by Grandjean and Goody (ref. 129) gave 13 times the Earth value, or 35±10 m-atm. (Note: this estimate was based on a total surface pressure of 85 millibars, and therefore, is of low accuracy.) From the rotational lines of carbon dioxide near λ8700 Å, Kaplan et al. (ref. 130) deduced the carbon dioxide abundance as 55±20 m-atm for a surface temperature of 230° K. They calculated the carbon dioxide partial pressure to be 4±2 millibars, proposing a total surface

[1] While comparing spectra of Mars and of the Moon in 1947, Kuiper found two slight depressions near 1.6 microns which suggested the presence of carbon dioxide on Mars. When the planet came closer in 1948, three characteristic bands of carbon dioxide at 1.96, 201, and 2.06 microns were observed, confirming the earlier result.

pressure of 25±15 millibars. Improved calibrations of the $5\nu_3$ band of carbon dioxide at λ8700 Å by several investigators led to various revisions of these results (refs. 131 and 132).

Carbon dioxide undergoes rapid photodissociation under radiation of wavelengths less than 1692Å. This mechanism is severely restricted in the Earth's upper atmosphere by the absorption of sunlight (the Schumann-Runge continuum, 1250–1760 Å) by oxygen molecules. On Mars, because molecular oxygen is insignificant, this dissociation was usually assumed to proceed rapidly. (Two recombination mechanisms were postulated to explain the continuous presence of carbon dioxide in the Martian atmosphere. These are discussed in the following paragraphs.) However, Chamberlain's calculations of the photochemical equilibrium between carbon dioxide, carbon monoxide, atomic and molecular oxygen indicate that the carbon dioxide dissociation is considerably slowed down by the rapid formation of molecular oxygen (reassociation of O+O) which shields the carbon dioxide from the ultraviolet radiation so conditions may be closer to terrestrial ones (ref. 133).

Data obtained from the Mariner IV mission have assigned the greatest atmospheric abundance on Mars to carbon dioxide.

Although the craft did not sample this atmosphere or even carry spectrographic equipment, the results of its physical probing by the radio occultation method—when interpreted in terms of refractivity and density (total density at surface and scale height) and when used in conjunction with previous spectrographic information of Kaplan et al. (ref. 130)—indicate with high probability that carbon dioxide constitutes at least 50 percent of the Martian atmosphere. Kliore et al. (ref. 134) in fact have chosen for their plots of mass density versus refractivity several possible model compositions with carbon dioxide ranging from 50 to 100 percent, the rest being either nitrogen or argon. These models are tentative but the preliminary conclusion about the preponderance of carbon dioxide appears reasonably consistent with the ionospheric measurements of Mariner IV. Indeed high abundances of carbon monoxide and atomic oxygen from photodissociation of carbon dioxide, and the resulting greater radiative cooling, are in line with the very cold ionosphere found.

NITROGEN

Nitrogen was generally thought to be the bulk constituent of the Martian atmosphere until probing of the latter's physical characteristics by Mariner IV proved otherwise. Indeed, the high mean

molecular weight determined, around 40—definitely above that of nitrogen (N_2=28)—indicated that a heavier gas or mixture of gases must be present.

It used to be customary, by making a simple analogy with Earth, to place the proportion of nitrogen in the Martian atmosphere at about 95 percent, since oxygen was known to be practically absent. Obviously, this was very precarious, since nothing is yet known of the relative abundances of the main constituents of planetary atmospheres other than that of Earth.

Speculation on the unknown primary gases constituting the Martian atmosphere considers nitrogen and argon as most likely candidates. The gases should be either cosmologically abundant and chemically unreactive elements (such as argon or nitrogen) or photochemically abundant and chemically stable compounds (such as carbon dioxide, carbon monoxide, . . .) and heavy enough so as not to escape under the low gravity of Mars (certainly atomic hydrogen or helium have been lost long ago). Thus, the concept of a mixture of carbon dioxide, argon, and nitrogen has been advocated by many investigators in the last 2 or 3 years and was a precursor to the Mariner IV information. One of the new pictures of the Mars' atmospheric composition, as interpreted from the Mariner results, is a mixture of 80 percent carbon dioxide and 20 percent argon and nitrogen (ref. 134).

ARGON

The relative cosmological abundance of argon, combined with its chemically inert nature and its atomic weight of 40 (relative to nitrogen's molecular weight of 28), makes it a very real possibility that argon is one of the main constituents of the Martian atmosphere. On Earth, argon is the product of the radioactive decay of the potassium isotope K^{40}, with a half-life of a billion years. K^{40} is concentrated near the Earth's surface, presumably because of processes associated with the differentiation of the crust and mantle (ref. 135). Brown (ref. 136) and Suess (ref. 137) independently concluded that within the proposed lifetime of the universe, 10^9 years, argon could have so accumulated as to become the major atmospheric constituent of Mars. The Mariner IV results have shown that argon may be the second most important constituent after carbon dioxide.

MOLECULAR OXYGEN

Persistent efforts in this century (pioneered around 1900 by the

Lowell, Slipher, and Very team at the Lowell Observatory and followed in the 1925–1935 period by Adams and Dunham at Mount Wilson Observatory), leading to the present work by Dunham (ref. 138), Richardson (ref. 139), Kiess and Corliss (ref. 140), and finally Kaplan et al. (ref. 130), have failed to detect any Martian oxygen spectroscopically. The latter team place an upper limit of 70 cm-atm for the presumed oxygen content, while Dunham had given the often-quoted upper limit of 250 mm-atm from determination of the spectroscopically detectable threshold.

Theoretical calculations of the possible oxygen concentration profile in Mars' atmosphere, based on carbon dioxide photochemistry and carbon monoxide, atomic and molecular oxygen and ozone chemistry, were undertaken by Marmo and Warneck (ref. 141). They found that significant amounts of oxygen were formed down from carbon dioxide photodissociation ($CO_2+h\nu \rightarrow CO+O$) through $O+O+M$ and $O+O_3$ reassociation reactions. The total abundance of molecular oxygen was estimated at some 0.2 cm-atm, with a maximum concentration on the order of 10^{-3} occurring somewhere between 110 and 160 kilometers, at a level at which the total carbon dioxide below is $\sim 10^{20}$ molecules/cm^2. Below this level the oxygen concentration decreases very rapidly to a negligible value near the ground. For comparison, Prabhakara and Hogan's (ref. 142) photochemical calculations, neglecting the carbon dioxide photochemistry, place at about 80 kilometers the level of total carbon dioxide just mentioned. Their concentration profiles are given in terms of O_2+O_3 only, as they were mostly concerned with evaluating the solar heating because of ultraviolet absorption by these two molecules.

Chamberlain and McElroy (ref. 133) also found a theoretical oxygen peak or maximum in their model calculations illustrating the strong coupling of the equilibrium abundances of oxygen and carbon dioxide. (See fig. 12–1.)

OZONE

Ozone is formed by association of molecular and atomic oxygen through the three-body process: $O_2+O+M \rightarrow O_3+M$. In the Martian middle atmosphere, photodissociation of carbon dioxide should supply sufficient atomic oxygen to promote this reaction. Marmo and Warneck (ref. 141) calculated the abundance of ozone, based on dissociation of carbon dioxide only, to be less than 0.0001 cm-atm, a negligible value in comparison to their predicted 0.2 cm-atm for molecular oxygen. They also calculated that for any molecular oxygen amounts up to 250 cm-atm the concentration of

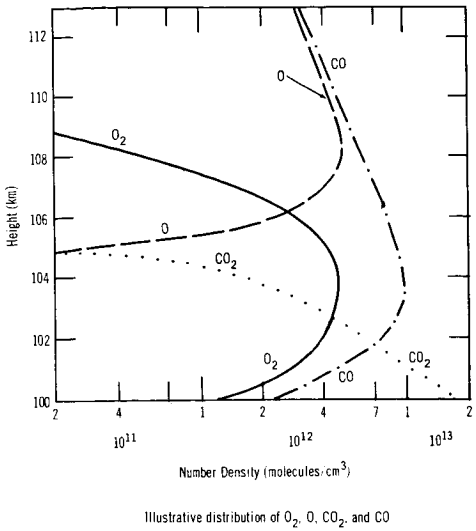

FIGURE 12–1.—Photodissociation of carbon dioxide. (After ref. 133.) Assumptions: 50 percent carbon dioxide (in lower atmosphere). Scale height: 7 kilometers. Same conditions as in structural model of figure 13–3.

ozone will not pass through a maximum as it does in Earth's atmosphere, but that it will increase gradually with decreasing altitude, even for surface pressures as low as 10 millibars (ref. 143). This agrees with the theory of Wildt (ref. 144) that the surface of Mars is highly oxidized. Of course, the total ozone was found to vary proportionately with the total oxygen present. If the concentration of molecular oxygen were actually slightly below the spectroscopically predicted threshold of 250 cm-atm, then there would be nearly the same amounts of ozone in the atmospheres of Mars and Earth (2 to 3 mm-atm), with a resulting similar opacity in the ultraviolet (Hartley bands) between 0.2 and 0.3 micron (ref. 135).

Recently, Prabhakara and Hogan (ref. 142) used fully the basic photochemical theory of ozone production to determine a vertical distribution of ozone consistent with a new radiative equilibrium temperature structure which takes into account absorption of solar energy by molecular oxygen and ozone in the ultraviolet and by carbon dioxide in the near ultraviolet. They assumed for their six models running from surface to 100-kilometer-altitude surface temperatures of 230° and 270° K, surface pressures ranging from 10 to 50 millibars, and carbon dioxide amounts of 35, 55 and 70 m-atm and oxygen amounts of 35 and 70 cm-atm. Their results clearly indicate that no temperature maximum is produced by the hypothesized absorptions. The total ozone amount found is ~0.3 cm-atm (or 1/10 Earth value). The ozone number density from

its maximum at the surface gradually decreases upward, in agreement with Marmo and Warneck. (Also, it was shown that below ~30 kilometers, the molecular oxygen and ozone absorption is comparable to carbon dioxide absorption, but above that it becomes considerably less.)

CARBON MONOXIDE AND ATOMIC OXYGEN

The products of the photodissociation of carbon dioxide are carbon monoxide and atomic oxygen. The reaction $CO_2+h\nu\rightarrow CO+O$ takes place under ultraviolet radiation of wavelengths $\lambda<1692$ Å (or $h\nu>7.33$ eV). An accumulation of carbon monoxide is prevented because of the reverse chemical reaction $CO+O+M\rightarrow CO_2+M$, using the momentum of any third molecule or atom (three-body recombination). Also, the photodissociation of carbon dioxide in a planetary atmosphere of the type of Mars may be considerably slowed down by the ultraviolet protecting effect of molecular oxygen formed at high altitudes by $O+O$ and $O+O_3$ recombinations. Consequently, the Martian abundances of carbon monoxide and atomic oxygen are likely to be much smaller than those of molecular oxygen and ozone.

Photochemical calculations by Marmo and Warneck (ref. 141) predicted total abundances of about 0.03 cm-atm for carbon monoxide and ozone, and an atomic oxygen maximum concentration occurring between 150 and 200 kilometers. This result is in agreement with the spectroscopic upper limit of 10 cm-atm obtained by Sinton (ref. 145) from negative results in infrared scans of Mars.

Chamberlain and McElroy (ref. 133), emphasizing the ultraviolet shielding effect of molecular oxygen on carbon dioxide dissociation, calculated illustrative concentration profiles for carbon dioxide, carbon monoxide, atomic and molecular oxygen under the new atmospheric-ionospheric conditions relayed by Mariner IV. Assuming a scale height of 7 km and 50 percent carbon dioxide, they obtain peaks of carbon monoxide and atomic oxygen at an altitude just above 100 kilometers, with a concentration of $\sim 10^{13}$ molecules/cm^3 for either gas. (See fig. 12–1.)

Of interest here is a possible process, serving as a carbon monoxide sink, suggested by Rosen (ref. 146). The fairly reactive carbon monoxide can combine with carbon dioxide to form the transitory carbon suboxide C_3O_2, which photolyzes and releases carbon. Thus, $2CO+CO_2+h\nu\rightarrow C_3O_2+2O$, and $C_3O_2+h\nu\rightarrow CO_2+C_2$ in the ultraviolet with $\lambda<3250$ Å (or $h\nu>3.81$ eV). The carbon would be released as an apparent smoke in the Martian atmosphere, under the right conditions. Both Rosen (ref. 146) and

Öpik (ref. 147) have based an explanation of the "blue haze" upon this mechanism (ch. 16).

WATER VAPOR

Water vapor has been suggested as a constituent of the Martian atmosphere for more than a century on the basis of observations of the polar caps, their variations with the seasons, and associated clouds. It is, however, a very minor constituent which, until the last few years, completely eluded all attempts at positive identification. Spectroscopists at the turn of the century mistakenly accepted as positive evidence the illusory effect of the very strong telluric lines on the very weak Martian lines of oxygen and water. This view was accepted fairly recently by workers such as Adams and St. John (ref. 148), Campbell (ref. 14[a]), and Slipher (ref. 150) until the powerful new spectrograph of the 100-inch Mount Wilson telescope became available. Using this new tool, Adams and Dunham (ref. 151), and Adams (ref. 152) obtained only negative results for water vapor, and concluded that it was unlikely that more than 0.01 millimeter of precipitable water existed over the Mars surface. Hess (ref. 153), however, took strong issue with such a low upper limit, criticizing both the spectrographic precision and the meteorological assumptions. His own calculations, based on aqueous clouds, gave an upper limit of 0.4 to 0.6 millimeter of precipitable water (ref. 154). This result approaches De Vaucouleurs' meteorological estimate of 0.7 millimeter (ref. 155). At the perihelic opposition of 1956, Kiess and Corliss (ref. 140) were still unable to detect any Martian water vapor. After immediate direct calibration they gave a spectrographic upper limit of 0.08 millimeter of water, a value considered more reliable than that of Adams and Dunham.

The repeated negative results with spectrography prompted a number of investigators to calculate theoretical estimates from various phenomena long observed on Mars, such as the following:

(1) Early morning haze (ref. 156).

(2) Rate of evaporation of polar caps, and the greenhouse effect (ref. 157).

(3) Condensation of polar mists into ice crystals (ref. 158).

(4) Dissociation pressure of the goethite in limonite (ref. 159).

The results of these efforts are listed in table 12–1 (refs. 130, 156–164), along with the recommended value of De Vaucouleurs (ref. 160) of 0.01 millimeter of precipitable water (1 mg/cm^2), based on broad general considerations.

TABLE 12-1.—*Abundance of Water in Mars' Atmosphere*

Method	Author	Water, mg/cm²
Calculation from morning haze.	Urey (ref. 156)	<5
Critical discussion.	De Vaucouleurs (ref. 160)	1
Calculation from greenhouse effect, and sublimation of polar cap edge.	Sagan (ref. 157)	2 to 20
Calculation from polar mists condensation, ice crystals precipitated.	Lebedinskii and Salova (ref. 158)	0.1
Calculation from goethite dissociation pressure.	Adamcik (ref. 159)	0.2 to 60
Polarizing spectrophotometry, 1.4-micron band.	Dollfus (ref. 161)	20
Infrared spectroscopy, 2.7-micron band.	Danielson et al. (ref. 162)	<4
Infrared spectroscopy, 0.82-micron band.	Spinrad et al. (ref. 163)	0.5 to 1.0
	Spinrad and Richardson (ref. 164)	≤3.5
	Kaplan et al. (ref. 130)	1.4 (±0.7)

Other experimenters have made high-altitude observations and detected water bands in the infrared. Dollfus (ref. 161) achieved this goal with broadband filter photometry near 1.4 microns, both from a balloon at 14-kilometer altitude and from a Swiss mountain peak at 3.5 kilometers. His estimate of water vapor is now considered unexpectedly high. Danielson and the Schwarzschild team (ref. 162) used the ground-controlled 36-inch telescope of Stratoscope II suspended at 24-kilometer altitude (80 000 ft) in March 1963 to obtain about 10 microns (0.01 mm) of precipitable water; however, they preferred to announce an upper limit of 40 microns because of uncertainties in their data reduction.

Finally, the Mount Wilson 100-inch reflector enabled Spinrad, Münch, and Kaplan (ref. 163) to obtain a good high-dispersion spectrogram of Mars, where, despite their faintness, 11 rotational lines of water were detected in the 8200-Å region, ascribable to the Martian atmosphere because the Doppler shifts from their telluric counterpart were of the expected amount (0.42 Å to the red). Measurements of the average equivalent width and intensity of three of these lines (unblended lines at λ 8176.97, 8189.27, and 8226.96 Å), coupled with the use of recent laboratory calibrations of line strengths by Rank, led the Mount Wilson team to a water abundance value of 14±7 microns of precipitable water. The estimated error is large because of uncertainties in measuring width and intensity of such faint lines. All of these results are entered in

table 12–1, summarizing recent determinations and estimates of water vapor in the Martian atmosphere.

These results tend to confirm De Vaucouleurs' estimate of 10 microns of water, and also agree with the maximum of 100 microns estimated by Hess (ref. 165). The uncertainty, therefore, is approximately 1 order of magnitude. Variations in water-vapor content on Mars could be expected if only from variability in atmospheric conditions with seasons, latitudes, and regions. It may be that ice-crystal clouds hold most of this maximum amount, while the residual actual water vapor may be as low as 10 microns. Martian air is indeed extremely dry—by comparison, even Arizona's desert air averages 1 millimeter of water in the winter. Neither rain nor snowfall should be expected on Mars.

SUMMARY

Table 12–2 gives a summary of the abundance of each of the probable major constituents of the Martian atmosphere as predicted a few years ago by De Vaucouleurs (ref. 160) and Hess (ref. 165). They assumed that nitrogen composed the bulk of the atmosphere, that the surface pressure was 85 millibars, and that argon was the second most important constituent.

Kuiper (ref. 166), renewing an earlier effort to determine trace constituents in Mars' atmosphere, has tested negatively for the presence of carbon monoxide, methane, ammonia, hydrogen sulfide, nitric oxide, nitrous oxide, carbonyl chloride, methylene oxide, and carbonyl sulfide (ref. 167). The upper limits are lower than before because of the lower threshold of spectrographic detectability. A sensitive test was also made for nitrogen dioxide by Marshall (ref. 168) in Kuiper's laboratories.

TABLE 12–2.—*Composition Model of Mars' Atmosphere*[a]

[Proposed by refs. 155, 160, and 165]

Major gases	De Vaucouleurs		Hess	
	Absolute, cm, STP	Relative volume percent	Absolute, cm, STP	Relative volume, percent
Nitrogen	165 000	93.8	163 600	93
Argon	7 000?	4.0	9 800	5.6
Carbon dioxide	4 000	2.2	2 400	1.3
Oxygen	<200	<.1	<260	.1
Water vapor			180	.04

[a] Assuming surface pressure 85 millibars.

Table 12–3 shows the preliminary model of atmospheric composition for Mars presented by Owen and Kuiper (ref. 169), including these trace constituents and assuming a surface pressure of 17 millibars. Here, carbon dioxide is the second most abundant constituent. An investigation of isotopic compositions was also attempted by Kuiper (ref. 166). The O^{18} isotopic band was definitely detected and indicates an O^{18}/O^{16} ratio in Mars' atmosphere that is greater than in Earth's atmosphere. A precise determination of this ratio should provide clues as to the photochemical history and rate of escape of the oxygen of Mars' atmosphere.

Table 12–4 shows partial surface pressures of the major atmospheric constituents carbon dioxide, argon, nitrogen, as deduced by Kaplan, Münch, and Spinrad (ref. 130) for three different surface pressures: 10, 25, and 40 millibars. It is interesting to note that in their 10-millibar model, carbon dioxide becomes a major constituent.

New models of Martian atmospheric composition incorporating the physicochemical restrictions inferred from the Mariner IV

TABLE 12–3.—*Preliminary Composition Model of Mars' Atmosphere*[a]

[Proposed by ref. 169]

Gas	Absolute cm, STP	Relative volume, (percent)	Gas	Absolute cm, STP
Nitrogen	30 000	85	Carbonyl sulfide	<0.2
Carbon dioxide	5 000	14	Methylene oxide	<.3
Argon	400	1.0	Nitrous oxide	<.08
Water	1		Nitric oxide	<20
Ozone	<0.05		Nitrogen dioxide	<.0008
Oxygen	<7.		Hydrogen sulfide	<7.5
Sulfur dioxide	<0.003		Methane	<.4
Carbon monoxide	<1		Ammonia	<.1

[a] Assuming surface pressure 17 millibars.

TABLE 12–4.—*Surface Pressures for Possible Major Constituents of Mars' Atmosphere*

[Ref. 130]

Constituents	Pressure, mb		
	Low	Mean	High
Total	10	25	40
Carbon dioxide	6	4	3
Argon 40	2	2	2
Nitrogen	2	19	35

mission have not yet appeared in published form. At present, the reader can be referred only to the speculations of the JPL team (ref. 134). These investigators considered as possible rough representations of the Martian atmospheric composition models such as: 100 percent carbon dioxide; 50 percent carbon dioxide and 50 percent argon; 80 percent carbon dioxide and 20 percent argon or nitrogen, or their mixture.

13

Atmospheric Structure

NUMEROUS MODELS OF THE MARTIAN ATMOSPHERE have been formulated in the past, before the Mariner IV encounter, but they were all highly speculative. They were based on the assumptions of a very high surface pressure (~85 mb), an almost pure nitrogen atmosphere (~95 percent), and very high exospheric temperatures (~1000° K). Also, generally implied was a structural subdivision in layers resembling that of Earth. It is interesting to give here such a tentative table of physically significant levels comparing Earth and Mars (table 13–1).

The successful occultation experiment of Mariner IV has altered our ideas on the physical structure of the Martian atmosphere and ionosphere. This atmosphere was found to be much thinner and colder than expected, and the ionosphere quite undeveloped. Carbon dioxide is now thought to be the dominant molecule.

After the release of such information by the JPL team, new models were constructed to account for the data. These will be reviewed here as fully as possible, but it should be noted that the great differences found in these early interpretations of the new data reflect many uncertainties.

For the sake of comparison and background, some important pre-Mariner models of the lower and upper atmospheres of Mars are also given.

THE MARINER IV OCCULTATION EXPERIMENT AND RESULTS

The Mars' atmosphere was probed by analyzing the radio signal as the spacecraft disappeared and reappeared (54 min later) from behind the planet. Phase, frequency, and amplitude changes of the S-band radio signal after refraction and diffraction by the Martian atmospheric (neutral and ionized) layers provided the possibility of estimating the refractivity profile and scale height and, finally, the surface density and pressure of the atmosphere, and similarly the electron scale-height and electron density profile

TABLE 13–1.—*Atmospheric Levels, Earth and Mars*

Region	Dominant heat-transfer process	Vertical temperature variation		Characteristics
		Earth	Mars	
Troposphere	Convection	Decreasing	Decreasing	Region immediately above the surface, with weather and cloud phenomena.
	Infrared radiation by CO_2 and H_2O.	A minor minimum	A minor inversion	Transition level between troposphere and stratosphere.
Stratosphere	Conduction and radiation	Increasing	Decreasing	Region above tropopause; temperature stabilization.
	Near UV absorption by ozone.	Major maximum	Not evident	Transition level between stratosphere and mesosphere.
Mesosphere	Convection and radiation	Decreasing	Decreasing	Region of increasing photolysis with altitude and breakdown of Kirchhoff's law for radiative transfer at the vibrational relaxation level just below the mesopause.
	Infrared radiation by CO_2	Major minimum	Major minimum	Transition level between mesosphere and thermosphere.
Thermosphere	Photolysis by X-ray and euv insolation; conduction.	Increasing	Increasing	Region showing rapid rise in temperature and the transition level (turbopause) just above mesopause, between mixed lower atmosphere (turbosphere) and diffusive upper atmosphere (diffusosphere).
	Photoionization	Constant	Constant	Transition level between thermosphere and exosphere.
Exosphere	Photoionization	Constant	Constant	Region of gravitational escape of atoms.

of the ionosphere. The method used by Fjeldbo and Eshleman (ref. 170) was to establish the refractivity mode, then the density for a postulated composition can be inferred. From the scale height determination and the temperature the surface pressure is derived. It appeared from the Fresnel diffraction pattern of the amplitude data that the rays had grazed a surface feature of some elevation—such as a mountain—which acted as a diffracting edge. These results of the occultation experiment, analyzed rapidly by the JPL investigators Kliore et al. (ref. 134), are presented in table 13–2, where three typical compositions each with a predominance of carbon dioxide were chosen. (More sophisticated analyses by the same team are to be released in the future.) The Martian atmospheric and ionospheric mass densities, temperatures, and scale heights are surprisingly lower than previously thought. Thus, for a composition model, with 50 percent carbon dioxide and 50 percent argon, the mass density found was 1.75×10^{-5} g/cm^3, the surface pressure 5 to 7 millibars, and the temperature 170° K.

EARLY MODELS OF MARS' ATMOSPHERE

LOWER ATMOSPHERE (Up to ~50 km).—A succession of radiative models of the troposphere were constructed by Goody (ref. 171), Ohring (ref. 172), and Arking (ref. 173), which bear a strong resemblance to the terrestrial troposphere in winter polar regions. They differ in the choice of surface temperature of the atmosphere. Goody took 270° K, Ohring chose the more realistic 230° K, and Arking 235° K. The tropopause is at 8- to 9-kilometer altitude, where the temperature is much lower than the surface temperature due to an adiabatic negative gradient.

The compositions were of 98 percent nitrogen and 2 percent carbon dioxide, and surface pressure was 85 millibars in Goody's and Ohring's models, which are represented in figure 13–1.

Other workers, including Schilling (ref. 174), and Evans and Wasko (ref. 175), considering the uncertainties in the assumed physical parameters, produced for more practical purposes, extreme limits (and means) of the temperature, pressure, and density profiles.

UPPER ATMOSPHERE (Above ~50 km).—The most consistent series of models, elaborated from classical radiative transfer theory (used for stellar atmospheres) and the use in the heat budget equation of conductive heat flux of solar heat, were presented by Chamberlain (ref. 176), and later refined by McElroy, L'Ecuyer, and Chamberlain (ref. 177). They emphasized for the first time the radiative cooling of carbon monoxide formed from

TABLE 13-2.—*Radio Occultation Experiment Results*

[Ref. 134]

Mars' atmosphere:

Surface refractivity: 3.6 ± 0.2 N units.
Scale height: 8–10 kilometers.

	Model 1	Model 2	Model 3
Postulated composition	100% CO_2.	80% CO_2; 20% A or N_2.	50% CO_2; 50% A
Surface number density, 10^{17} mol/cm^3	1.9 ± 0.1	2.1 ± 0.2	2.5 ± 0.15
Surface mass density, 10^{-5} g/cm^3	1.43 ± 0.1	1.5 ± 0.15	1.75 ± 0.10
Temperature, °K	180 ± 20	175 ± 25	170 ± 20
Surface pressure, mb	4.1–5.7	4.1–6.2	5.0–7.0

Mars' ionosphere:

Maximum electron density: $9 \pm 1.0 \times 10^4$ electrons/cm^3.
Altitude of maximum (peak): 120 to 125 kilometers.
Electron scale height (above maximum): 20 to 25 kilometers.
Temperature: <200° K at 120 to 200 kilometers.

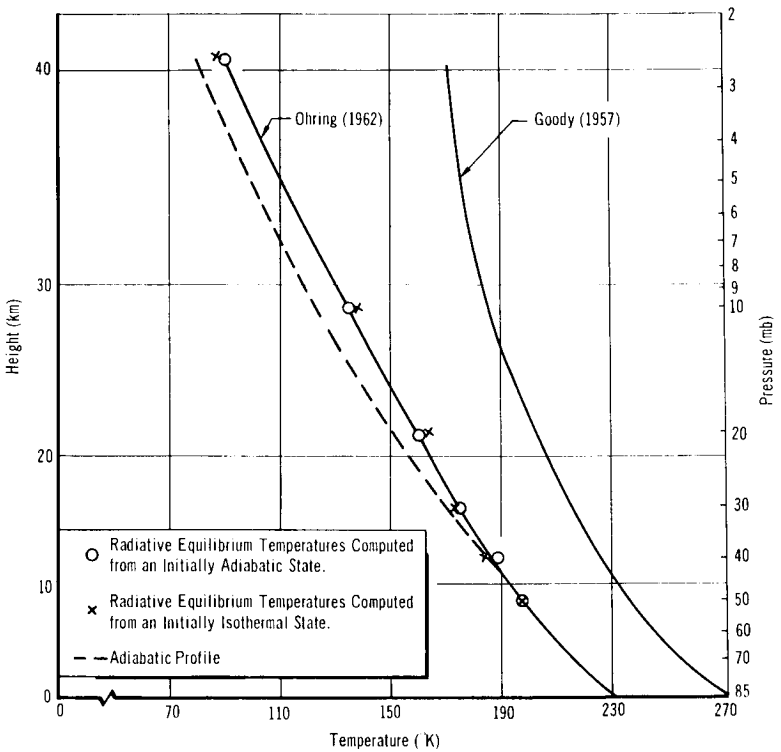

FIGURE 13-1.—Temperature profile in Mars' lower atmosphere. (After ref. 172.)

carbon dioxide photodissociation in the thermosphere. They are characterized by a strong mesopause minimum temperature, at above 120 kilometers, where vibrational relaxation of carbon dioxide molecules, and therefore cooling, is important. This thermostatic effect was found in the latter paper to be not as important as the radiative loss by carbon monoxide and atomic oxygen. Thermosphere temperature approaches some 1100° K at the thermopause (~1500 kilometers). Ionospheres were also sketched by Chamberlain with an F_2 and an F_1 region, resembling Earth regions. Figure 13–2 gives Chamberlain's original model of Mars' upper atmosphere.

POST-MARINER MODELS OF THE MARS ATMOSPHERE AND IONOSPHERE

Chamberlain (ref. 133) proposed a model upper atmosphere with an E-region (ionization from solar X-rays) and characterized by only weak dissociation of carbon dioxide, contrary to his previous models. The lower and middle atmospheres adopted were essentially the radiative-equilibrium model I of Prabhakara and Hogan (ref. 142), starting with 10-millibar pressure at surface, and containing 44 percent carbon dioxide gas with nitrogen as the remainder. The gases are assumed thoroughly mixed in the computation of the radiative losses by carbon dioxide emission. Chamberlain uses his previously developed methods based on inclusion of conduction, radiation, and diffusion in the heat-budget equation.

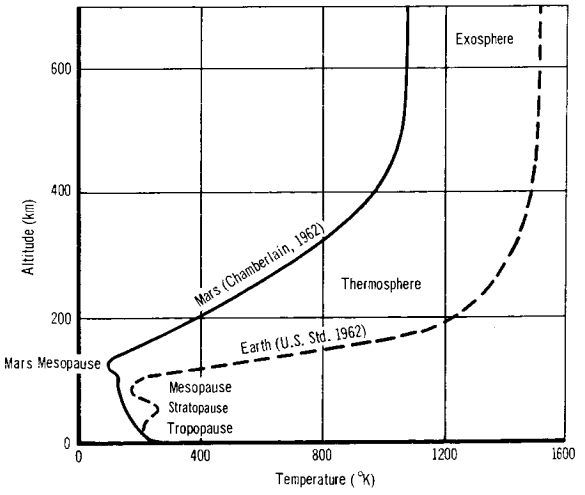

FIGURE 13–2.—Mars model atmosphere. (After ref. 176.)

He finds that a true thermosphere (where temperature increases with altitude) develops as a result of the radiative losses by carbon dioxide and molecular oxygen. Indeed molecular oxygen, formed readily with oxygen atoms resulting from ultraviolet (1750 Å) photodissociation of carbon dioxide, in turn shields carbon dioxide from extensive photodissociation; and appreciable amounts of carbon dioxide (and molecular oxygen) can thus extend to great heights. Chamberlain's new calculations show that although carbon dioxide still serves as an effective thermostat (keeping the overall temperature low), there is a buildup of temperature (forming the thermosphere) from solar ionizing and dissociating radiation and downward conductive heating. The top of the thermosphere, or base of the exosphere, is about 400° K or higher, while the base is about 160° K. Figure 13–3 gives a picture of Chamberlain's thermal profile for Mars' atmosphere. His ionosphere, which is in the thermospheric layer, has no F_1 or F_2 regions, only an E-region as was suggested by the preliminary analysis by Kliore et al. (ref. 134), of Mariner occultation results (electron scale height of 20 to 25 kilometers, and a maximum electron density, in late afternoon, of 9×10^4 electrons cm^{-3} at 125 kilometers). A complete analysis is underway by Chamberlain, of the various processes competing to form the structure of the Mars' atmosphere (radiative exchange, conductive heating, turbulent mixing, diffusive separation, photodissociation, and ionization).

Johnson (ref. 178) proposed a semiempirical atmospheric model based on the postulate that the main ionospheric peak was of the F_2 type (as on Earth), and that the predominant ions at and above this peak are atomic oxygen O^+. The main constituent is carbon dioxide, with possible additions of argon and nitrogen. Surface

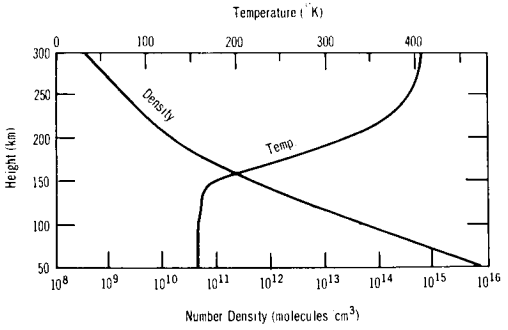

FIGURE 13–3.—Upper atmosphere model (suggested by Mariner IV results). (After ref. 133.) Assumptions: Negligible carbon dioxide dissociation and strong mixing. The exospheric temperature, T_e, is 410° K.

temperature at 210° K (compatible with Mariner observation conditions; late afternoon, late winter at 55° S latitude), and surface pressure of 8 millibars were taken as boundary conditions. Johnson's model has a very cold temperature profile, in order to fit the 25-kilometer scale height determined by Mariner IV. Figure 13–4 gives the obtained temperature and pressure curves. The model consists of three layers: a 14-kilometer troposphere, or lower convective layer with an adiabatic temperature gradient of ~5° C/kilometer, and a tropopause at 140° K; then a stratosphere, or middle atmosphere of constantly decreasing temperature at the rate of 0.64° C/kilometer, following the carbon dioxide-ice vapor-pressure curve up to the stratopause at 100 kilometers and 85° K; finally, an isothermal thermosphere (and ionosphere) at 85° K. This structure implies exact heat balance between absorption of solar ultraviolet radiation and emission by carbon dioxide and its dissociation product carbon monoxide at great heights. Objections to this model were presented by Chamberlain (ref. 133): that the F_2 postulate and abundance of O^+ ions, as well as the cold isothermal thermosphere, are unrealistic in fitting the Mariner data.

Gross, McGovern, and Rasool (ref. 179) calculated an upper atmosphere based on predominant carbon dioxide completely dissociated in the thermosphere. Starting with a surface temperature of 200° K and pressure of 8 millibars, and assuming radiative equilibrium conditions in the lower atmosphere up to 80 kilometers, where the carbon dioxide dissociation is effective, they computed a temperature profile for the lower atmosphere by applying the method of Prabhakara and Hogan (ref. 142). Above 80 kilometers, the thermal structure, based on the diffusive equilibrium of carbon dioxide, carbon monoxide, and atomic oxygen, is treated according to the methods of Chamberlain (ref. 176) developed by his students (ref. 177). Here the heating by the Sun is through

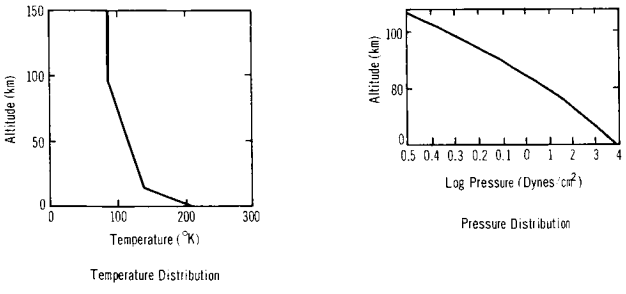

FIGURE 13–4.—Lower atmosphere model (suggested by Mariner IV results) (late afternoon, late winter, 55° S latitude). (After ref. 178.)

the extreme ultraviolet ionization of oxygen atoms, while the cooling is by radiation of carbon dioxide and especially carbon monoxide. The exospheric temperature turns out to be as low as 550° K, with a large uncertainty of 150° K, and this prevents the escape of oxygen atoms. The temperature structure obtained is given in figure 13–5. It is quite different from Johnson's profile in the thermosphere. Note the mesopause at 80 kilometers, which is a minimum. The temperatures are lower than in the models of McElroy et al. Chamberlain finds objections to the implied F_2 ionization and O^+ ions diffusion theory adopted in this model, on the ground that an F_2 peak would be well formed above 125 kilometers, which is not consistent with the Mariner findings.

SURFACE PRESSURE

The atmospheric surface pressure, p_0, of a planet is directly proportional to the columnar air mass, m, and gravitational acceleration, g; that is, $p_0 = m \times g$. A reasonable estimate of Martian gravity has been available for some time (see ch. 6), but "m" remained a controversial factor until the Mariner IV occultation experiment. The value of the columnar air mass was based upon the observed optical thickness of the atmosphere. Various methods, using photometry, polarimetry, spectroscopy, occultation, twilight arc, and meteorology, have been devised to determine the Martian surface pressure. (See table 13–3 (refs. 181–184).) These are briefly reviewed below. See also Chamberlain and Hunten (ref. 180). The pre-Mariner results are presented in table 13–4.

(1) Photometry is a potentially sound method but not yet perfected. The primary difficulty is that the optical properties

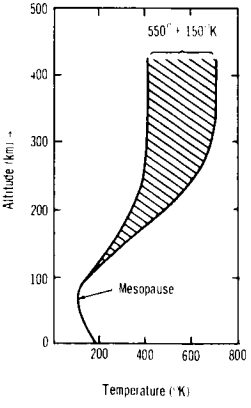

FIGURE 13–5.—Upper atmosphere model (suggested by Mariner IV results). (After ref. 179.) Assumptions: 100 percent carbon dioxide, $p_0 = 8$ millibars.

TABLE 13–3.—*Methods for Determining Surface Pressure for Mars*

Method	Remarks
Photometry (visual or photographic).	Measurement of mean albedos at different wavelengths; assumptions on absorption and scattering (ref. 184) or: Brightness distributed across disk; assumptions on absorption and scattering (ref. 181).
Polarimetry (visual or photographic).	Brightness and polarization across disk; assumptions on absorption and scattering (refs. 182 and 183).
Spectroscopy	Infrared absorption of pressure-dependent bands of a gas like carbon dioxide, whose abundance is known or determinable from pressure-independent bands. Calibration of spectrometer in the laboratory (refs. 130 and 166).
Occultation	Signal strength and frequency versus time curves from Doppler-shift, atmospheric refraction and diffraction of light or radio signal from a star or spacecraft. Star not yet used for Mars, but Mariner IV acted as radio signal source in passing behind Mars.
Twilight Arc	Residuals in measurements of planet's diameters. Never applied (ref. 184).
Meteorology	Temperature and heights of the tops of convective clouds (cumuli, assumed aqueous). Application of formulas of theoretical meteorology. Proposed and applied (ref. 153).

of the Martian atmosphere and surface have not been accurately differentiated. Photographic photometry, as first applied by Barabashov and Timoshenko (ref. 43), Sharonov (ref. 44), Sytinskaya (ref. 185), and Fessenkov (ref. 186), gave values appreciably higher than those obtained from visual photometry by De Vaucouleurs (ref. 181) and Dollfus (ref. 187).

(2) Polarimetry had, for sometime, provided a generally accepted and apparently reliable method. Dollfus obtained, by this means, a value of surface pressure, p_0, between 80 and 90 millibars (refs. 182 and 183). De Vaucouleurs' (refs. 160 and 188) often-quoted value of 85 ± 4 millibars was the weighted mean of primarily polarimetric results. However, serious doubts concerning the application of the polarimetric method have arisen in recent years, because it has become apparent that some of the simplifying assumptions are unwarranted. The various empirical corrections attempted by Öpik (ref. 147) and Deirmendjian (ref. 189) only emphasize the uncertainty of polarimetric results. Dollfus (ref. 190) then stated that his 85-millibar value should be regarded as an upper-limit. Sekera (ref. 191) stated on theoretical grounds

TABLE 13–4.—*Pre-Mariner Surface Pressure Determinations*
[*Based on Nitrogen Atmosphere*]

Method	Author	Surface pressure, mb
Photometry—mean albedos	Menzel (ref. 195)	67
Photographic photometry	Barabashov and Timoshenko (ref. 43)	116
	Sharonov (ref. 44)	120
	Sytinskaya (ref. 185)	112
	Fessenkov (ref. 186)	125
Visual photometry	De Vaucouleurs (ref. 181)	80
Theoretical meteorology	Hess (ref. 153)	80
Visual polarimetry	Dollfus (ref. 182)	80
Visual polarimetry	Dollfus (ref. 187)	95
Visual polarimetry	Dollfus (ref. 187)	83
Visual polarimetry	Dollfus (ref. 183)	90
Theoretical meteorology	Shapiro (ref. 194)	75
Weighted mean	De Vaucouleurs (ref. 160)	85±4
Absorption correction	Öpik (ref. 147)	116
Scattering and polarization correction	Deirmendjian (ref. 189)	95±40
Spectrographic-infrared (CO_2 bands at 0.87 and 2.06 microns)	Kaplan et al. (ref. 130)	25±15
Spectrographic-infrared ($2CO_2$ bands near 1.6 microns)	Owen and Kuiper (ref. 169)	17±3
Proposed correction to Kaplan's value (recalibration of 0.87-micron CO_2 band)	Hanst (ref. 192)	50±30
Proposed correction to Kaplan's value (effective path length for 0.87-micron band on Mars)	Swan (ref. 193)	65±35

three major objections to the method: (*a*) multiple scattering was neglected; (*b*) solid surface reflection was assumed to be independent of atmospheric scattering; and (*c*) pure molecular scattering (Rayleigh scattering) was assumed.

The critical evaluation by Chamberlain and Hunten (ref. 180) corroborating these objections placed the position of the polarimetric method in the range of 30 to 200 millibars.

(3) Spectrometry is accurate and reliable under the proper observational conditions. There is some doubt of its reliability in the observation of the planets through the Earth's atmosphere. Kaplan et al. (ref. 130) and Kuiper (ref. 166) made spectrographic observations of Mars in the carbon dioxide rotational bands and determined surface-pressure values for Mars appreciably lower (by about 60 to 70 mb) than the average value deduced from previous measurements. Additional measurements based on refined

calibration techniques are desirable to substantiate the spectrographic observation for the following reasons:

(a) The Earth's atmospheric turbulence causes varying degrees of scintillation which blurs the line contours.

(b) The rotational line widths of carbon dioxide are difficult to measure accurately because of the low intensity of the lines.

(c) The trajectory of light traversing the Martian atmosphere may not actually lie in the Martian equatorial plane, as assumed, for determining the path length in the spectrographic calculations. Aerosols may also affect the effective path length. Hanst (ref. 192), Swan (ref. 193), and Sekera (ref. 191) are among those who have noted the uncertainty of the exact effective path length.

(4) Occultation can be very valuable, as provided by Mariner IV (table 13–3). By this method, information concerning the refractive index and scale height of the atmosphere may be obtained.

(5) The twilight arc method is mentioned only for its historical interest; it has not yet been applied to Mars.

(6) Meteorology as a method would be helpful if more observations of the Martian clouds were available. The results obtained by Hess (ref. 153) and Shapiro (ref. 194) appear to agree with polarimetric results, but this may be coincidental.

SURFACE PRESSURE VALUES

The exact value of surface pressure for Mars over many years had been subject to much debate, as shown by the diverse findings in table 13–4. Recent spectrographic results indicate the lowest values (17 and 25 mb). Before these results, 85 millibars was provisionally accepted as the most likely surface pressure. The additional observations made in 1965 from the radio-occultation experiment of Mariner IV's flyby of Mars have now settled this long controversy, by giving the unexpected result of a surface pressure value of 4 to 7 millibars (ref. 134). Kliore (ref. 195) later stated the possibility that due to mountainous terrain the pressure value may be 7 to 10 millibars.

14

Atmospheric Circulation

THE ATMOSPHERIC CIRCULATION on Mars has been estimated both theoretically and through observations of cloud movements. Early work by Hess (ref. 105) on Martian surface temperatures led to his formulation of a consistent isotherm map of the surface. He combined this with cloud motion data to form a crude circulation map. The result is very similar to an Earth weather map (fig. 14–1).

More recently, Miyamoto and Matsui (ref. 196), drawing upon theory and observation, have suggested that Martian circulation is earthlike in spring and autumn, and uniquely Martian in summer and winter. The terrestrial circulation consists of heat transfer from the equator to both poles via circulating airmasses. During the Martian summer or winter, however, heat is transported directly from the warm to the cool pole. This hypothesis is supported by the alternate appearance of the polar caps, as if moisture had migrated from pole to pole.

Mintz (ref. 111) has carried out a theoretical analysis of the flow regimes resulting from the expected poleward temperature

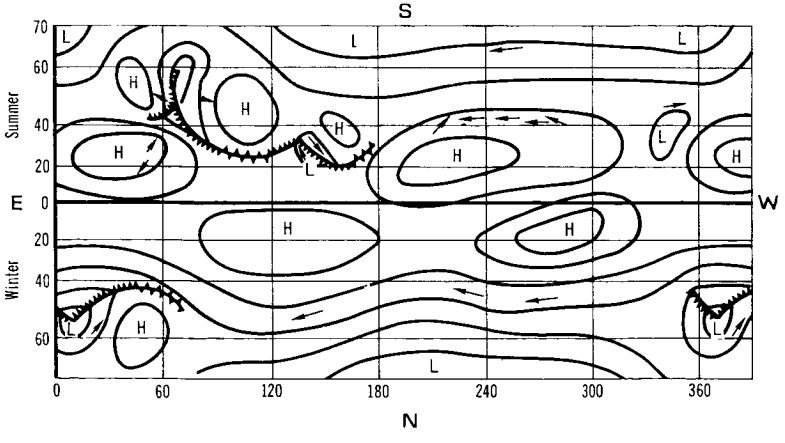

FIGURE 14–1.—Schematic streamline map of Mars (northern winter). (Based on 18 cloud drift observations.) (After ref. 105.)

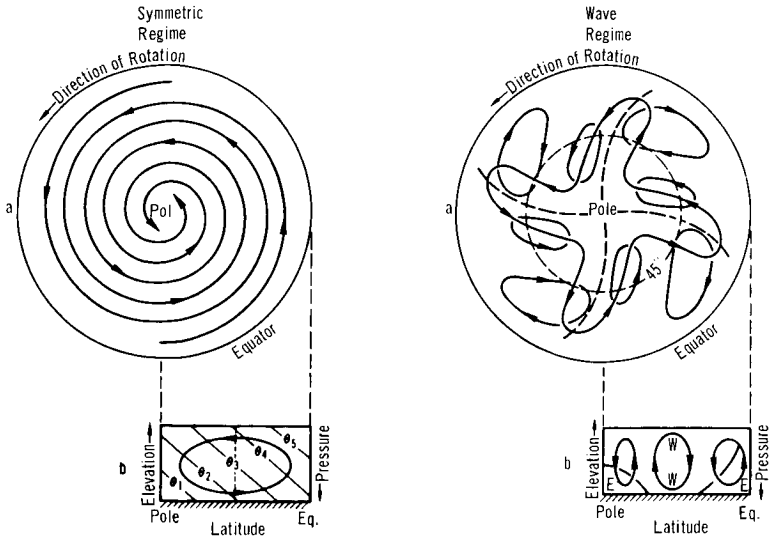

FIGURE 14–2.—General circulation model for Mars. Symmetric regime: (*a*) Streamlines of flow at upper levels; (*b*) Mean meridional circulation and isotherms of potential temperature θ. Wave regime: (*a*) Streamlines of flow in middle and upper levels; (*b*) Mean meridional circulation and mean zonal wind. (After ref. 111.)

gradient on Mars as a function of season. He postulated a generally stable symmetric regime in early fall and late spring with a change to a wave regime in winter. In summer, a reversal in the temperature gradient is postulated, which sets up a reversed symmetric circulation. The symmetric and wave regimes are represented in figure 14–2. In the former, the atmosphere is heated near the equator and ascends, moves toward the poles, descends and returns to the equator. Since the globe is rotating, there is an atmospheric velocity component in the direction of rotation which increases with altitude within the troposphere.

In the wave regime, large-amplitude horizontal waves exist in the upper troposphere accompanied by large horizontal eddies near the surface. The tongues of warm fluid moving poleward in some latitudes are balanced by cold tongues flowing toward the equator at other latitudes to produce a net poleward transport of heat. These large-scale disturbances are analogous to the familiar migrating highs and lows of the daily weather map.

Tang (refs. 197 and 198), firstly from analysis of yellow cloud observations, and secondly from model computations using recent input parameters based on the Mariner IV radio-occultation experiment, has found that a wave-type circulation regime must prevail over the Martian year.

15
Clouds

THREE MAIN CLOUD TYPES have been distinguished in the thin, dry, cold Martian atmosphere: white, blue, and yellow clouds, so named for the colors which they predominantly reflect.

WHITE CLOUDS

White clouds vary considerably in thickness, brilliance, extent, and location. They can be subdivided into three categories:

(1) Dense, brilliant, white clouds frequently observed as large systems in motion in the equatorial and temperate zones, or as thick, white shrouds over the winter pole lasting several months. In the midlatitudes they last for days or weeks, change shape irregularly, and, at times, extend conspicuously over the terminator.

(2) Thin, white mists detected polarimetrically as extensions of the thick, white clouds, or as mists of brief duration occurring with sudden temperature drops. Thus, mists formed during the night appear on the sunrise limb, but are quickly dissipated. Thin mists of this kind have also been detected migrating in spring from pole to pole.

(3) Orographic clouds appearing repeatedly over what are presumed to be high-altitude surface areas such as the Nix Olympica and Candor ranges.

Dollfus has demonstrated that the polarization of all Martian white clouds closely resembles those of the terrestrial ice-crystal clouds or fogs. He has concluded that the white clouds on Mars are analogous to the terrestrial cirrus clouds (refs. 199, 200, and 201).

BLUE CLOUDS

The distinction between blue and white clouds is not always clear. The blue clouds frequently appear along with white clouds

and mists, but are probably at higher altitudes. Strictly speaking, blue clouds are those which reflect blue and ultraviolet light only. Generally, however, classification is a question of degree.

Blue clouds appear at the winter pole and are reduced to mists in summer. Blue mists also appear commonly over the terminator at sunrise, and sunset in the equatorial belt. Finally, orographic blue clouds are evident periodically over certain preferred areas. For example, a large W-shaped cloud formed repeatedly over the Tharsis region in 1926, 1954, and 1958. Blue clouds frequently appear as bumps or distortions of the blue disk of Mars. When associated with white cloud systems, the blue seems to dominate. These facts have led to the conclusion that blue clouds are relatively high in the Martian atmosphere. Wilson (refs. 202 and 203) estimates their elevations as 15 and 25 kilometers, with a possible maximum of 100 kilometers. By comparison with terrestrial noctilucent clouds, he maintained that blue clouds are simply condensed blue haze. Estimates of cloud-particle size range from 0.1 micron by Goody (ref. 171) for ice crystals, to 2 to 2.5 microns by Dollfus for fine water droplets.

YELLOW CLOUDS

Yellow clouds, generally explained as Martian duststorms, are relatively infrequent but have shown a great deal of variability. Subdivision by size (or extent) results in three broad categories.

(1) Major formations are generally opaque, mobile, and enduring. They were observed on a planetary scale in 1924 and 1956.

(2) Smaller formations in the form of localized yellow clouds are more frequent. Their properties are similar to those of major formations, but they are less intense (table 15–1 (ref. 204)).

(3) Faint yellow veils which are detected photometrically or polarimetrically are believed to be the "tail end" of duststorms.

A dusty nature for the yellow clouds is generally accepted for the following reasons:

(1) Polarimetry indicates that the bright areas of Mars' surface are composed of a powdery material.

(2) The cloud motions suggest the likelihood of strong local winds capable of lifting and carrying dust to great heights.

(3) The low gravity on Mars allows a long settling time.

(4) The rapid increase of polarization in the yellow veils going toward the limbs can be explained only by particles greater than molecules.

Yellow clouds, and particularly major formations, have been

observed most frequently during perihelic or near perihelic oppositions (ref. 205).

The polarization curve of an opaque yellow cloud most closely resembles that of tobacco smoke and not that of ordinary Earth dust. The negative polarization led Dollfus (ref. 200) to believe that they are composed of minute highly absorbent particles. Earth dust is primarily transparent quartz sand and polarizes in the positive sense. By applying Stokes' law for the rate of falling particles, Dollfus has obtained from 2 to 5 microns as an estimate of the yellow-cloud-particle diameters. However, this size is largely underestimated, according to Ryan (ref. 206).

DUSTSTORMS

In view of the importance of duststorms to future landing missions, it is perhaps appropriate to give here quantitative details arising from two recent studies. A comprehensive search and study of available reliable records of observations of yellow clouds which displayed motion was undertaken by Gifford (refs. 204 and 207) in an attempt to analyze their probable nature and properties and, hopefully, to gain a factual insight into Martian circulation patterns. The data were separated into two groups of large moving yellow clouds, observationally distinct and also, as the study proved, physically distinct: (1) yellow clouds observed against the disk as obscuring some surface features, and (2) yellow clouds observed as limb or terminator projections. Table 15–1 lists for each group the results of Gifford's search and analysis of the locations, dates, and average direction and speed of the clouds.

The tabulations indicate clearly that the yellow clouds on the disk are primarily found in lower latitudes, near the thermal equator of the planet (see ch. 10), whereas the projection yellow clouds are primarily found in the middle latitudes. The latter group exhibit no special latitudinal drift, but the former, originating in Martian desert locations (bright areas), drift toward the equator. In view of the great dryness of Mars, their short duration (1 to 3 days usually), and their origin in regions of maximum temperature (isotherms at 280° K or greater), the yellow clouds on the disk can be called the Martian "duststorms." They are probably initiated by gusty winds caused by thermal convection over the powdery deserts (the limonite or goethite-coated "sands" of Mars). Their general equatorward drift seems to imply a low-altitude phenomenon (altitudes below 5 to 10 km), and possibly also, in view of their localized character or small extent (several hundred to one thousand km), that they are steered by the tropical

TABLE 15-1.—*Observations of Martian Yellow Cloud Motions*

[After ref. 204[a]]

Year	Earth date	Mars date, Southern Hemisphere	Latitudes[b]		Longitude		Drift		
			from	to	from	to	Mars region	Direction[c]	Average speed, mph
Yellow clouds on disk									
1873	May 24 to 25	Feb. 11 to 12	15	15	315	305	Aeria	W	16
1905	July 27 to 29	Mar. 11 to 16	11	20	210	215	Cerberus-I to Elysium	SSE	4
1907	July 29 to 30	Apr. 20 to 21	0	—20	270	220	Libya to M. Cimmerium	WNW	12
1911	Oct. 11 to 18	Aug. 2 to 7	0	—40	270	210	Libya to Eridania	NW	13
1911	Nov. 13 to 14	Aug. 21 to 22	—70	—70	335	315	Hellas	W	20
1922	July 9 to 12	Mar. 29 to 31	0	30	30	40	Margaritifer S. to Chryse	SE	9
1924	Aug. 9 to 10	May 14 to 15	15	0	280	290	Isidis R. to Libya	NNE	22
1926	Oct. 25 to 26	July 31 to Aug. 1	10	—30	270	255	Libya-Isidis to Ausonia	NNW	55
1937	May 25 to 29	Feb. 22 to 24	10	25	80	60	Candor to Niliacus L.	SW	8
1941	Nov. 12 to 28	July 31 to Aug. 10	30	—40	270	140	Libya to Phaethontis	NW	10
1943	Oct. 3 to 5	Aug. 3 to 4	0	—20	270	240	Libya to Hesperia	NW	25
1954	June 2	Mar. 13	—5	—10	115	108	Ulysses to Phoenicia L.	NNW	.....
1956	Aug. 22 to 25	May 29 to 31	—42	—38	20	350	Argyre to Noachis	WSW	15
1956	Aug. 28 to Sept. 4	June 2 to 6	—38	10	350	290	Noachis to Syrtis Major	SW	18
1958	Oct. 12 to 15	July 29 to 31	20	—25	265	230	Isidis R. to Hesperia	NW	24
1961	Jan. 19 to 21	Oct. 13 to 14	40	40	260	230	Casius to Elysium	W	20

Yellow projection clouds

1890	July 5 to 6	Mar. 21 to 22	40	40	52	41	Tempe	W	13
1892	July 2 to 3	Apr. 12 to 13	—50	—50	335	326	Hellespontus	W	18
1892	July 11 to 13	Apr. 19 to 20	—47	—46	344	357	Noachis	E	7
1894	Nov. 25 to 26	Aug. 10	—32	—23	44	49	Protei	SE	13
1900	Dec. 7 to 8	Oct. 24 to 25	—4	—1	336	322	Sabaeus S. to Icarium	WSW	27
1903	May 26 to 27	Jan. 23 to 24	18	26	40	32	Chryse	SW	15
1911	Oct. 6 to 7	Aug. 18 to 19	—45	—40	295	255	Hellas to Ausonia	W	77
1912	Jan. 15 to 16	Sept. 23 to 24	—40	—45	340	300	Noachis to Hellas	W	48
1913	Dec. 31 to Jan. 1	Oct. 7 to 8	—45	—45	65	50	Argyre	W	16
1914	Jan. 25 to 26	Oct. 20 to 21	—45	—45	10	25	Argyre	E	14
1914	Jan. 28 to 29	Oct. 21 to 22	—45	—45	347	356	Argyre	E	10
1914	Feb. 2 to 3	Oct. 23	—15	—15	333	318	Deucalionis R	W	38
1914	Feb. 6 to 7	Oct. 25	—10	—40	345	10	Sabaeus S. to Argyre	NE	55
1914	Feb. 10 to 11	Oct. 27	—45	—45	260	193	Hellas to Eridania	W	85
1914	Feb. 17 to 18	Oct. 30 to 31	—42	—42	155	150	Phaethontis	W	5
1915	Dec. 24 to 25	Oct. 20	—45	—40	165	135	Phaethontis to Icaria	W	33
1915	Dec. 28 to 29	Oct. 27 to 28	—10	10	210	190	Aeolis to Elysium	SE	30
1924	Oct. 10 to 13	June 25 to 26	—44	—32	313	319	Yaonis to Hellas	S	5
1924	Oct. 20 to 27	June 30 to July 5	—40	—40	287	236	Hellas	W	8
1937	May 2 to 5	Feb. 10 to 12	10	10	285	270	Syrtis Major to Isidis	W	6

[a] Each reported instance of cloud drift is referenced by Gifford to the original source.

[b] In latitudes, the minus sign indicates Southern Hemisphere.

[c] Direction is that from which motion occurred.

portion of a symmetric general-circulation cell. Some of the clouds, however, are large enough so that their motion can be explained by the transition from a symmetric regime to a wave regime, a feature of the general circulation of Mars predicted theoretically by Mintz (ref. 111). There are too few cases of the second group (the projection clouds) in each season to permit evaluation of the circulation pattern by means of the construction of maps such as that by Hess for the Southern Hemisphere summer (see ch. 14). However, they do exhibit motions that may possibly have analogies with terrestrial circulation patterns at higher latitudes. Their altitudes seem much greater, since they are sometimes observed as projections illuminated by the setting Sun, with their tops estimated to reach 30 kilometers or even 50 kilometers. Also they are of much longer duration (several weeks). They may consist in part of aqueous condensations.

The conditions governing the formation of Martian yellow clouds have been examined quantitatively by both Gifford (ref. 204) and Ryan (ref. 206) with similar conclusions.

According to calculations of Ryan:

(1) The horizontal wind velocities necessary to initiate grain movement are considerably greater than on Earth (unless the Martian surface is extremely rough, which is unlikely). For a surface atmospheric pressure of p_0=80 millibars, the velocities required do not exceed those observed; but, if p_0=25 millibars, then they would have to be greater, implying undetectable initial winds of short duration (1 day or so), or small cyclonic systems (like our dust devils).

(2) The vertical wind velocities necessary to maintain particles aloft are less than on Earth over a rather large range of grain sizes (diameters: 1 to 300 microns for p_0=80 mb, but 4 to 200 microns for p_0=25 mb).

Ryan concludes that Martian duststorms should generally be much more violent than terrestrial duststorms; that is, on Mars a large amount of material is quickly carried aloft and sustained for a long period. Also, it is possible that particles significantly larger than 20 microns could cause most obscurations, particularly if the cloud is higher than a few kilometers and the air is turbulent.

Since Mariner IV showed surface pressures on Mars of $p_0 \sim 10$ millibars, another theory by Newbauer (ref. 208) has attempted to explain the formation of dust clouds. Newbauer's calculations explain them by the action of dust devils of diameters larger than 100 meters, which are initiated by the thermal convection due to the considerable variation in the daily atmospheric temperature on Mars.

16

Blue Haze

A HAZE NORMALLY EXISTS over the planet Mars which completely obscures the surface markings, when photographed through blue or ultraviolet filters. Effectively, this "blue haze," or "violet layer," is increasingly opaque at wavelengths shorter than about 4600 Å, and at about 4500 Å there is an abrupt transition to total opacity. Its characteristics below 3000 Å cannot be observed through the Earth's atmosphere.

De Vaucouleurs (refs. 39 and 120) estimated that the blue haze has an optical thickness between 0.1 and 0.2, that it transmits about 85 percent of visible light, and that its reflectivity or albedo in the blue is approximately 0.05 in the region of 4000 to 3300 Å. (See ch. 11.) Thus, in transmission, the haze has a reddish appearance, that is, to an observer on Mars, and in reflection it is gray and dark with a yellowish tendency (ref. 209). Blue images of Mars, although characterized by a hazy aspect, will show the polar caps to be strikingly brilliant, and display blue clouds of varying brightness, especially on the morning side.

Limb brightening is present as a rule, especially on the morning side, while cases of darkening were reported on the evening side (Mt. Wilson photographs (ref. 210)). Also, it was pointed out by Sagan and Kellogg (ref. 211) that the limb brightening may not extend to the very edge of the limb, but a thin dark border may appear, as predicted by Harris (ref. 113) for an intermediate optical depth ($\tau \simeq 0.25$). The existence of both pure scattering, with expected limb brightening, and pure absorption, with expected limb darkening, in varying relative importance seems to illustrate the general computations of Harris. Not until more observational data are secured will the debate on absorption supported by Öpik (ref. 209) versus scattering supported by Sharonov (ref. 212) be settled as to the primary physical mechanism responsible for the above optical effects. However, Rayleigh scattering can be ruled out by the abrupt transition to opacity below 4550 Å.

The blue haze appears to be a high-level atmospheric phenomenon, as evidenced by the larger diameters in the blue (Wright's

effect) and the near absence of flattening in the blue (Gifford, quoted by ref. 213), as compared to the yellow, orange, or red images. Kuiper (refs. 91 and 166), however, finds a haze layer markedly higher over the equator than over the poles. The average height of the haze layer, or its top, is not known even today; it has been placed by a variety of theories between 6 and 200 kilometers. Sagan (ref. 214) believes 150 kilometers to be a high maximum. It is possible that it consists of several layers.

The haze is generally uniform in spread, but Slipher (ref. 213) and others have noticed inhomogeneities such as darker clouds, mottled patterns, and even weather bands. The latter suggests changes in circulation and temperature. Attempts to correlate haze opacity with latitude, rotation, season, or solar activity have so far been inconclusive.

BLUE CLEARINGS

An outstanding phenomenon concerning the blue haze was discovered by Slipher (ref. 215), on comparing blue and yellow photographs taken at the same time. He found that there are occasions when the blue haze clears up enough to allow full visibility in the blue of Martian surface details. These "blue clearings" are usually patchy, with a greater or lesser degree of transparency, but they can also, on very rare occasions, be planetwide, or complete. Both clearing and recovery generally require a few days, or at least a few hours, to take place. The duration of a blue clearing is quite variable, the atmosphere remaining clear for days, or even weeks; one recorded instance lasted 2 months. Table 16–1 (refs. 216–221) gives a list of instances of blue clearings,

TABLE 16–1.—*Some Instances of Blue Clearing*

Dates of clearing		Opposition	Observer
1890	May 26 to June 1	May 27	Pickering (ref. 216)
1926	Nov. 2, 3	Nov. 5	Slipher (refs. 213 and 217)
1928	Dec.	Dec. 21	Slipher (ref. 213)
1937	May 20, 21	May 19	Slipher (refs. 213 and 215)
1939	July 18 to 25	July 23	Martz (ref. 221)
1941	Oct. 10	Oct. 10	Slipher (ref. 213)
1954	May to July 2	June 24	Slipher (ref. 213)
1956	Aug. 25 to Sept. 3	Sept. 10	De Vaucouleurs (ref. 218)
1958	Sept. 3 (ended)	Nov. 16	Richardson and Roques (ref. 219)
1958	Nov. 22	Nov. 16	Wilson (ref. 203)
1961	Jan. to Feb.	Dec. 30, 1960	Focas (ref. 220)
1961	Jan. 1 to 11	Dec. 30, 1960	Robinson (ref. 221)

many of them traced back on older photographs by Martz (ref. 222) or Slipher (ref. 213). There is an apparent greater frequency of blue clearings during opposition, which Slipher and Wilson (ref. 223) noticed and studied carefully. It became more firmly established through a statistical analysis performed by De Vaucouleurs and Young (ref. 224), who showed that observational selectivity of Mars (its observations being confined largely to the few weeks before and after oppositions) was not solely responsible. Slipher provided evidence of a tendency for a correlation between clearing and oppositional approaches of Mars. However, more definitive evidence is needed to substantiate this hypothesis, despite the wide irregularities of oppositional clearings. For example, one well-recorded instance took place 74 days before exact opposition. (See table 16–1 (ref. 219).) No correlation with heliocentric longitude has ever been found, but a weak correlation with areocentric longitude (greater frequency near 250° or 270°) was reported recently by both Slipher (ref. 213) and Robinson (ref. 221). A 4-month survey of Mars indicated that partial weak clearings are probably more common than was generally supposed (ref. 225). A recent investigation by Palm and Basu (ref. 226), based on Slipher's records for 1926 to 1958 and Robinson's for 1960 to 1961, reports "a small but statistically negative correlation between the extent of blue clearing and meteor shower activity."

NATURE AND THEORIES OF THE BLUE HAZE

At present, no satisfactory explanation of the nature of the blue haze and its clearings exists. A number of theories have been advanced since 1950, but all seem to have weaknesses.

WATER-ICE CRYSTAL THEORY.—Proposed by Schatzmann (ref. 227), and studied by Kuiper (ref. 91) and Hess (ref. 228), this theory is based on the Mie scattering of tiny water-ice crystals presumably suspended in the Martian atmosphere. A rise in temperature would cause a clearing, and the return to normal cold temperatures would cause the reappearance of the haze. The major objection to this theory (or any based on a condensable substance) raised by Urey (ref. 228) is that it is difficult to account for planetwide clearings by a temperature change of several degrees, 10° C or more, over the planet. A second objection was voiced by Öpik (ref. 209) against any scattering explanation; in fact, microscopic ice crystals floating in the air should scatter appreciably in the blue to ultraviolet, which conflicts with the known very low albedo of Mars (0.05) from 4000 to 3300 Å. However, an

unconfirmed rocket measurement by Boggess and Dunkelmann (ref. 128) indicated the high albedo of 0.24 at 2700 Å.

Kuiper (ref. 166) explains clearings by invoking deposition and growth of ice, as soon as temperature falls below the local frost point, upon suspended silicate dust particles acting as nuclei, and subsequent fallout. The process is supposedly controlled by atmospheric circulation and evaporation of (ground) frost, especially over the polar areas. As in the case of the dust theory, objections based on the settling rates of particles can be raised.

CARBON DIOXIDE-ICE CRYSTAL THEORY.—First advocated by Hess (ref. 105), and similar in principle to the water-ice crystal theory, this theory depends also on Mie scattering. In application, this theory requires decidedly lower temperatures to form carbon dioxide-ice crystals than those required to form water-ice crystals. In fact, the frost point of carbon dioxide, which depends, of course, on atmospheric pressure, and therefore on altitude, is so low, about 120° K at $p \simeq 15$ millibars, that Hess himself withdrew his support in favor of the water theory (ref. 229).

More recently, however, Ohring (ref. 172) tried to revive the carbon dioxide crystallization possibility as a consequence of his very low atmospheric temperature profiles (90° K at 40 km); likewise did Chamberlain (ref. 176) with his extremely cold mesopause, a minimum 76° K at 130 kilometers. (See ch. 13.)

One objection is that the carbon dioxide-ice layer formed in the carbon dioxide-rich Martian atmosphere would produce a far too opaque blue haze. Urey's major objection also applies to clearings.

NITROGEN DIOXIDE GAS THEORY.—This theory was proposed by Kiess et al. (ref. 230) on the untenable assumption of large amounts of nitrogen dioxide on Mars. (See ch. 12.) It was revived by Warneck and Marmo (ref. 231) and developed by Sagan et al. (ref. 210) on the assumption that only about 1 mm-atm of nitrogen dioxide exists in Mars' atmosphere. This theory is attractive in that the observed transmission characteristics of the blue haze as well as its limb effects, that is, the dependence of opacity on both wavelength and position across the disk, can be reproduced theoretically under suitable Martian temperature conditions. While the nitrogen dioxide is strongly opaque at $\lambda > 3300$ Å, its dimmer N_2O_4 formed at decreasing temperatures is essentially transparent for $\lambda < 3600$ Å.

The sensitivity of the $NO_2 \rightleftharpoons N_2O_4$ system to temperature and pressure is very great. Blue clearings are explained as the result of the dimerization from a temperature drop of a few degrees, perhaps 10°, in Mars' upper atmosphere.

Objections to this theory include Urey's major one regarding all condensable substances, the coexistence of water vapor with nitrogen dioxide in the atmosphere, and the uncertain photochemical abundances of nitrogen oxides on Mars.

DUST THEORY.

(1) Meteoritic dust of microscopic sizes was suggested by Link (ref. 23) and again by Kviz (ref. 233) as being the cause of the blue haze, since Mars' orbit is in a region of apparently plentiful meteor debris. The many meteor showers would supply the upper atmosphere with extensive dust that would cause almost constant opacity in the blue.

The main objection is that no correlation has been found between blue-haze opacity or clearings and Mars' heliocentric longitudes indicative of shower frequencies.

(2) Yellow ground dust, presumably limonitic, from duststorms or yellow clouds was invoked first by Goody (ref. 171) in the form of extremely minute particles responsible for the strong absorption by the blue haze, with no appreciable scattering being involved. The minute particles would be transported to the upper atmosphere, forming an almost permanent veil. An important contradiction was cited by Slipher (ref. 213) from the case of the great yellow duststorm of the 1956 opposition, which did not prevent the occurrence of an extensive blue clearing at the same time.

Most fatal, perhaps, to any dust theory of the blue haze is that the settling rates for small particles (Stokes' law) cannot account for the numerous instances, such as at the 1960–1961 opposition, of rapid clearings.

CARBON SMOKE THEORY.—Suggested by Rosen (ref. 146) and developed by Öpik (ref. 147), this theory is similar to the dust theory, except for the fact that the particles are assumed to be carbon C_3 polymers arising from the photolysis of carbon monoxide and carbon dioxide in the Martian upper atmosphere. Rosen and others have suggested a volcanic gas origin, such as from methane or C_2H_2. Öpik interprets the optical characteristics of the blue haze as due to this highly absorbent "soot." Practically no scattering is envisioned.

Objections to the theory are that it cannot explain rapid clearings, nor can it adequately explain limb brightening in the blue.

FLUORESCENCE THEORY.—Urey and Brewer (ref. 234) attempted to explain the blue haze in terms of fluorescence of ions such as CO_2^+, CO^+, and N_2^+, supposedly abundant in the high Martian atmosphere and formed by incoming solar particle radiation (protons). It was suggested that during opposition, the Earth's

magnetic field deflects the solar protons, thus preventing ionization and fluorescence on Mars, and consequently creating a blue clearing.

Objections are many: the blue spectrum of Mars shows no evidence of characteristic bands or lines; furthermore, Sagan (ref. 214) showed that abnormally large proton energies (above 2 MeV) and fluxes (10^{11} protons/cm^2/sec) would be required to produce the postulated ionization at the blue-haze level (maximum 150 km).

CONCLUSIONS

Disregarding the last theory, it appears that any explanation of the blue haze and clearings in terms of one type of substance or particle and one layer leads to a dead end. Apparently both absorption and scattering of the blue haze are present in different manners which cannot be accounted for by one substance or one particle type. An explanation in terms of two substances or particle types, such as water-ice crystals and carbon smoke, or nitrogen dioxide and dust, and of two distinct layers, a scattering one and an absorbing one, may indeed prove to be more satisfactory. In any case, it seems that more observational data are needed to guide the theoretical work.

17

Surface Features

OBSERVATIONS OF MARS over the past three centuries have resulted in the production of a wide variety of drawings and photographs of its surface. Table 17–1 lists and locates the basic 128 areographic designations recently adopted by the International Astronomical Union Committee, Mars section, as a nucleus for future studies. (See refs. 235 and 236.) The positions of these features are shown in figure 17–1.

MARS MAP

A project to construct a Mars map—or, rather, a series of maps at opposition times—with first-order reference points accurate to within 1° areocentric (~60 km on the surface) was initiated in 1958 by De Vaucouleurs (refs. 237 and 238) at the Harvard College Observatory and is approaching completion. (See the latest report by Menzel et al. (ref. 239).) The program is based on all usable areographic coordinates recorded from 1877 to 1958; that is, from Schiaparelli's initial work up to modern times. It incorporates a particularly desirable novel feature; that is, the systematic reduction of all coordinates to a revised physical ephemeris of Mars for all oppositions from 1877 to 1965. This provides a homogeneous, modern basis for constructing the maps at each opposition. (See ch. 5.) However, the accuracy of any given map is transient because of the continual variation in the dark areas.

The Mars map project, when completed, together with the revised physical ephemeris, is planned to provide the most accurate basis for relating the computed areographic locations of the Mariner IV photographs (not yet established precisely) to the known Martian surface features (ref. 240).

RELIEF

Surface relief on Mars is generally believed to be moderate. Lowell (ref. 241) estimated that Martian mountains (if they are

TABLE 17-1.—*International Astronomical Union Basic Surface Area Designations*

Name	Number	Location, deg
Acidalium Mare	1	30, +45
Aeolis	2	215, —5
Aeria	3	310, +10
Aetheria	4	230. +40
Aethiopis	5	230, +10
Amazonis	6	140, 0
Amenthes	7	250, +5
Aonius Sinus	8	105, —45
Arabia	9	330, +20
Araxes	10	115, —25
Arcadia	11	100, +45
Argyre	12	25, —45
Arnon	13	335, +48
Aurorae Sinus	14	50, —15
Ausonia	15	250, —40
Australe Mare	16	40, —60
Baltia	17	50, +60
Boreum Mare	18	90, +50
Boreosyrtis	19	290, +55
Candor	20	75, +3
Casius	21	260, +40
Cebrenia	22	210, +50
Cecropia	23	320, +60
Ceraunius	24	95, +20
Cerberus	25	205, +15
Chalce	26	0, —50
Chersonesus	27	260, —50
Chronium Mare	28	210, —58
Chryse	29	30, +10
Chrysokeras	30	110, —50
Cimmerium Mare	31	220, —20
Claritas	32	110, —35
Copaïs Palus	33	280, +55
Coprates	34	65, —15
Cyclopia	35	230, —5
Cydonia	36	0, +40
Deltoton Sinus	37	305, —4
Deucalionis Regio	38	340, —15
Deuteronilus	39	0, +35
Diacria	40	180, +50
Dioscuria	41	320, +50
Edom	42	345, 0
Electris	43	190, —45
Elysium	44	210, +25
Eridania	45	220, —45
Erythraeum Mare	46	40, —25
Eunostos	47	220, +22

TABLE 17-1.—*Continued*

Name	Number	Location, deg
Euphrates	48	335, +20
Gehon	49	0, +15
Hadriacum Mare	50	270, —40
Hellas	51	290, —40
Hellespontica Depressio	52	340, —60
Hellespontus	53	325, —50
Hesperia	54	240, —20
Hiddekel	55	345, +15
Hyperboreus Lacus	56	60, +75
Iapigia	57	295, —20
Icaria	58	130, —40
Isidis Regio	59	275, +20
Ismenius Lacus	60	330, +40
Jamuna	61	40, +10
Juventae Fons	62	63, —5
Laestrygon	63	200, 0
Lemuria	64	200, +70
Libya	65	270, 0
Lunae Palus	66	65, +15
Margaritifer Sinus	67	25, —10
Memnonia	68	150, —20
Meroe	69	285, +35
Meridianii Sinus	70	0, —5
Moab	71	350, +20
Moeris Lacus	72	270, +8
Nectar	73	72, —28
Neith Regio	74	270, +35
Nepenthes	75	260, +20
Nereidum Fretum	76	55, —45
Niliacus Lacus	77	30, +30
Nilokeras	78	55, +30
Nilosyrtis	79	290, +42
Nix Olympica	80	130, +20
Noachis	81	330, —45
Ogygis Regio	82	65, —45
Olympia	83	200, +80
Ophir	84	65, —10
Ortygia	85	0, +60
Oxia Palus	86	18, +8
Oxus	87	10, +20
Panchaïa	88	200, +60
Pandorae Fretum	89	340, —25
Phaethontis	90	155, —50
Phison	91	320, +20
Phlegra	92	190, +30
Phoencis Lacus	93	110, —12
Phrixi Regio	94	70, —40
Promethei Sinus	95	280, —65

TABLE 17-1.—*Concluded*

Name	Number	Location, deg
Propontis	96	185, +45
Protei Regio	97	50, —23
Protonilus	98	315, +42
Pyrrhae Regio	99	38, —15
Sabaeus Sinus	100	340, —8
Scandia	101	150, +60
Serpentis Mare	102	320, —30
Sinaï	103	70, —20
Sirenum Mare	104	155 —30
Sithonius Lacus	105	240, +45
Solis Lacus	106	90, —28
Styx	107	200, +30
Syria	108	100, —20
Syrtis Major	109	290, +10
Tanaïs	110	70, +50
Tempe	111	70, +40
Thaumasia	112	85, —35
Thoth	113	255, +30
Thyle I	114	180, —70
Thyle II	115	230, —70
Thymiamata	116	10, +10
Tithonius Lacus	117	85, —5
Tractus Albus	118	80, +30
Trinacria	119	268, —25
Trivium Charontis	120	198, +20
Tyrrhenum Mare	121	255, —20
Uchronia	122	260, +70
Umbra	123	290, +50
Utopia	124	250, +50
Vulcani Pelagus	125	15, —35
Xanthe	126	50, +10
Yaonis Regio	127	320, —40
Zephryia	128	195, 0

abrupt) must be less than 2500 feet high from the fact that neither he nor anyone else had been able to detect prominences at the terminator. Tombaugh, as quoted by Wilson (ref. 242), argues against the validity of Lowell's upper limit because of limitations imposed by the turbulent atmosphere of Earth on the angular resolution of ground-based telescopes. Tombaugh points out that Martian abrupt mountains of less than 15 500 feet (4700 m) in height would not be observable if a realistic limit of resolution of 0.15 arc-second is adopted.

The observation of a few areas or spots in midlatitudes, which periodically whiten, are suggestive of high plateaus or summits

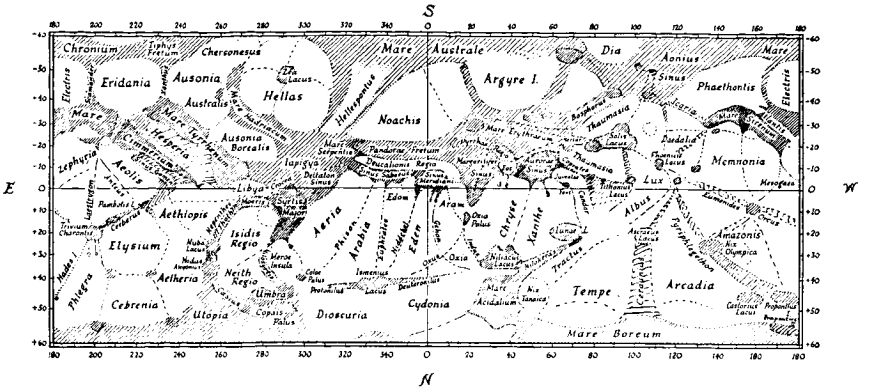

FIGURE 17-1.—Locator map of Mars. (After ref. 188.)

covered with snows or frosts, such as Hellas, Argyre, and Elysium. Polar areas annually exhibit very distinct patterns during melting. Finally, mountainous relief is suggested by the recurrence of orographic clouds over fixed locations, such as Olympia and Candor.

Depressions seem indicated in some cases; for instance, the Trivium Charontis, a large oasis which is conspicuously dark green in any season. Tombaugh (refs. 243 and 244) believes it may be a deeply depressed area several thousand feet below the level of the surrounding desert plain, perhaps capable of retaining water and maintaining vegetation without dependence upon the season.

The surface of Mars, although generally believed to consist of rather flat or rolling terrain, may include some massive but eroded mountain chains.

The Mariner IV photographs covered a strip of only 1 percent the total surface area of the planet, but they revealed a fairly cratered surface of moonlike aspect. According to Leighton et al. (ref. 245), nothing in the pictures suggests mountain chains, great valleys, ocean basins, continental masses, or any earthlike geological features. It appears that no orogenesis took place. The absence of a magnetic field suggests no molten core for Mars. There apparently has been no internal activity over a long time.

The surface appears to be in a primitive form, as in the case of the Moon, although water and erosion could have existed in the very early history of Mars. The actual atmosphere is insignificant and cannot hold much water.

The existence of craters on Mars startled the scientific community, although some 15 years ago Öpik (ref. 246) and Tombaugh (ref. 247) had predicted that the surface of Mars should be covered with thousands of impact craters resulting from asteroidal collisions, since Mars is close to the asteroid belt.

Mars' surface is at least partially covered with large craters; 70 craters are clearly distinguishable on pictures 5 through 15, and ranging from 3 to 75 miles in diameter (ref. 245). Larger and smaller craters are surely in existence. Crater rims rise several hundred feet above the surrounding surface with depths of a few thousand feet below the rims. Crater walls seem to slope at angles up to 10°. The total number of craters of sizes observed is expected to be about 10 000 on Mars. They appear to be impact craters (ref. 248).

Öpik (ref. 249) believes that they are all "later" craters, the primeval craters having been erased by very early erosion (water or ice age and a denser atmosphere). Martian craters are more numerous than craters in the lunar maria, but not as thick as in the continents. Anders (ref. 250), gives an area density of Martian craters of 20 kilometers wide or more of 3.4 times that in lunar maria, but only 19 percent that in lunar continents. He also proposes a limit age of 800 million years, earlier craters being erased by saturation cratering. Öpik found Anders' rate of Martian crater production (25 times the lunar rate) too high, if one considers the actual list of asteroids crossing the Mars orbit and the actual population density of other stray bodies in the solar system. Öpik calculated that Mars received in its history of 4.5 billion years about 8.8 craters larger than 20 kilometers per million km^2 surface area from comet nuclei, asteroids, and other objects. Leighton et al., however, find from Mariner IV pictures 36 craters per 10^6 km^2, a large excess of observed craters over predicted numbers. For both Mars and the lunar maria, this ratio is about 4–5 to 1. Anders obtains even larger values for Mars: 220 craters larger than 20 kilometers accumulated in 4.5×10^9 years per 10^6 km^2 (a ratio of 20 for Martian versus lunar crater densities). Öpik finds no theoretical grounds for postulating excessive rates of erosion on Mars, except in the very beginning, so that the oldest craters can be as old as the surface itself, perhaps 4.5 billion years.

Later investigations by Witting et al. (ref. 251) and Baldwin (ref. 252) arrive at a much lower age for the Martian craters: 300 million and 340 million years, respectively. In other words, the Mars surface appeared to them quite young, with previous active erosion. But Öpik (ref. 249) points out that these investigators did not use a collision theory and the actual data for the stray bodies populations around Mars and near Earth.

BRIGHT AREAS

The surface of Mars, as seen from Earth-based telescopes, can

be divided into three main area types: bright areas, dark areas, and polar caps.

The bright areas compose two-thirds to three-quarters of the total area of the surface, their colors ranging from salmon-pink to reddish or yellowish ocher, give Mars its familiar ruddy color. The characteristic brightness of these areas (0.28 candle/cm^2), albedo (0.15 to 0.20), and color are representative of the planet because the effects of dark areas and polar caps virtually cancel each other. The optical properties of bright areas are largely invariable, except for seasonally whitening areas presumed to be high plateaus covered with frost. Bright areas are generally assumed to be the expanses of moderate relief, constituting the background of the planet's surface.

The various bright areas named individually on the map are hardly distinguishable from each other by brightness or color measurements. When adjacent, their separation is rather ill-defined by faint lines representing the "canals," most of them being very faint or elusive. (See ch. 17.) The most clear-cut demarcation of bright areas is provided by the bordering dark areas; however, these borders may become altered with season and year according to growth or retreat of the dark areas.

The evaluation of the regional colors on Mars is somewhat difficult, and often depends on the optics used and the observer. Thus, the bright yellows and reds frequently reported for bright areas in the early literature are now believed mostly caused by chromatic aberration in refractors or ascribed to contrast effects between bright and dark regions. Kuiper (ref. 253), with the 82-inch reflector of McDonald Observatory, reported only a relatively slight difference between colors of bright and dark regions.

The bright areas are believed to be extremely dry and desertlike regions covered by a fine dust. Using polarimetry and photometry data, Dollfus (refs. 183 and 200) tentatively identified this ocher powder as limonite, a hydrated ferric oxide ($Fe_2O_3 \cdot nH_2O$). The polarimetric curve, visual albedo, brightness, and color index of limonite (out of several hundred mineral samples tested) most closely match those of bright areas on Mars. Partial confirmation was offered by several investigators, principally Sharonov (ref. 254). The limonite interpretation was supported by Adamcik (ref. 159) on thermodynamic grounds. His calculation of the dissociation pressure of goethite ($Fe_2O_3 \cdot H_2O$), the primary constituent of limonite, matches the expected partial pressure of water vapor in Mars' atmosphere. (See ch. 12.) Finally, Sagan et al. (ref.

255), testing varieties of natural limonite in a program of diffuse reflection spectrophotometry, arrived at the conclusion that powdered ferric oxides must be the dominant constituent of the bright areas. The mineralogical model of limonite for the bright areas was once challenged by Kuiper (ref. 91), who proposed a brownish felsitic rhyolite as best reproducing the spectrophotometry. Recently, however, Binder and Cruikshank (ref. 256) obtained the match only with some weathered igneous rocks (rhyolite, granite, andesite, and basalt).

From a geological standpoint, however, it may be difficult to accept the interpretation that the surface of Mars consists primarily of hydrated iron oxides. Silicates are far more common than iron oxides in the Earth's crust. Van Tassel and Salisbury (ref. 257) proposed a desert surface model in which silicate grains (fine or coarse) are coated with finely divided limonite. According to them, most of the powdery limonite formed by prolonged and active mechanical (aeolian) weathering is being gradually transported by winds into the vegetated dark areas. Objection to this dust-sink hypothesis was raised by Rea (ref. 258) who prefers the limonite model and suggests that atmospheric fractionation would separate silicates and limonite particles so that the top layer would be fine limonite dust. Salisbury and Van Tassel (ref. 259) believed the result of a fractionating process would be the reverse (the denser limonite layer under the lighter silicates).

Salisbury and Van Tassel found that many finely powdered minerals have infrared emission spectra (8 to 14 microns) characteristic of graybodies; that is, their emissivities become nearly constant throughout the spectrum and little information is contained in their spectrograms, in particular, as to whether silicates are present or absent upon Mars.

DARK AREAS

The dark areas cover roughly one-third of the surface of Mars, giving it a semipermanent pattern suggestive of some distorted map of the terrestrial surface. Because of their frequent variation in spread, apparent color variation, and general blue-green hue, the dark areas were formerly believed to be Martian oceans, and were named "maria." Of the many dark areas mapped, Syrtis Major (extending across the equator), Mare Tyrrhenum, Mare Sirenum, and Sinus Sabaeus in the south; and Mare Acidalium in the north, are probably the regions most consistently dark and, therefore, most clearly observable by small telescopes.

Under excellent observing conditions, the dark areas can be

resolved into groups of small dark spots (nodosities), or dark granules. Focas (ref. 260) concluded that the fine structure consisted of two elements: (1) a dusky background of a rather granular appearance patched by dark blocks, and (2) groups of spots or isolated spots of various sizes constituting the fundamental nuclei of dark matter.

Kuiper (ref. 253), in his general conclusions regarding the dark areas, found various types of maria shorelines (soft, sharp, frayed, or shredded) without evidence of a distinct geometric pattern, systematic streakiness, preferred patch dimensions, or oasis formation. He found the dark areas to be predominantly gray, with possible blue or green overtones. He reported no seasonal color changes, although Antoniadi (ref. 205) and numerous observers in the past had done so.

From examination of the Mariner photographs, Öpik (ref. 249) came to conclusions about the Martian surface areas:

(1) There is great spottiness in the shadings of both dark areas (maria) and bright areas (continents). Both of these area types are not uniform in surface texture, and they differ from one another by the varying proportions of small dark and bright elements (of dimensions roughly 10 to 100 km). Some dark round spots are most likely old crater bottoms, but many other dark spots and irregular patches seem covered with some genuine dark material, possibly the presumed vegetation, such as the complicated wiggly dark lanes noticed in pictures 3 and 11.

(2) There are gradual transitions between dark areas and bright areas, instead of the sharp borders usually depicted by telescope observers. Thus, Mare Sirenum merges gradually into bright Zephyria in picture 8, and into darker Atlantis in picture 9.

VARIATIONS IN DARK AREAS

Syrtis Major and the Pandorae Fretum provide two of the many possible examples of regular variation in dark areas which follow the seasonal melting and re-forming of the polar caps. Syrtis Major in southern spring and early summer is relatively narrow; however, in midsummer it starts spreading east, overlapping Libya and Moeris Lacus. The isolated Pandorae Fretum area darkens conspicuously in late spring (paralleling the Sinus Sabaeus), disappears again in late autumn, and repeats this cycle every year.

Seasonal variations in brightness have been observed in many dark areas by De Vaucouleurs (ref. 261) and Focas (quoted by (ref. 235)). Generally, a dark wave spreads from the spring pole toward the equator. In the work by Focas (refs. 220 and 260), two

facts were noted: (1) there is a propagation of the darkening wave from either pole to a point approximately 22° across the equator, and (2) there is a decrease in the amplitude of the wave going from pole to equator. This seems valid because a darkening effect from one or the other pole is always in evidence in equatorial latitude. Focas calculated that the wave progresses approximately 30 kilometers per day. The most common explanation for this darkening wave is that it is caused by an increase in atmospheric humidity as the water sublimes from one polar cap and moves toward the other.

Some dark areas irregularly produce new patterns of darkening. Solis Lacus, the "eye of Mars," is particularly noted for variations of this nature (fig. 17–2). Casius, Utopia, Nepenthes-Thoth, Trivium Charontis, Propontis, and Panchaia have been observed undergoing similar variations.

Other dark areas have been observed undergoing sudden changes which remained permanent for several Martian years. Mare Cimmerium has extended 15° further north since 1939, while its other side, along the Zephyria desert, also changed but returned to normal in 1948. A second example is the round, dark spot which appeared in 1956 in the Arcadia desert. This spot had definitely not been present in previous years. Other examples of long-lasting changes are contained in the monograph by Antoniadi (ref. 204) summarizing the Martian surface observations from 1659 to 1929, and the book by Slipher (ref. 262) covering the period from 1905 to 1961.

NATURE OF DARK AREAS

Many efforts have been made to explain the physical cause of the dark areas. In general, these theories are either inorganic or organic. The volcanic-aeolian theory, perhaps the best inorganic theory, is generally discredited today, while the classical vegetative theory is the most widely accepted organic theory. (See ch. 18.)

McLaughlin, noticing a systematic southeast orientation of many south tropical dark bands and their termination in funnel-shaped bays curving northeast after crossing the equator, attributed the pattern to the wind-driven ashes of intermittent volcanoes located at the points of the bays. Seasonal changes in circulation would produce the seasonal variations in dark areas. (See refs. 263 through 267.) Ingenious as it is, the theory contains many discrepancies: many exceptions to the oriented funnel pattern are found, the presumed atmospheric circulation is questionable, and the low quantity of water vapor (which should be released by active volcanism).

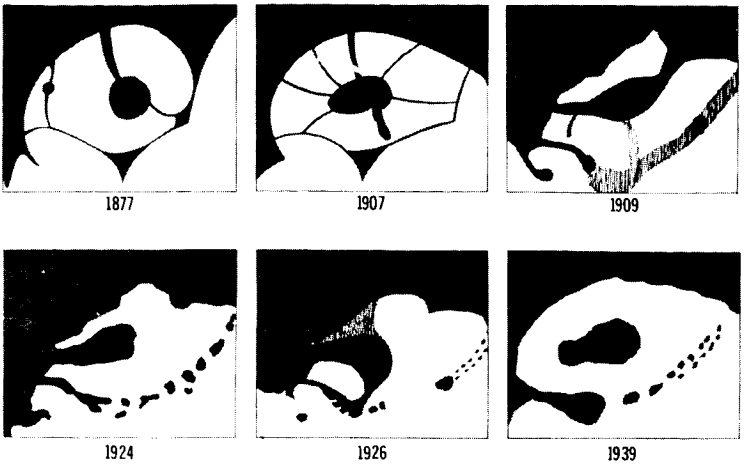

FIGURE 17-2.—Changes in shape of Solis Lacus. (After refs. 205 and 287.)

Other inorganic theories include the suggestion by Arrhenius (ref. 268) that the dark areas are hygroscopic salt beds able to respond to small changes in atmospheric humidity; and Kuiper's theory of lava beds emerging from the desert sands, where dust-storms periodically clear their smooth surfaces, and with, perhaps, a partial vegetal cover (refs. 91 and 253). A hypothesis was proposed by Kiess et al. (ref. 230) assuming that large quantities of nitrogen oxides had accumulated on Mars. The heavy tetroxide gas N_2O_4 was supposed to crystallize at the low polar temperature to form the polar caps. As the pole warmed up, N_2O_4 would begin to dissociate into NO_2, and sublimation would occur. The heavy gases would then flow away along the depressed dark areas. The theory is unacceptable, however, because spectral evidence points to only minute quantities of nitrogen dioxide ($\leq$1 mm-atm) in the Martian atmosphere.

The organic theories advanced to explain the dark areas on Mars generally vary in the selection of the life form believed most likely to exist in the dark areas. For example, micro-organisms were suggested as the life form by Dollfus (ref. 200); lower vegetation resembling lichens or mosses was suggested by Kuiper (ref. 91), and even higher vegetation (plants with leaves) of an unknown type was suggested by Salisbury (ref. 269). Whatever the nature of these life forms, it is generally agreed that they must be specifically adapted to Martian conditions.

The nature of the dark areas could not be clarified by the photographs obtained during the Mariner IV mission. Further analysis

of the photographs may bring out facts favoring one of the various theories. The task appears unsurmountable when it is realized that even on photographs of Earth surface taken by our meteorological satellites, one cannot distinguish vegetation from geological features. Even the question of the relief character of the dark areas, that is, whether they generally represent elevations above, or depressions below, the main surface level of the surrounding bright areas, remains a controversial subject (refs. 270, 271, and 272).

POLAR CAPS

The polar caps, by their great brilliance, were conspicuous to the earliest observers of Mars. The south cap becomes entirely visible only during perihelic opposition and the north cap during aphelic opposition. A heavy white mist shrouds them throughout the winter, making observation virtually impossible.

The polar caps seasonally grow and shrink with great regularity (ref. 262). The cap formation begins in the fall with the appearance of heavy white mists in the polar region, and proceeds through winter hidden by a bright polar veil. In early spring, the veil thins and clears, and the polar cap emerges gleaming white and at its maximum breadth; the south cap then spans a mean areocentric arc of 60° to 70° (averaged over many years and assuming its shape to be circular), and the smaller north cap, some 50° to 55°. Table 17–2 schematizes the evolution of the caps according to observations by Focas (ref. 220). Table 17–3, constructed by Antoniadi (ref. 205), predicts their mean sizes at any time, exhibiting the alternating rhythm. The maximum dimension varies from year to year; in 1960, an unusual breadth of 100° of arc was reached by both caps. The southern cap is always more extensive, produced by the longer, colder southern winter season, while its rapid, near-complete melting is the result of the shorter, hotter southern summer. (See ch. 2.) Shrinkage of the south cap in summertime usually reduces it to below 5° in arc, with possible complete disappearances (as in 1894). The minimum north cap always remains above 6° in angular breadth. Another, not seasonal, but topographic difference between the summertime cap remnants is the eccentric displacement from the true areographic pole: while the center of the north cap is only 1° away from the north pole (to lat. 89° N; long. 290°), the south cap is off-centered by 6°.5 (to lat. 83°.5 S; long. 30°).

The photographic scan of Mariner IV may have reached the edges of the south polar cap of late midwinter but very late in the

TABLE 17–2.—*Seasonal Evolution of the Polar Caps*

[Based on ref. 220]

Evolutionary phase and meteorological process	North cap		South cap	
	Duration (fraction of Martian year)	Heliocentric longitude, η, deg	Duration (fraction of Martian year)	Heliocentric longitude, η, deg
Condensation of ice crystals (indicated by polarimetry) forms thin mist. Visible cap gradually obscured	~0.30	~264 to 15	[a]	? to 225
Growth from a thin mist to maximum thickness of polar cloud. Polar snow deposit starts on ground. Cap entirely invisible	.11	~15 to 55	0.12	~225 to 270
Regression of polar cloud. Cap snow deposits appear through cloud, or at its boundary	.21	55 to 130	.11	270 to 310
Polar snow cap entirely visible (cloud free). Snow sublimates soon after.	.37	130 to 265	.32	310 to 65

[a] Data missing.

TABLE 17-3.—*Mars Polar Cap Sizes*

[After ref. 205]

Heliocentric longitude of Mars, η, deg	Altitude of Sun, deg	Mean areocentric arc of polar cap	
		South cap, deg	North cap, deg
0	—25	14	[a]
10	—24	12	[a]
20	—22	10	[a]
30	—20	9	[a]
40	—18	8	[a]
50	—14	7	[a]
60	—11	6	50
70	—7	5	48
80	—3	[a]	46
90	+1	[a]	44
100	+5	[a]	42
110	+9	[a]	40
120	+13	[a]	37
130	+16	[a]	34
140	+19	[a]	31
150	+21	[a]	27
160	+23	[a]	24
170	+24	[a]	21
180	+25	[a]	18
190	+24	[a]	16
200	+22	[a]	14
210	+20	[a]	12
220	+18	[a]	11
230	+14	[a]	10
240	+11	60	9
250	+7	58	8
260	+3	56	7
270	—1	54	6
280	—5	52	[a]
290	—9	49	[a]
300	—13	45	[a]
310	—16	40	[a]
320	—19	34	[a]
330	—21	27	[a]
340	—23	22	[a]
350	—24	17	[a]

[a] Cloud-veiled cap.

afternoon, so nothing could be seen. In pictures 13 to 15, the ground seems to be partially frost covered, especially on crater rims and peaks.

In melting, the polar cap breaks up in a quite regular and predictable manner. Brilliant white patches and dark bands appear,

giving strong evidence of the presence of rifts, plateaus, and mountains (e.g., Mountains of Mitchel) in the polar regions. When the polar caps start to shrink, sometime in midspring, the receding white edge of the cap becomes permanently bordered by a very dark, bluish band, or fringe, noted in 1830 by Beer and Madler. This dark band (well singled out with a red filter) follows the receding cap closely until the disintegration of the final area is underway. Figure 17–3, a relief map of the polar areas drawn from observation of the manner in which the caps recede, shows depressed areas as darkly shaded, for example, Rima Angusta, from which the cap disappears most quickly. Lightly shaded islands are believed to be high plateaus, for example, Argyre, and the unshaded areas are believed to be mountains, for example, Hypernotius Mons which is able to retain the white cap material until late in the season. An attempt to relate the rate at which polar caps diminish in size to the sunspot cycle was made by Antoniadi (ref. 273). While he did show some correlation between these phenomena, the theory is still held in doubt.

From knowledge of the insolation of Mars, and observations of the rate at which the caps disappear, estimates of the cap thickness have been made which range from a few millimeters to several centimeters. A 1-centimeter average cap thickness has been adopted by De Vaucouleurs (ref. 274) who also estimated that the central core of the cap is between 5 and 10 times thicker than its surroundings. However, Lebedinskii and Salova calculated the snow cover to be appreciably lower, at 1 mg/cm^2 to 1 g/cm^2.

The caps are generally whitish, or pale bluish in color, with shades ranging from brilliant white (on the periphery) to gray; the possible result of varying cap thickness or the growth of vegetation in sheltered areas. In spring, a yellowish tinge can be noticed which De Vaucouleurs (ref. 188) suggested results from selective transmission of mists over the poles. Duststorms may also be responsible for giving the poles a yellow tone, as for example, the great duststorm of 1956.

The average brightness of the caps, free of mist in spring, is 1.53, while that of its wintry veil is 1.31 relative to a reference bright area at disk center (ref. 220). Polarization studies of the caps by Dollfus (ref. 200) have resulted in the conclusion that the variation of polarization with phase angle is not marked for the main cap. However, the bright white regions at the periphery of the cap show an extremely strong negative dip, characteristic of ice-crystal clouds. Dollfus has concluded that these persisting spots

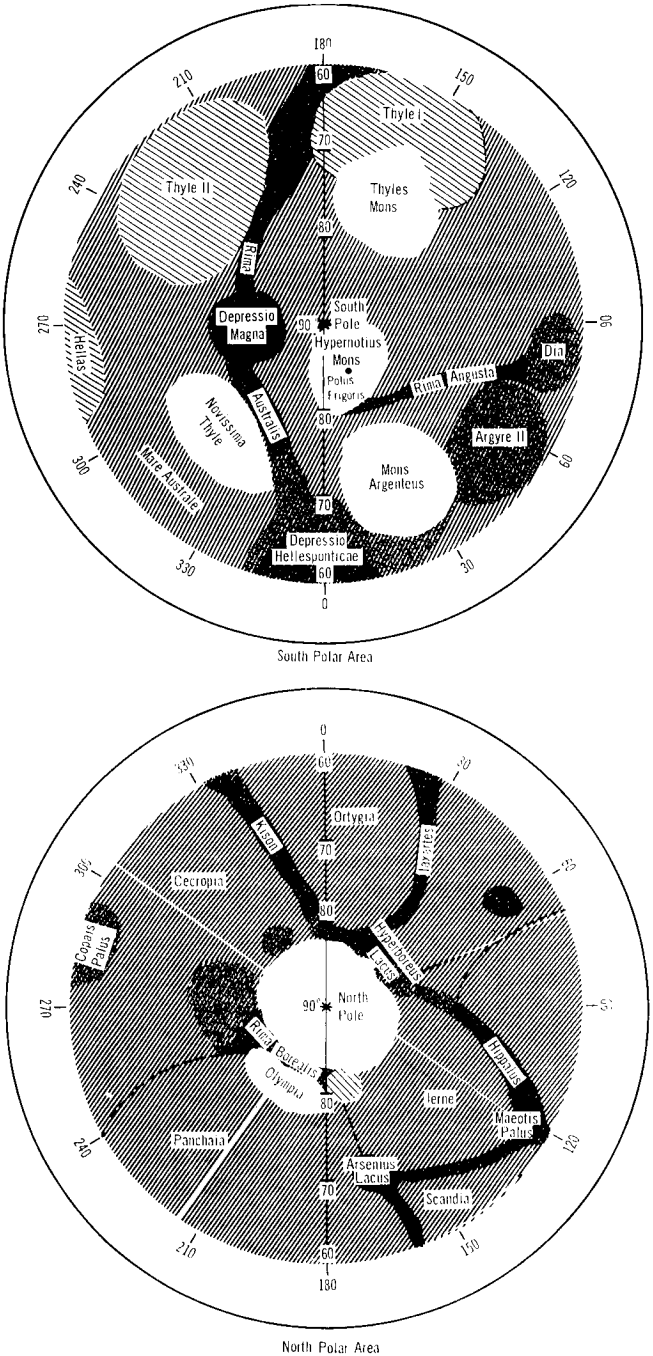

FIGURE 17-3.--Map of Martian polar areas.

must be evidence of recondensation at a high altitude of material sublimated from the cap.

The composition of the polar caps has been the subject of much speculation. Before 1948, the caps were generally believed to be composed of frozen water or frozen carbon dioxide. Tikhov (ref. 275) and Sharonov (ref. 44), using colorimetry and photometry, demonstrated that the caps might be ice, or a substrate of ice covered by hoar frost. In 1948, Kuiper demonstrated that hoar frost and not frozen carbon dioxide, constitute the caps, by comparing their infrared reflection spectra with those of laboratory deposits of the materials in question. Dollfus (ref. 200) confirmed this by polarimetric matching with sublimating hoar frost deposited under simulated Martian conditions.[1] As to the dark polar fringe, Dollfus found it similar to a dark area, and different from a sample of damp earth. The popular theory, that the dark fringe is simply damp earth following the regressing cap, is therefore not supported by polarimetry, although it is still held by many to be the best of the available explanations.

CANALS

Schiaparelli (ref. 277) was the first to systematically observe the famous and controversial canals of Mars in 1877. He called them "canali," which is more precisely translated from Italian as "channels." Since that time, many observations and interpretations have been made. The canals appear as a network of thin gray lines with occasional dark gray, blue, or green tones. It is generally agreed that these lines run between dark areas, and never end abruptly in a bright area. They seem closely related to the dark areas, for they undergo the same changes in color and contrast.

If two canals intersect, a dark area is generally observed. These intersections were first noticed by Pickering (ref. 278), who named them "oases." Although the network of canals does not form a geometric pattern, several canals may radiate outward from an oasis in a spokelike arrangement, as from Trivium Charontis,

---

[1]Recent evidence, obtained from the Mariner IV occultation experiment, indicating a very thin, very cold, and predominantly carbon dioxide atmosphere around Mars, is likely to revive again the former frozen carbon dioxide hypothesis for the polar-cap deposit. Leighton and Murray (ref. 276), in fact, have already proposed a carbon dioxide frost cap model in equilibrium with the carbon dioxide atmosphere, with occasional thin coatings of water-ice on top and a permafrost layer beneath trapping most of the Martian water as ice.

which is a large oasis. It is unfortunate that the Mariner IV photographic scan just missed this interesting feature.

The Mariner IV photographic scan seems to have crossed areas with only a few canals. (See, for example, ref. 279.) According to the JPL report by Leighton et al. (ref. 245), no "canals" were seen nor were any canallike markings discerned with certainty. Burgess (ref. 280), however, pointed out the existence, on at least one photograph, of parallel thin straight lines, and Tombaugh (ref. 270) spoke of definite indications of a canal system being present.

MAPPING

The detection and mapping of Martian canals is difficult. Frequently, the width of an individual narrow canal is less than the theoretical resolving power of the telescope employed, and it is only because of the increased ability of optical systems to distinguish long lines that they are detected at all (refs. 165 and 242). Photography is of little help, as relatively slight atmospheric turbulence can cause the canal image to fade into the background, even in short exposures. Examples of photographed canals are found in the book by Slipher on Mars (ref. 262). Dollfus (refs. 281 and 282), under good visual conditions, classified the apparent linear markings into (1) wide, hazy bands; (2) narrow, more regular streaks; and (3) threadlike, dark, artificial-looking canals. He claims that excellent visual conditions will resolve these canals into a series of small dots irregularly alined and of natural character (fig. 17–4). Experiments made with dots on a board placed at some distance have repeatedly proved that under less than ideal visual conditions, the human eye tends to blend dots into a line.

FIGURE 17–4.—Resolution of Martian canals into irregular dots. (After ref. 282.)

NATURE OF CANALS

Several theories have been advanced to explain the canals. Undoubtedly, the most controversial and sensational theory was presented by Lowell in his book (ref. 283). Until his death in 1916, Lowell mapped several hundred Martian canals into a distinctly geometric network, perhaps exaggerating their artificial aspect (see maps in his books). Lowell believed that the canals were artificial waterways, that is, pipelines bordered by cultivated areas, built by intelligent Martian beings to irrigate their drying planet. With the present spectroscopic evidence that there is little water on Mars, the earlier arguments that the canali and maria (dark areas) contain water are no longer tenable.

A more plausible explanation given was that the canals are either ancient canyons or surface cracks filled with vegetation, according to Tombaugh (refs. 243 and 244) or, as explained by Arrhenius (ref. 268), hygroscopic salts. Katterfeld (ref. 284) suggested that the canals are tectonic fractures sheltering and providing water for dense vegetation. Gifford (ref. 285) speculated that the canals may be long, straight, narrow systems of sand dunes, but this seems unlikely in view of Mariner IV photographs which showed craters so distinctly. None of these explanations is generally accepted today.

The parallel straight lines found by Burgess (ref. 280) were interpreted by him as evidence of a depressed strip of land. Whatever these Martian features are geologically, it seems that their enigma has not been solved by the Mariner IV photographs.

MARS PHOTOGRAPHY BY MARINER IV

On July 14, 1965, when the Mariner IV spacecraft was some 20 000 miles from Mars, a command was sent to warm up the TV scanning system. When Mariner was at 10 500 miles, a planet sensor responding to sunlight reflected from Mars switched on the actual photographing sequence. A series of 22 pictures of the Martian surface were taken in 26 minutes. During this time the spacecraft approached to within approximately 7400 miles of the planet's surface. Some 18 minutes afterward, it reached the closest distance to the surface, only 6118 miles away. One hour and 18 minutes later, Mariner disappeared behind Mars and for 54 minutes its radio signals were occulted. Eight and one-half hours later (or 11 hours after the last picture was taken) the slow playback of the digitized pictures began. At the rate of 8.33 bits per second, it took 8.66 hours to transmit each picture and

it took until July 24 for the complete playback of the 22 pictures.

Each photograph was divided into 40 000 elements to be transmitted to Earth. The picture consisted of 200 lines, each line containing 200 elements. Each picture element had a brightness identified by a six-bit code, providing a scale of 64 steps from full black to full white. Therefore each picture required 240 000 binary digits to be transmitted. The very slow transmission rate of 8.33 bits per second was necessitated by the enormous communication distance of more than 134 million miles. Pictures of Mars were taken through red or green filters, in overlapping pairs so as to obtain more information about the surface coloration.

Less than 1 percent of the Martian surface, an area totaling about 600 000 square miles, was photographed. The camera scanned a strip some 4000 miles long passing across the equator from northwest to southwest. The first picture, taken when Mariner was about 8000 miles below the Martian orbit showed the bright limb, while the 19th picture was thought to include the

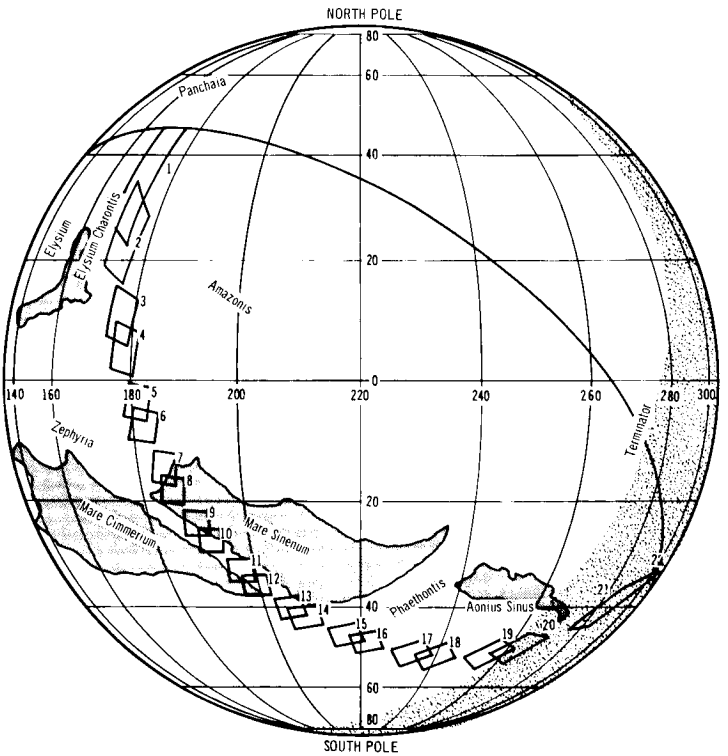

FIGURE 17–5.—The photographic scan of the surface of Mars by Mariner IV. (After ref. 286.)

evening terminator and the last three, the darkness beyond. This meant a brightness variation from full subsolar illumination to almost total darkness. The pictures were taken at various slant ranges, the closest being 7400 miles. The areographic strip photographed is shown in figure 17–5. It is seen that picture 1 was of a bright area between Trivium Charontis and Propontus II Phlegra (on the limb) ; number 5, a bright area in east Zephyria; number 9, the dark area Mare Sirenum; numbers 10 and 11, a bright area between Mare Sirenum and Mare Cimmerium; numbers 12 and 13, the dark area Mare Cimmerium; numbers 14, 15, and 16, the bright area Phaethontis; numbers 17, 18, and 19, the dark area Aonius Sinus; numbers 20, 21, and 22 are in darkness. The Sun's position was high, within 30° of zenith, in the first seven pictures, and therefore little shadow relief was afforded. As the craft swept into the Southern Hemisphere, the Sun altitude was lower and lower, until twilight in picture 19.

The most interesting pictures are the ten from number 5 to 15. Picture 5 first showed Martian craters. Picture 7 revealed a heavily cratered surface, of lunar aspect. Picture 9 showed clusters of craters. Picture 11 is remarkable, showing distinctly a large crater 75 miles across, and all crater sizes down to 3 miles wide. The Sun was low (47° from zenith), the area was viewed from 7800 miles, and was about 170 by 150 miles. Picture 14 has frost-rimmed craters (this is not surprising since it was late midwinter in the south), and brightly illuminated peaks, as the Sun was quite low (at 60° from zenith). Picture 15 also has white ringed craters, and the Sun is even lower (at 66° from zenith).

The 22 pictures of Mariner IV have been distributed by the Jet Propulsion Laboratory, Pasadena, and have appeared in several scientific magazines. The pictures were commented upon by Leighton et al. (ref. 245) and Leighton (ref. 286).

18
Life

SPECULATION AS TO WHETHER LIFE EXISTS on Mars dates back to the earliest telescopic observations of its surface. The introduction of spectroscopic analysis and continued advances in our understanding of terrestrial life processes have provided a firmer scientific basis for the continuing debate on theories and conjectures about Martian life. Nevertheless, the controversies still retain elements of imagination.

ORIGIN

Kuiper (ref. 91) and Urey (ref. 156) are of the opinion that Mars may once have been warmer, with a thicker, more humid atmosphere. Extensive cloud cover would have kept temperature fluctuations much smaller than they are now. Photolysis of water vapor would have provided oxygen to the atmosphere. Under such conditions, plantlife could have developed, adding further oxygen through photosynthesis.

It is suggested, however, that these conditions were not stable; and that the relatively small mass of Mars allowed oxygen to escape to space. Oxidation of the iron on the surface might have hastened this loss of oxygen, and could account for the characteristic yellow-red color of the planet's surface.

The result of such a continuing process would be a thin, dry, cold atmosphere, and an accompanying increase in the intensity of ultraviolet radiation, X-rays, and solar protons at the surface. This is the harsh physical environment to which any surviving vegetation would have had to adapt.

VISUAL EVIDENCE

One of the earliest and most fundamental bases for the theory that life exists in at least the dark areas of Mars is the observations of contrast changes in these areas with the Martian seasons. As spring comes and the polar cap begins to diminish in size, the color of the dark areas beings to deepen, first near the pole and

then farther and farther from it, toward the equator and even across it. If the polar caps are frozen water, evaporation in early spring and the corresponding increase in humidity might cause Martian life of some form to flourish.

The sudden appearance or disappearance of certain of these surface dark areas lends further credibility to the theory that they maintain life. McLaughlin (refs. 263 and 264) has suggested that the dark areas may be regions where volcanic ash has settled, and reduced to a fertile soil with vegetal cover. Volcanic activity, with its release of sulfur dioxide into the atmosphere, might also provide local ultraviolet shielding. Hess (ref. 288) suggests that the blue haze offers adequate protection from ultraviolet.

SPECTROGRAPHIC EVIDENCE

Since 1948, the following spectrographic data have increased the likelihood that life exists on Mars:

(1) Detection of carbon dioxide in the Martian atmosphere, from infrared absorption spectra (ref. 289).

(2) Detection and traces of water vapor in the Martian atmosphere, from infrared absorption spectra (ref. 161).

(3) Evidence from infrared reflection spectra that the polar caps are frozen water, confirmed by polarimetry (ref. 200).

(4) Compatibility of infrared reflection spectra of Mars dark areas with those of certain terrestrial plants, such as mosses and lichens (ref. 91).

The overall evaluation of the spectrographic evidence would seem to be that at least some of the conditions necessary to support life are found on Mars.

SINTON'S CONTROVERSIAL BANDS.—In 1956, using the 200-inch telescope of Mount Palomar, Sinton (ref. 290) obtained infrared spectra of the very dark areas of Mars, such as Syrtis Major which indicated the presence of three absorption bands at 3.43, 3.56, and 3.67 microns. The bands seemed much less pronounced in spectra of bright areas (Amazonis). Later, from data obtained in 1958, he modified the location of the bands to 3.45, 3.58, and 3.69 microns (ref. 145). Since organic compounds with C—H bonds characteristically absorb in the 3- to 4-micron region, it was immediately thought that strong evidence had been discovered suggesting life on Mars, or at least the presence of large organic molecules. For several years, the carbohydrates of Martian plants were believed responsible for these phenomena. Colthup (ref. 291) suggested the –CHO radical of aldehydes, as a cause, citing acetaldehyde as

conforming best to the Martian situation. However, Rea maintained that volatile acetaldehyde released into the atmosphere should be detectable over the entire disk. Investigating further, Rea et al. (refs. 292 and 293) demonstrated that for the spectral region of 2.5 to 4 microns, there were possible complications in spectra of bioorganic materials, perhaps caused by superimposed transmission and reflection spectra; however, they were unable to offer any satisfactory explanation of Sinton's bands, despite tests of inorganic compounds, including carbonates.

The whole question of the Martian origin of Sinton's bands was reopened by Shirk et al. (ref. 294) who found that the bands at 3.58 and 3.69 microns were similar to those of an equal mixture of water (H_2O) and heavy water (HDO and D_2O). Discarding as highly improbable the suggestion by these authors that extensive fractionation of the escaping Martian water had taken place in the course of history, Rea, O'Leary, and Sinton (ref. 295) proposed that the spectral features are caused by heavy water (HDO) in the Earth's atmosphere. They remeasured the original 1958 Martian spectra for the percentage absorption at 3.58 and 3.69 microns, comparing them to solar spectra, and the expected absorption in the Earth's atmosphere, using radiosonde data from San Diego to calculate the amount of water vapor in the vertical path above Mount Palomar. The result was not conclusive but, allowing for various uncertainties, a correlation seemed to exist between the intensities of the 3.58- and 3.69-micron features and the amount of telluric water vapor in the optical path. If this correlation is valid, Sinton's bands cannot be attributed to Mars. (Variations in the telluric HDO could account for the differences observed in the 1958 spectra attributed to dark or bright areas. Also, poor resolution of the disk and other measuring difficulties may contribute to erroneous conclusions.)

EXPERIMENTAL EVIDENCE

One approach to the question of Martian life is to examine the behavior of terrestrial micro-organisms under simulated Martian conditions of pressure, atmosphere, humidity, and temperature fluctuations. Fulton (ref. 296), Kooistra et al. (ref. 297), and Hawrylewicz et al. (ref. 298) proceeded in this manner. They found that certain micro-organisms (facultative anaerobes) not only survived, but actually multiplied in some cases, under these severe conditions. Packer, Scher, and Sagan (ref. 299) found that many micro-organisms survived freeze-thaw cycles of —60°

to +20° C over a 6-month period, and some withstood the expected Martian ultraviolet dosages of 10 ergs/cm² at 2537 Å. These micro-organisms came from soil samples of various locales. When additional water is available, many more micro-organisms can survive and even grow in similar cycles (ref. 300). This finding points up the increased possibility of contamination from spacecraft which land in areas of potentially great water supply. These areas include the dark fringes of "melting" polar caps and regions of possible geothermal activity. Lederberg and Sagan (ref. 301) emphasize the possibility of finding havens of Martian life in the warmer and more humid spots of geothermal penetration of the hypothesized permafrost layer of the Mars subsurface. Availability of water is the principal controlling factor for life on Mars.

CRITERIA FOR THE EXISTENCE OF LIFE ON MARS

Salisbury (ref. 269) has concluded that if life on Mars produces telescopically observable features, it should meet the following five criteria:

(1) It must form colonies covering large areas visible from Earth.

(2) Its color must be consistent with that observed and must respond to variations in temperature and humidity.

(3) It must account for the observed rapid changes in size and shape of the dark areas and be able to reemerge rapidly from a yellow dust cover.

(4) It must be able to exhibit these characteristics within the severe Martian environment.

(5) It must conform to certain fundamental principles of ecology, such as cycling of elements.

Salisbury believes it unlikely that any of the lower terrestrial life forms can meet criteria 1, 2, and 3. A great variety do exhibit the ability to survive the most diverse physical conditions. Lichens, for example, found both in the Sahara and in Antarctica, seemingly meet criterion 4 better than any other known organism; however, they fail to meet the remaining criteria. They show virtually no seasonal change in color; they grow extremely slowly; their shape and height is such that they would not readily emerge from dust cover; they could hardly form colonies visible from Earth in an atmosphere of such low humidity.

It is more plausible that higher vegetation exists on Mars because this satisfies all the criteria, with the possible exception of

the fourth. Vegetation in some modified form is a possibility, with a pigment capable of shielding it from strong ultraviolet radiation. This pigment might absorb solar radiation, enabling the vegetation to maintain a reasonable temperature. In spite of the extreme dryness and lack of oxygen, it may be possible for Martian vegetation to carry on either the terrestrial photosynthesis-respiration cycle or a biogeochemical process involving other elements. Besides Salisbury, Tikhov (ref. 302) has also discussed these alternatives and described examples of terrestrial plants which exhibit pertinent modifications.

The possibility of an exotic type of Martian biochemistry has been suggested again recently by Pimentel et al. (ref. 303), but they point out that the Martian environment—although harsh—is still comparable to the terrestrial one.

The Mariner IV mission was not intended to detect life on Mars. Its experiments were centered on the physical characteristics of the planet. To detect life, a landing probe would be necessary (such as planned for the later Voyager missions in the 1970's). The remarkable TV photographs obtained have resolutions insufficient to detect any vegetation growth as was proved by similar experiments with Tiros and Nimbus Satellites orbiting Earth (ref. 304). The Mariner results, however, seemed to have narrowed down the possibility of some advanced form of life. The very low surface pressures found by Mariner point to even harsher conditions than anticipated for a Martian life form to survive.

19

Satellites

MARS HAS TWO SMALL SATELLITES which revolve rapidly around the planet in orbits which are nearly circular and lie close to the equatorial plane of their primary. Their diameters are so small that measurement of their angular diameters is entirely beyond the reach of present-day giant telescopes. Hall (ref. 305) discovered them both within a few days in August 1877, at the perihelic approach of Mars, as the result of a deliberate search with the new 26-inch refractor of the U.S. Naval Observatory. They were christened Phobos and Deimos, meaning Fear and Terror, after the two attendants of the God of War.

The closer satellite, Phobos, approximately 10 miles in diameter, is unique in the entire solar system in that it rotates around its planet Mars about three times each day, and rises in the west. Its period of revolution is only 7 hours and 39 minutes, and its average altitude is about 6000 kilometers above the surface of Mars. Deimos revolves around Mars in 30 hours and 18 minutes, at approximately 20 000 kilometers above it. Its diameter is believed to be about half that of Phobos, or about 5 miles. These estimates of diameter are based on brightness, arbitrarily assuming satellite albedo equal to that of Mars. There are also no direct measurements of their masses.

The photometry of such faint and close satellites is difficult. At the 1956 opposition, Kuiper (see ref. 113) obtained reduced visual magnitudes V(1,0) of 12.1 for Phobos, 13.3 for Deimos; and a color index B–V of 0.6 for both.

SATELLITE ORBITS

The orbits of the satellites have been observed and studied at the U.S. Naval Observatory in Washington, D.C., ever since their discovery in 1877; their exact characteristics are still unknown. Hall (ref. 305) determined orbital elements of the satellites and published tables of their motions (ephemerides) which were used for a number of years thereafter. Struve (refs. 306 and 307) restudied the elements and their variations between 1877 and 1909.

The ephemerides which appeared annually until 1963 in *The American Ephemeris and Nautical Almanac* were based upon his set of elements.

The best set of orbital elements available today for both satellites are those revised by Burton (ref. 308) from the 49-year period of observations, 1877 to 1926. Table 19–1 presents these elements with their secular variations, after some theoretical improvements by Woolard (ref. 50). The elements are complicated by the fact that they are referred to the fixed Laplacian plane of the satellite

TABLE 19–1.—*Orbital Elements of Satellites*

Element	Phobos	Deimos
a	12″.895 at 1 A.U.	32″.389 at 1 A.U.
e	0.0210	0.0028
η	1128°.844 per tropical day	285°.1619
π	342° + 158°.5 (T–1900.0)[a]	195° + 6°.544 (T–1900.0)
	Orbital plane (referred to Laplacian plane)	
i	1°.13	1°.77
θ	243°.4–158°.5 (T–1900.0)	354°.0–6°.544 (T–1900.0)
K	158°.5 (per Julian year of 365.25 days)	6°.544 (per Julian year of 365.25 days)
	Laplacian plane (referred to Earth's equinox and equator of 1880.0)	
N_1	47°.17	45°.76
I_1	37°.43	36°.86
	Orbital plane (referred to Earth's equinox and equator of 1880.0)	
$(N-N_1)\sin I_1$	$1°.13 \sin\{243°.4-158°.5\,(T-1900.0)\}$	$1°.77 \sin\{354°.0-6°.544\,(T-1900.0)\}$
$I-I_1$	$1°.13 \cos\{243°.4-158°.5\,(T-1900.0)\}$	$1°.77 \cos\{354°.0-6°.544\,(T-1900.0)\}$
	Mean Orbital Longitude of Satellite $L = L_0 + \eta\,(t-t_0)$[b] $+ i \tan \tfrac{1}{2} I_1 \sin\{\theta_0 - K(T-T_0)\}$	
L	$19°.67 + 1128°.844\,(t-2415020.5) + 0°.38 \sin\{243°.4-158°.5\,(T-1900.0)\}$	$286°.71 + 285°.1619\,(t-2415020.5) + 0°.59 \sin\{354°.0-6°.544\,(T-1900.0)\}$

[a] (T–1900.0) = Julian years of 365.25 days reckoned from 1900.0 (epoch T_0) or J.D. 2415020.5.

[b] (t–t_0) = ephemeris days reckoned from J.D. 2415020.5 (epoch t_0).

Symbols:

θ Longitude of the ascending node R of satellite orbit upon Laplacian plane, measured along the Laplacian plane from its ascending node N_1 on Earth's equator (thus, $\theta = N_1 R$).

π Longitude of pericenter P of satellite orbit, measured similarly to L (therefore, $\pi = \Upsilon N + NP$).

γ Vernal equinox of Earth, or ascending node of Earth orbit upon its equator on the celestial sphere.

a Semimajor axis of satellite orbit, measured as the apparent angle at unit distance (1 A.U.).

e Eccentricity of satellite orbit.

at epoch 1900.0, itself referred to the Earth equatorial plane and equinox of 1880.0. Figure 19–1 illustrates the orbit of a Martian satellite with its various possible reference planes depicted as great circles on the areocentric celestial sphere.

The secular variations of these elements are large, as a consequence of the fact that the satellites, being so close to their primary, are under the strong disturbing force of the planet's oblateness. The disturbing influence of the Sun is more significant for Deimos, the more distant satellite of the two. For each satellite, the line of apsides of the orbit advances in its orbital plane. Meanwhile, the pole of this orbit describes a small, nearly circular path on the celestial sphere around the fixed pole of the Laplacian plane, in a retrograde direction. (See fig. 19–2.) These two rotative motions are approximately uniform and equal to each other, because the satellites are of the regular type. The rate (K) of the motion observed for Phobos is about 158°.5 per year, which is very high, and for Deimos it is about 6°.5 per year. The angular radius $\rho(=i)$ of the circle described is small, and about the same for both: for Phobos, $\rho=1°.13$; for Deimos, $\rho=1°.77$. Figure 19–2 illustrates the relative position of the various planes involved; table 19–2 gives the angular values of their respective inclinations.

---

i Inclination of satellite orbit to the Laplacian plane.

K Rate of regression of the ascending node R of satellite orbit upon Laplacian plane $K=d\theta/dt$.

L Mean orbital longitude of satellite $\bar{S}$, measured along Earth's equator from the vernal equinox Υ to the ascending node N of the satellite orbit and then along the orbit (thus $L=\Upsilon N+N\bar{S}$).

L_0 Mean orbital longitude of satellite $\bar{S}$, but measured along equator from Υ to N_1, then along Laplacian plane from N_1 to R, and finally along orbit from R to $\bar{S}$ (therefore, $L'=\Upsilon N_1+N_1R+R\bar{S}$).

N Ascending node (point and longitude) of satellite orbit on the Earth equator, measured from Υ (thus $N=\Upsilon N$).

η Mean daily motion (tropical) of satellite $\bar{S}$.

N_1 Ascending node (point and longitude) of Laplacian plane on the Earth equator, measured from Υ (thus $N_1=\Upsilon N_1$).

N_0 Ascending node (point and longitude) of Laplacian plane on the Earth equator, measured from Υ (thus $N_0=\Upsilon N_0$).

P Pericenter ("periareon") of satellite orbit.

R Ascending node (point only) of satellite orbit upon Laplacian plane.

$\bar{S}$ Mean position of satellite.

T Time measured in Julian years of 365.25 ephemeris days from the epoch T_0.

t Time measured in Ephemeris days from the epoch t_0.

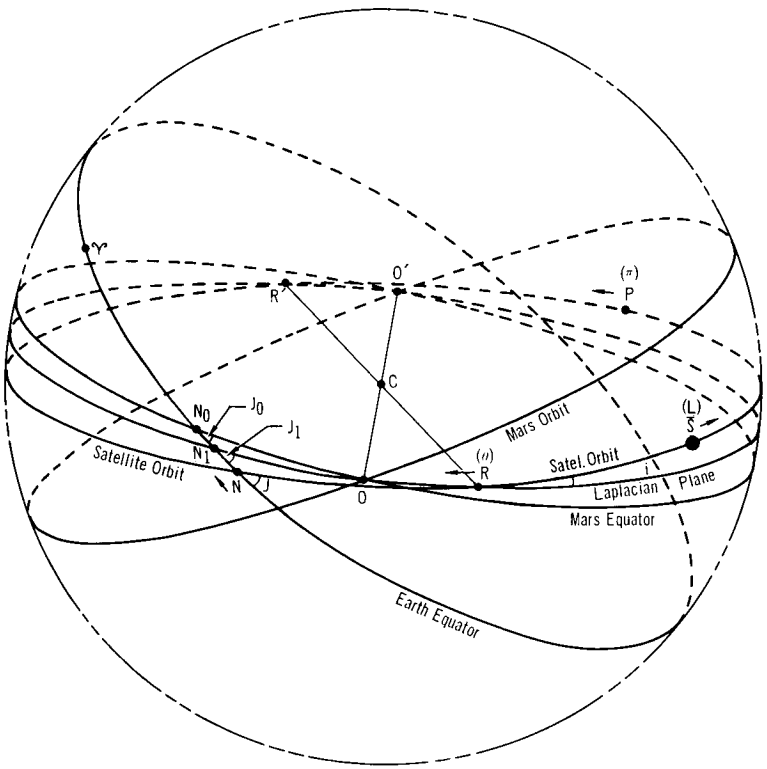

FIGURE 19-1.—Areocentric celestial sphere (with satellite orbital plane and its Laplacian plane).

- θ Longitude of the ascending node R of satellite orbit upon Laplacian plane, measured along the Laplacian plane from its ascending node N_1 on Earth's equator (thus, $\theta = N_1R$).
- π Longitude of pericenter P of satellite orbit, measured similarly to L (therefore, $\pi = \Upsilon N + NP$)
- Υ Vernal equinox of Earth, or ascending node of Earth orbit upon its equator on the celestial sphere.
- C Center of mass of Mars.
- i Inclination of satellite orbit to the Laplacian plane.
- J Inclination of satellite orbit on the Earth equator.
- J_1 Inclination of Laplacian plane on the Earth equator.
- J_0 Inclination of Mars equator on the Earth equator.
- L Mean orbital longitude of satellite $\overline{S}$, measured along Earth's equator from the vernal equinox Υ to the ascending node N of the satellite orbit and then along the orbit (thus $L = \Upsilon N + N\overline{S}$).
- N Ascending node (point and longitude) of satellite orbit on the Earth equator, measured from Υ (thus $N = \Upsilon N$).
- N_1 Ascending node (point and longitude) of Laplacian plane on the Earth equator, measured from Υ (thus $N_1 = \Upsilon N_1$).
- N_0 Ascending node (point and longitude) of Laplacian plane on the Earth equator, measured from Υ (thus $N_0 = \Upsilon N_0$).
- O Intersection point common to Mars orbit, Mars equator, and Laplacian plane on the celestial sphere. Line OO', then, is the common intersection of the three planes.
- P Pericenter ("periareon") of satellite orbit.
- R Ascending node (point only) of satellite orbit upon Laplacian plane. Line RR', then, is the line of nodes.
- $\overline{S}$ Mean position of satellite.

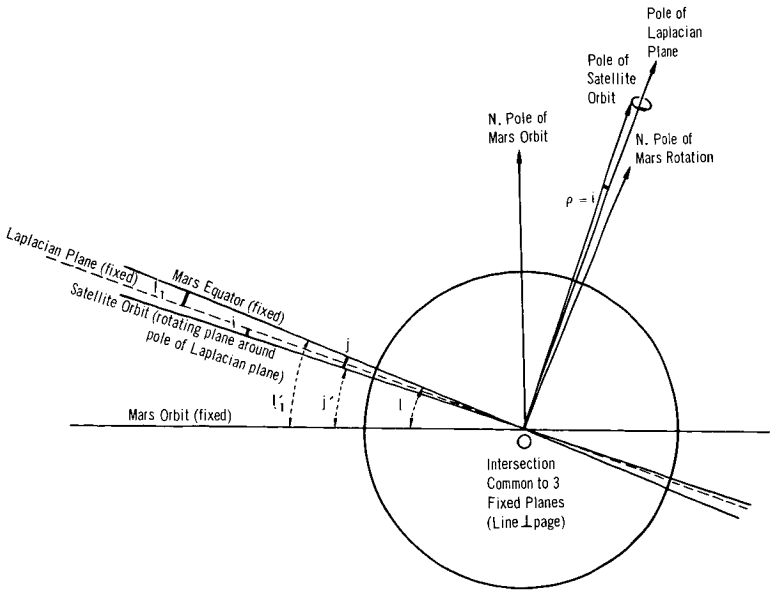

FIGURE 19-2.—The Laplacian plane of a Martian satellite.

TABLE 19-2.—*Inclination of the Planes in the Mars Satellite System*

Inclination angle[a]	Intersecting planes	Phobos	Deimos
Fixed, i	Satellite orbit to its Laplacian plane	1°13	1°77
Variable, j	Satellite orbit to Mars equator plane	1°12–1°14	0°85–2°69
Variable, j'	Satellite orbit to Mars orbit plane	24°06–24°08	22°51–24°35
Fixed, I_1	Laplacian plane to Mars equator plane	0°01	0°92
Fixed, I_1'	Laplacian plane to Mars orbit plane	25°19	24°28
Fixed, I	Mars equator plane to Mars orbit plane	25°20	

[a] Constant angular values for i, I, I_1 are Burton's (1929).

APPARENT SECULAR ACCELERATION OF PHOBOS

Sharpless (ref. 309) reported a secular acceleration in longitude for Phobos but not for Deimos from an investigation of positions during the 1877 to 1941 period. He obtained an acceleration coefficient of $+0°001882$ per (year)^2 with a probable error of $\pm 0°000171$, which corresponds to a fractional increase in mean motion $\Delta\eta/\eta$ of $(+7.98\pm0.73)\times10^{-12}$ for Phobos. Whether this acceleration is real is still a disputed subject. Clemence (quoted in ref. 310), after first pointing out that the probable error in η was "likely to have been underestimated, perhaps by a factor of 2," seemed later to be of the opinion that the data available to

Sharpless were of somewhat questionable accuracy and their interpretation was therefore "based on a false premise."

Nevertheless, theories have been put forth in the last decade to explain the mysterious acceleration of the Martian satellite (assuming it to be real). First, Kerr and Whipple remarked that such an effect could be due to either: (1) a resisting interplanetary medium (of meteoritic or gaseous character), or (2) tides (body tides) between planet and satellite. After investigating the first possible cause, they concluded that the meteoritic density of the space near Mars could not account for the motion of Phobos without predicting an unlikely motion for Deimos too.

Renewed interest was generated when the Russian astronomer Shklovskiy (ref. 311) proposed the idea that Phobos must be of artificial origin and in the shape of a very large hollow sphere. The nonnegligible drag caused by Mars' exosphere was supposed to account for the acceleration reported. Öpik (ref. 209) pointed out that such a fantastic hypothesis was not necessary, since tidal friction alone could cause an appreciable loss of momentum, and calculated that the resulting gradual inward spiraling of Phobos could last another 30 million years until it falls on Mars—a lifetime 10 times longer than Shklovskiy's, but "short enough to be still rather exceptional." It must be remarked, however, that the friction constant of Mars is entirely unknown. Redmond and Fish (ref. 312), developing Öpik's hypothesis, assumed upper and lower limits for the rigidity of Mars which enabled them to calculate the required minimum (1°1) and maximum (1°4) values of the lunitidal interval (angle measuring the tidal bulge lag). Such calculations unfortunately have to be based upon very uncertain assumptions about Phobos' mass. Also, the magnitude of the lunitidal bulge rests upon assumptions of the anelastic properties of Mars. Using most recent Earth-Moon tidal data, the predicted tidal phase lag in Mars appears strong enough to account for the reported acceleration of Phobos by Sharpless.

Schilling (ref. 313), following the alternative approach, explored the possibilities of Martian exospheric drag. His calculations were based on his 1963 exosphere model and suggested that the densities at the orbital altitude of Phobos (6000 km) could exert observable drag effects on the satellite without requiring it to be hollow. The physical parameters (temperature and density) were found, as expected, to be extremely sensitive to solar heating efficiency, but insufficient observational data on Phobos prevented validation of the postulated correlation between solar activity and the accelerations reported.

SEARCH FOR OTHER SATELLITES

During the favorable oppositions of 1954, 1956, and 1958, a photographic search for fainter and more distant satellites was undertaken by Kuiper (ref. 314) with the 82-inch reflector of McDonald Observatory. Use was made of an eccentric diaphragm at the Cassegrain focus to eliminate the diffraction cross of the planet. The survey failed to find any new satellites above the threshold of detectability, thus placing an upper limit of 1.4 kilometers (about 1 mile) on its diameter, assuming that its photographic albedo is that of Mars (about 0.05).

References

1. American Ephemeris and Nautical Almanac. Issued in annual volumes numbered by year, Nautical Almanac Office, U.S. Naval Observatory, U.S. Government Printing Office.
2. ALLEN, C. W.: Astrophysical Quantities. University of London, Athlone Press, 1955, pp. 155–164, 263 pp.
3. NEWCOMB, S.: The Elements of the Four Inner Planets and the Fundamental Constants of Astronomy. Supplement to American Ephemeris for 1897, Government Printing Office, 1895, 202 pp.
4. NEWCOMB, S.: Tables of the Four Inner Planets, Part IV, Tables of the Heliocentric Motion of Mars. Astronomical Papers Prepared for the Use of The American Ephemeris and Nautical Almanac, vol. 6, pt. 4, 1898, pp. 383–586.
5. Ross, F. E.: New Elements of Mars and Table for Correcting the Heliocentric Positions Derived from Astronomical Papers, vol. VI, pt. IV. Astronomical Papers Prepared for the Use of The American Ephemeris and Nautical Almanac, vol. 9, pt. 2, 1917, pp. 251–274.
6. KIRBY, D. S.: Summary of Orbital and Physical Data for the Planet Mars. Rand Corp. Res. Memo. RM-2567. Aug. 1960.
7. CLEMENCE, G. M.; AND SCOTT, F. P.: Note on the Mass of Venus Derived From Observations of Mars. Astron. J., vol. 49, 1940, pp. 188–190.
8. CLEMENCE, G. M.: First-Order Theory of Mars. Astronomical Papers Prepared for the Use of The American Ephemeris and Nautical Almanac, vol. 11, pt. 2, 1949, pp. 224–333.
9. CLEMENCE, G. M.: Theory of Mars—Completion. Astronomical Papers Prepared for the Use of The American Ephemeris and Nautical Almanac, vol. 16, pt. 2, 1961, pp. 261–333.
10. DUNCOMBE, R. L.: Provisional Ephemeris of Mars 1800–1950. U.S. Naval Observatory Circular No. 95, Apr. 30, 1964, 82 pp.
11. DUNCOMBE, R. L.; AND CLEMENCE, G. M.: Provisional Ephemeris of Mars 1950–2000. U.S. Naval Observatory Circular No. 90, Dec. 16, 1960, 48 pp.
12. BLANCO, V. M.; AND MCCUSKEY, S. W.: Basic Physics of the Solar System. Addison-Wesley Publishing Co. (Reading, Mass.), 1961, 307 pp. (Clemence, unpublished results.)
13. Explanatory Supplement to The Astronomical Ephemeris and The American Ephemeris and Nautical Almanac. H.M. Nautical Almanac Office, H.M. Stationery Office (London), 1961, pp. 206–207.
14. Planetary Coordinates for the Years 1800–1940 Referred to the Equinox of 1950.0. H.M. Nautical Almanac Office, H.M. Stationery Office (London), 1933.
15. Planetary Coordinates for the Years 1940–1960 Referred to the Equinox of 1950.0. H.M. Nautical Almanac Office, H.M. Stationery Office (London), 1939.

16. Planetary Coordinates for the Years 1940–1960 Referred to the Equinox of 1950.0. H.M. Nautical Almanac Office, H.M. Stationery Office (London), 1958.
17. HEATH, M. B. B.: Oppositions of Mars, 1956 to 1999. J. Brit. Astron. Assoc., vol. 66, no. 5, Apr. 1956, p. 166.
18. MEEUS, J.: Oppositions of Mars, 1960 to 1980. J. Brit. Astron. Assoc., vol. 70, no. 3, 1960, pp. 144–145.
19. HALL, A.: Observations and Orbits of the Satellites of Mars With Data for Ephemerides in 1879. U.S. Government Printing Office, 1878.
20. VAN DEN BOSCH, C. A.: De Massa's van de groote Planeten. Dissertation, University of Utrecht, 1927.
21. CLEMENCE, G. M.; AND BROUWER, D.: The Accuracy of the Coordinates of the Five Outer Planets and the Invariable Plane. Astron. J., vol. 60, 1955, pp. 118–126.
22. BROUWER, D.; AND CLEMENCE, G. M.: Orbits and Masses of Planets and Satellites. Planets and Satellites. Vol. III of The Solar System, G. P. Kuiper and B. M. Middlehurst, eds., University of Chicago Press, 1961, pp. 31–94.
23. CLEMENCE, G. M.: As reported in Astronomical Notes from Hamburg, 2. Sky and Telescope, vol. 29, no. 1, 1965, pp. 19–22.
24. LEVEAU, G. M.: Tables de Vesta. Compt. Rend., Acad. Sci., vol. 113, 1891, p. 681.
25. LEVEAU, G. M.: Determination des Elements solaires et des Masses de Mars et Jupiter par les Observations meridiennes de Vesta. Compt. Rend., Acad. Sci., vol. 141, 1907, pp. 903–906.
26. DE SITTER, W.; AND BROUWER, D.: On the System of Astronomical Constants. Bull. Astron. Inst. Neth., vol. 8, 1938, pp. 213–231.
27. RABE, E.: Derivation of Fundamental Astronomical Constants from the Observations of Eros During 1926–1945. Astron. J., vol. 55, 1950, pp. 112–126.
28. UREY, H. C.: The Planets, Their Origin and Development. Yale University Press (New Haven), 1952.
29. MAKEMSON, M. W.; BAKER, R. M. L., JR.; AND WESTROM, G. B.: Analysis and Standardization of Astrodynamic Constants. J. Astronaut. Sci., vol. 8, 1961, pp. 1–13.
30. CAMICHEL, H.: Détermination photographique du Pole de Mars, de son Diamètre et des Coordonnées areographiques. Bull. Astron., ser. 2, vol. 18, 1954, fasc. 2, pp. 83–174; fasc. 3, pp. 175–191.
31. CAMICHEL, H.: Observations photographiques de Mars faites au Pic du Midi en 1954. Bull. Astron., ser. 2, vol. 20, 1956, fasc. 2, pp. 131–139.
32. DE VAUCOULEURS, G.: Geometric and Photometric Parameters of the Terrestrial Planets. Icarus, vol. 3, no. 3, 1964, pp. 187–235; or Rand Corp. Res. Memo. RM-4000-NASA, 1964, 121 pp.
33. VAN DE KAMP, P.: Photographic Determination of the Diameter of Mars. Publ. Astron. Soc. Pacific, vol. 37, no. 219, 1925, pp. 261–264.
34. VAN DE KAMP, P.: A Determination of the Diameter of Mars, From Photographs Taken With the 26-inch Visual Refractor of the Leander McCormick Observatory. Astrophys. J., vol. 38, no. 894, 1928, pp. 61–71.
35. REUYL, D.: Photographic Determination of the Diameter of Mars. Astron. J., vol. 49, no. 1136, 1942, pp. 125–129.
36. TRUMPLER, R. J.: Observations of Mars at the Opposition of 1924. Lick Obs. Bull., vol. 13, no. 387, 1927, pp. 19–45.

37. WRIGHT, W. H.: Photographs of Mars Made With Light of Different Colors. Lick Obs. Bull., vol. 12, 1925, p. 48.
38. ROSS, F. E.: Photographs of Mars, 1926. Astrophys. J., vol. 64, 1927, pp. 243–249.
39. DE VAUCOULEURS, G.: The High-Level Absorbing Layer. Pt. I, ch. 2 of Physics of the Planet Mars. Faber & Faber (London), 1954, pp. 55–76.
40. MENZEL, D. H.: The Atmosphere of Mars. Astrophys. J., vol. 63, 1926, pp. 48–59.
41. FESSENKOV, B.: On the Atmosphere of Mars; Photometrical Analysis of Wright's Phenomenon. Astron. Nachr., vol. 228, no. 5450, 1926, pp. 25–32.
42. BARABASHOV, N.; AND SEMEJKIN, B.: Photometrische Untersuchung der Marsoberfläche und seiner Atmosphäre durch Farbfilter. Z. Astrophys., vol. 8, 1934, pp. 44–55.
43. BARABASHOV, N.; AND TIMOSHENKO, I.: Photographic Photometry of Mars in Red and Blue Light. Astron. Zh., Akad. Nauk, vol. 17, 1940, p. 52.
44. SHARONOV, V. V.: The Brightness Contrasts Observed on the Surface of Mars. Poulkovo Obs. Circular, no. 32, 1941, pp. 62–73.
45. MÜLLER, P.: Sur un nouveau Micromètre à double Image, ses Possibilités, et quelques Questions connexes. Bull. Astron., ser. 2, vol. 14, fasc. 3 and 4, 1949, pp. 177–313.
46. SEE, T. F. F.: Preliminary Investigation of the Diameter of Mars. Astron. Nachr., vol. 157, no. 3750, 1901, pp. 97–114.
47. WIRTZ, C.: Beobachtungen der grossen Planeten. Ann. Kaiserl. Universitäts-Sternwarte in Strassburg, vol. 4, pt. 2, 1912, pp. 243–286.
48. WRIGHT, W. H.: Photographs of Mars and of Jupiter Taken by Light of Different Colors During 1926. Lick Obs. Bull., vol. 13, no. 389, 1927, pp. 50–67.
49. STRUVE, H.: Bestimmung der Abplattung und des Aequators von Mars. Astron. Nachr., vol. 138, no. 3302, 1895, pp. 217–228.
50. WOOLARD, E. W.: The Secular Perturbations of the Satellites of Mars. Astron. J., vol. 51, no. 2, Aug. 1944, pp. 33–36.
51. DOLLFUS, A.: Mesure des Dimensions du Globe de la Planète Mars. Compt. Rend., Acad. Sci., vol. 255, Oct. 29, 1962, pp. 2229–2231.
52. DE VAUCOULEURS, G.: The Physical Ephemeris of Mars. Icarus, vol. 3, no. 3, Sept. 1964, pp. 236–247.
53. MEILLER, V.: Physical Ephemeris of Mars 1887–1967. U.S. Naval Observatory Circular No. 98, June 12, 1964, 87 pp.
54. STRUVE, H.: Beobachtungen der Marstrabanten in Washington, Pulkowa, und Lick Observatorium. Mem. Acad. Imperiale Sci. St. Petersbourg, ser. 8, vol. 8, 1898, pp. 1–73; p. 64.
55. LOWELL, P.: Precession of the Martian Equinoxes. Astron. J., vol. 28, 1914, pp. 169–171.
56. LOWELL, P.: Position of the Axis of Mars. Lowell Obs. Bull., no. 24, vol. 1, 1905, pp. 157–161.
57. FISH, F. F.: Precession of Mars. Spaceflight, vol. 6, no. 6, Nov. 1964, pp. 214–215.
58. WISLICENUS, W.: Beitrag zur Bestimmung der Rotationszeit des Planeten Mars. Strassburg inaugural dissertation, Karlsruhe, 1886.
59. BAKHUYZEN, H. G.; AND VAN DE SANDE: Untersuchungen über die Rota-

tions zeit des Planeten Mars und über Aenderungen seiner Flecke. Ann. Leidener Sternwarte, vol. 7, 1897, p. 1.

60. ASHBROOK, J.: A New Determination of the Rotation Period of the Planet Mars. Astron. J., vol. 58, no. 6, 1953, pp. 145–155.
61. CROMMELIN, A. C. D.: Ephemeris for Physical Observations of Mars, 1900–01. Monthly Notices Roy. Astron. Soc., vol. 60, no. 3, 1900, pp. 232–243.
62. CROMMELIN, A. C. D.: Ephemeris for Physical Observations of Mars, 1902–03. Monthly Notices Roy. Astron. Soc., vol. 62, no. 8, 1902, pp. 604–615.
63. CROMMELIN, A. C. D.: Ephemeris for Physical Observations of Mars, 1904–06. Monthly Notices Roy. Astron. Soc., vol. 64, no. 5, 1904, pp. 506–521.
64. SCHIAPARELLI, G.: Osservazioni astronomiche e fisiche sull Asse de Rotazione e sulla Topografia del Pianeta Marte. Rome, 1878.
65. MARTH, A.: Ephemeris for Observations of the Physical Features of the Planet Mars During the Opposition of 1869. Monthly Notices Roy. Astron. Soc., vol. 29, no. 2, 1869, pp. 53–55.
66. DE VAUCOULEURS, G.; AND WRIGHT, R.: Sources of Areographic Coordinates, 1909–1954. AFCRL Rept. No. 257, Harvard College Obs., Rept. 2, 1961.
67. DE VAUCOULEURS, G.: Sources of Areographic Coordinates, 1877–1907. Rand Corp. Res. Memo. RM-3991-NASA, Jan. 1964, 81 pp.
68. Nautical Almanac and Astronomical Ephemeris for the Year 1909. H.M. Nautical Almanac Office, Edinburgh: H.M. Stationery Office, pp. 32–48 of the appendix.
69. KIRBY, D. S.: Studies of the Physical Properties of the Moon and Planets. Rand Corp. Res. Memo. RM-2769-JPL, Apr. 28, 1961, pp. 68–73.
70. RINGWOOD, A. E.: The Constitution of the Mantle—I. Thermodynamics of the Olivine-Spinel Transition. Geochim. Cosmochim. Acta, vol. 13, 1958, pp. 303–321.
71. RINGWOOD, A. E.: The Constitution of the Mantle—II. Further data on the Olivine-Spinel Transition. Geochim. Cosmochim. Acta, vol. 15, 1958, pp. 18–29.
72. RINGWOOD, A. E.: The Constitution of the Mantle—III. Consequences of the Olivine-Spinal Transition. Geochim. Cosmochim. Acta, vol. 15, 1958, pp. 195–212.
73. RAMSEY, W. H.: On the Constitution of the Terrestrial Planets. Monthly Notices Roy. Astron. Soc., vol. 108, 1948, pp. 406–413.
74. CLAIRAUT, A. C.: Théorie de la Figure de la Terre, tirée des Principes de l'Hydrostatique. David Fils (Paris), 1743, 305 pp.
75. JEFFREYS, H.: The Density Distributions in the Inner Planets. Monthly Notices Roy. Astron. Soc., Geophysical Suppl., vol. 4, 1937, pp. 62–71.
76. BULLEN, K. E.: On the Constitution of Mars. Monthly Notices Roy. Astron. Soc., vol. 109, 1949, pp. 688–692.
77. WILDT, R.: Planetary Interiors. Planets and Satellites, ch. 5. Vol. III of The Solar System, G. P. Kuiper and B. M. Middlehurst, eds., University of Chicago Press, 1961, pp. 159–212.
78. MACDONALD, G. J. F.: On the Internal Constitution of the Inner Planets. J. Geophys. Res., vol. 67, no. 7, July 1962, pp. 2945–2974.

79. LYTTLETON, R. A.: On the Internal Constitution of the Terrestrial Planets. JPL Tech. Rept. No. 32–552, Sept. 21, 1963, 62 pp.
80. LAMAR, D. L.: Optical Ellipticity and Internal Structure of Mars. Icarus, vol. 1, 1962, pp. 258–265.
81. JOBERT, G.: Modèles de Répartition des Densités dans les Planètes Terrestres. Ann. Géophys., vol. 18, 1962, pp. 133–149.
82. LEVIN, B. J.: Comparative Analysis of the Internal Constitution and Development of Planets. La Physique des Planètes. Institut d'Astrophysique, Cointe-Sclessin, 1963, 604 pp.
83. KOVACH, R. L.; AND ANDERSON, D. L.: The Interiors of the Terrestrial Planets. J. Geophys. Res., vol. 70, no. 12, June 1965, pp. 2873–2882.
84. KOPAL, Z.: Thermal History of the Moon and of the Terrestrial Planets: Numerical Results. JPL Tech. Rept. No. 32–225, Jan. 9, 1962, 108 pp.
85. KOPAL, Z.: Stress History of the Moon and of the Terrestrial Planets. Icarus, vol. 2, 1963, pp. 376–395.
86. SINGER, S. F.: Some Considerations of Expected Radiation Belts of Planets Mars and Venus, Advances in the Astronautical Sciences. Proc. Am. Astronaut. Soc., vol. 6, Macmillan Co., 1961, pp. 781–793.
87. SMITH, E. J.; DAVIS, L., JR.; COLEMAN, P. J., JR.; AND JONES, D. E.: Magnetic Field Measurements Near Mars. Science, vol. 149, no. 3689, Sept. 10, 1965, pp. 1241–1242.
88. VAN ALLEN, J. A.; FRANK, L. A.; KRIMIGIS, S. M.; AND HILLS, H. K.: Absence of Martian Radiation Belts and Implications Thereof. Science, vol. 149, no. 3689, Sept. 10, 1965, pp. 1228–1233.
89. O'GALLAGHER, J. J.; AND SIMPSON, J. A.: Search for Trapped Electrons and a Magnetic Moment at Mars by Mariner IV. Science, vol. 149, no. 3689, Sept. 10, 1965, pp. 1233–1239.
90. ALLEN, C. W.: Astrophysical Quantities. University of London, Athlone Press (London), 1963, 2d ed., 291 pp.
91. KUIPER, G. P.: Planetary Atmospheres and Their Origin. The Atmospheres of the Earth and Planets, ch. 12, 2d ed., G. P. Kuiper, ed., University of Chicago Press, 1952, pp. 308–405 (1st ed., 1949).
92. OHRING, G.; TANG, W.; AND DESANTO, G.: Theoretical Estimates of the Average Surface Temperature on Mars. J. Atm. Sci., vol. 19, 1962, pp. 444–449.
93. ELSASSER, W. M.: Heat Transfer by Infrared Radiation in the Atmosphere. Harvard Meteorological Studies No. 6, Harvard University Press (Cambridge, Mass.), 1942.
94. ELSASSER, W. M.; AND CULBERTSON, M. F.: Atmospheric Radiation Tables. Meteorological Monographs, vol. 4, no. 23, 1960, Am. Meteorol. Soc., Boston, 43 pp.
95. COBLENTZ, W. W.: Temperature Estimates of the Planet Mars. Sci. Papers Nat. Bur. Std., vol. 20, 1925, pp. 371–397.
96. COBLENTZ, W. W.: Temperature Estimates of the Planet Mars, 1924 and 1926. J. Res. Nat. Bur. Std., RP 1458, vol. 28, pp. 297–309.
97. COBLENTZ, W. W.; AND LAMPLAND, C. O.: Measurements of Planetary Radiation. Lowell Obs. Bull., vol. 3, no. 85, 1923, pp. 91–134.
98. COBLENTZ, W. W.; AND LAMPLAND, C. O.: Further Radiometric Measurements and Temperature Estimates of the Planet Mars. Sci. Papers Nat. Bur. Std., vol. 22, 1927, pp. 237–276.
99. PETTIT, E.; AND NICHOLSON, S. B.: Measurements of the Radiation From the Planet Mars. Popular Astron., vol. 32, 1924, pp. 601–608.

100. GIFFORD, F., JR.: Surface Temperatures of the Planet Mars: 1926 to 1943. The Study of Planetary Atmospheres, a Final Report, Lowell Obs., Flagstaff, Ariz., Sept. 30, 1952, pp. 208–249.
101. GIFFORD, F., JR.: The Surface Temperature Climate of Mars. Astrophys. J., vol. 123, 1956, pp. 154–161.
102. SINTON, W. M.: Recent Radiometric Studies of the Planets and the Moon. Plants and Satellites, ch. 11. Vol. III of The Solar System, G. P. Kuiper and B. M. Middlehurst, eds., University of Chicago Press, 1961, pp. 429–441.
103. SINTON, W. M.; AND STRONG, J.: Radiometric Observations of Mars. Astrophys. J., vol. 131, 1960, pp. 459–469.
104. MILANKOVITCH, M.: Théorie Mathématique des Phénomènes thermiques produits par la Radiation Solaire. Gauthiers-Villars (Paris), 1920, 340 pp.
105. HESS, S. L.: Some Aspects of the Meteorology of Mars. J. Meteorol., vol. 7, no. 1, 1950, pp. 1–13.
106. DE VAUCOULEURS, G.: The Climatology of Mars. Pt. II of Physics of the Planet Mars. Faber & Faber (London), 1954, pp. 139–189.
107. MAYER, C. H.: Radio Emission of the Moon and Planets. Planets and Satellites, ch. 12. Vol. III of The Solar System, G. P. Kuiper and B. M. Middlehurst, eds., University of Chicago Press, 1961, pp. 442–472.
108. MAYER, C. H.; MCCULLOUGH, T. P.; AND SLOANMAKER, R. M.: Observations of Mars and Jupiter at a Wavelength of 3.15 cm. Astrophys. J., vol. 127, 1958, pp. 11–16.
109. GIORDMAINE, J. A.; ALSOP, L. E.; TOWNES, C. H.; AND MAYER, C. H.: Observations of Jupiter and Mars at 3 cm. Wavelength. Astrophys. J., vol. 64, 1959, pp. 332–333.
110. RASOOL, S. I.: Structure of Planetary Atmospheres. AIAA J., vol. 1, no. 1, 1963, pp. 6–19.
111. MINTZ, Y.: The General Circulation of Planetary Atmospheres. The Atmospheres of Mars and Venus, W. W. Kellogg and C. Sagan, eds., National Academy of Sciences—National Research Council, Washington D.C., Publ. 944, 1961, pp. 107-146.
112. ZÖLLNER, J. C. F.: Photometrische Untersuchungen. W. Engelmann (Leipzig), 1865.
113. HARRIS, D. L.: Photometry and Colorimetry of Planets and Satellites. Planets and Satellites, ch. 7. Vol. III of The Solar System, G. P. Kuiper and B. M. Middlehurst, eds., University of Chicago Press, 1961, pp. 272–342.
114. MÜLLER, G.: Helligkeitsmessungen der bei Planetenbeobachtungen benützen Vergleichsterne. Publ. Astrophys. Obs. Potsdam, vol. 8, no. 4, 1893, pp. 197–355.
115. KING, E. S.: Photovisual Magnitudes of Stars and Planets. Ann. Harvard College Obs., vol. 81, 1919, pp. 201–215, or: Color Index of Planets. Popular Astron., vol. 27, 1919, pp. 570–571.
116. KING, E. S.: Revised Magnitudes and Color Indices of the Planets. Ann. Harvard College Obs., vol. 85, no. 4, 1923, pp. 63–71.
117. LIVLÄNDER, R.: On the Colour of Mars. Publ. Obs. Astron. Université de Tartu, vol. 27, no. 6, 1933, pp. 1–29.
118. RADLOVA, L. N.: Photometrical and Colorimetrical Observations of Mars During the Opposition of 1939. Astron. Zh., vol. 17, no. 4, 1940, pp. 30–36.

119. JOHNSON, H. L.; AND GARDINER, A. J.: The Magnitude and Colour of Mars during the 1954 Opposition. Publ. Astron. Soc. Pacific, vol. 67, no. 395, Apr. 1955, pp. 74–77. (See also correction by A. T. Young, ibid., vol. 69, 1957, p. 568.)
120. DE VAUCOULEURS, G.: Multicolor Photometry of Mars in 1958. Planetary and Space Science, vol. 2, no. 1, Oct. 1959, pp. 26–32.
121. WOOLLEY, R.: Monochromatic Magnitudes of Mars in 1952. Monthly Notices Roy. Astron. Soc., vol. 113, 1953, pp. 521–525.
122. WOOLLEY, R.; ET AL.: Monochromatic Magnitudes of Mars in 1954. Monthly Notices Roy. Astron. Soc., vol. 115, 1955, pp. 57–59.
123. MÜLLER, G.: Die Photometrie der Gestirne. W. Engelmann (Leipzig), 1897, 556 pp.
124. DANJON, A.: Nouvelles Recherches sur la Photométrie de la Lumière cendrée et l'Albedo de la Terre. Ann. Obs. Strasbourg, vol. 3, fasc. 3, 1936, pp. 139–180.
125. LAU, H. E.: Variabilité de la Planète Mars. L'Astronomie, vol. 28, 1914, pp. 421–422.
126. GUTHNICK, P.; AND PRAGER, R.: Photoelektrische Untersuchungen an spektroskopischen Doppelsternen und an Planeten. Veroeffentl. königlichen Sternwarte zu Berlin-Babelsberg, Bd. I, Heft 1, 1914, pp. 1–68. (Also see ibid., Bd. II, Heft 3, 1918, p. 117.)
127. DE VAUCOULEURS, G.: Etude physique de la Planète Mars, Opposition de 1939. Ann. Obs. Houga. vol. 1, fasc. 1, 1942, pp. 1–75.
128. BOGGESS, A.; AND DUNKELMANN, L.: Ultraviolet Reflectivities of Mars and Jupiter. Astrophys. J., vol. 129, no. 1, 1959, pp. 236–257.
129. GRANDJEAN, J.; AND GOODY, R. M.: The Concentration of Carbon Dioxide in the Atmosphere of Mars. Astrophys. J., vol. 121, 1955, pp. 548–552.
130. KAPLAN, L. D.; MÜNCH, G.; AND SPINRAD, H.: An Analysis of the Spectrum of Mars. Astrophys. J., vol. 139, 1964, p. 1.
131. BOESE, R. W.; MILLER, J. H.; AND INN, E. C. Y.: The $5\nu_3$ Band of Carbon Dioxide-R-Branch Integrated Intensity. Astrophys. J., vol. 142, 1966, pp. 1272–1273.
132. RANK, D. H.; FINK, V.; FOLTZ, J. K.; AND WIGGINS, T. A.: Intensity Measurements on Spectra of Gases of Planetary Interest—H_2, H_2O, and CO_2. Astrophys. J., vol. 140, no. 1, 1964, pp. 366–373.
133. CHAMBERLAIN, J. W.; AND MCELROY, M. B.: Martian Atmosphere: The Mariner Occultation Experiment. Science, vol. 152, no. 3718, Apr. 1, 1966, pp. 21–25.
134. KLIORE, A.; CAIN, D. L.; LEVY, G. S.; ESHLEMAN, V. R.; FJELDBO, G.; AND DRAKE, F. D.: Occultation Experiment: Results of the First Direct Measurement of Mars' Atmosphere and Ionosphere. Science, vol. 149, no. 3689, Sept. 10, 1965, pp. 1243–1248.
135. KELLOGG, W. W.; AND SAGAN, C.: The Atmospheres of Mars and Venus. Space Sci. Board Rept., Publ. 944, National Academy of Sciences—National Research Council, Washington, D.C., 1961, pp. 29–151.
136. BROWN, H.: Rare Gases and the Formation of the Earth's Atmosphere. The Atmospheres of the Earth and Planets, ch. 9, G. P. Kuiper, ed., University of Chicago Press, 2d ed., 1952, pp. 258–266. (1st ed., 1949.)
137. SUESS, H. E.: On the Radioactivity of K^{40}. Phys. Rev., vol. 73, 1948, p. 1209.
138. DUNHAM, T., JR.: Spectroscopic Observations of the Planets at Mount

Wilson. The Atmospheres of the Earth and Planets, ch. 11, G. P. Kuiper, ed., University of Chicago Press, 2d ed., 1952, pp. 288–305.

139. RICHARDSON, R. S.: Preliminary Report on Observations of Mars Made at Mount Wilson in 1956. Publ. Astron. Soc. Pacific, vol. 69, 1957, pp. 23–30.
140. KIESS, C. C.; CORLISS, C. H.; KIESS, H. K.; AND CORLISS, E. L.: High-Dispersion Spectra of Mars. Astrophys. J., vol. 126, 1957, pp. 579–584.
141. MARMO, F. F.; AND WARNECK, P.: Laboratory and Theoretical Studies in the Vacuum Ultraviolet for the Investigation of the Chemical Physics of Planetary Atmospheres. Geophysics Corp. of Am. Quart. Prog. Repts., Contract NASw-124, Bedford, Mass., Aug. 3, 1960, and Aug. 3, 1961.
142. PRABHAKARA, C.; AND HOGAN, J. S.: Ozone and Carbon Dioxide Heating in the Martian Atmosphere. J. Atmospheric Sci., vol. 22, no. 2, Mar. 1965, pp. 97–109.
143. MARMO, F. F.; SHARDANAND; AND WARNECK, P.: Ozone Distribution in the Atmosphere of Mars. J. Geophys. Res., vol. 70, no. 9, May 1965, pp. 2270–2272.
144. WILDT, R.: Ozon und Sauerstoff in den Planeten Atmosphären. Veroeffentl. Univ.-Sternwarte in Göttingen, no. 38, 1934, p. 9.
145. SINTON, W. M.: Further Evidence of Vegetation on Mars. Science, vol. 130, 1959, pp. 1234–1237.
146. ROSEN, B.: Orgine possible de la Couche violette dans l'Atmosphere de Mars. Ann. Astrophys., vol. 16, 1953, pp. 288–289.
147. ÖPIK, E.: The Atmosphere and Haze of Mars. J. Geophys. Res., vol. 65, no. 10, 1960, pp. 3057–3063.
148. ADAMS, W. S.; AND ST. JOHN, C. E.: An Attempt to Detect Water Vapor and Oxygen Lines in the Spectrum of Mars With the Registering Microphotometer. Astrophys. J., vol. 63, 1926, pp. 133–137.
149. CAMPBELL, W. W.: Note on the Spectrum of Mars. Observatory, vol. 51, 1928, pp. 322–323.
150. SLIPHER, V. M.: On the Spectral Proof of Water and Oxygen on Mars. Observatory, vol. 53, 1930, pp. 79–81.
151. ADAMS, W. S.; AND DUNHAM, T., JR.: Water Vapor Lines in the Spectrum of Mars. Publ. Astron. Soc. Pacific, vol. 49, 1937, pp. 209–211.
152. ADAMS, W. S.: Some Results With the Coude Spectrograph of the Mount Wilson Observatory. Astrophys. J., vol. 93, 1941, pp. 11–23.
153. HESS, S. L.: A Meteorological Approach to the Question of Water Vapor on Mars and the Mass of the Martian Atmosphere. Publ. Astron. Soc. Pacific, vol. 60, 1948, pp. 289–302.
154. HESS, S. L.: Water Vapor on Mars. Lowell Obs. Rept., The Project for the Study of Planetary Atmospheres, vol. 9, 1951, p. 96.
155. DE VAUCOULEURS, G.: The Spectrographic Quest for Water Vapor. Physics of the Planet Mars, ch. 3, Pt. II, Faber & Faber (London), 1954, pp. 211–219.
156. UREY, H. C.: The Atmospheres of the Planets. Handbuch der Physik, vol. 52, S. Flugge, ed., Springer-Verlag (Berlin), 1959, pp. 363–418.
157. SAGAN, C.: The Abundance of Water Vapor on Mars. Astron. J., vol. 66, Mar. 1961, p. 52.
158. LEBEDINSKII, A. I.; AND SALOVA, G. I.: Amount of Water Available in Free State on Mars. Astron. Zh., SSSR, vol. 39, no. 3, 1962, pp. 494–505.

159. ADAMCIK, J. A.: The Water Vapor Content of the Martian Atmosphere as a Problem of Chemical Equilibrium. Planetary and Space Science, vol. 11, 1963, pp. 355–359.
160. DE VAUCOULEURS, G.: The Physical Environment on Mars. Physics and Medicine of the Atmosphere and Space, ch. 39, O. Benson and H. Strughold, eds., John Wiley & Sons, Inc., 1960, pp. 584–605.
161. DOLLFUS, A.: Mesure de la Quantité de Vapeur d'Eau contenue dans l'Atmosphere de la Planète Mars. Compt. Rend., Acad. Sci., vol. 256, 1963, pp. 3009–3011.
162. DANIELSON, R. E.; GAUSTAD, J. E.; SCHWARZCHILD, M.; WEAVER, H. F.; AND WOOLF, N. J.: Mars Observations from Stratoscope II. Astronaut. J., vol. 69, no. 5, June 1964, pp. 344–352.
163. SPINRAD, H.; MÜNCH, G.; AND KAPLAN, L. D.: The Detection of Water Vapor on Mars. Letter to the Editor, Astrophys. J., vol. 137, no. 4, May 15, 1963, pp. 1319–1321.
164. SPINRAD, H.; AND RICHARDSON, E. H.: High Dispersion Spectra of the Outer Planets, II: A New Upper Limit for the Water Vapor Content of the Martian Atmosphere. Icarus, vol. 2, no. 1, June 1963, pp. 49–53.
165. HESS, S. L.: Mars as an Astronautical Objective. Advan. Space Sci. and Tech., vol. III, F. I. Ordway III, ed., Academic Press (New York), 1961.
166. KUIPER, G. P.: Infrared Spectra of Stars and Planets, IV: The Spectrum of Mars, 1–2.5 Microns, and the Structure of its Atmosphere. Commun. Lunar and Planetary Lab., vol. 2, no. 31, 1964, pp. 79–112.
167. KUIPER, G. P.; AND CRUIKSHANK, D. P.: Laboratory Spectra for Testing the Presence of Minor Constituents in Planetary Atmospheres, I: CH_4, NH_3, N_2O, CO, COS, Region 1–2.5μ. Commun. Lunar and Planetary Lab., vol. 2, no. 34, 1964, pp. 141–165.
168. MARSHALL, J. V.: Improved Test for NO_2 on Mars. Commun. Lunar and Planetary Lab., vol. 2, no. 35, 1964, pp. 167–173.
169. OWEN, T. C.; AND KUIPER, G. P.: A Determination of the Composition and Surface Pressure of the Martian Atmosphere. Commun. Lunar and Planetary Lab., vol. 2, no. 32, 1964, pp. 113–132.
170. FJELDBO, G.; AND ESHLEMAN, V. R.: The Bistatic Radar-Occultation Method for the Study of Planetary Atmospheres. J. Geophys. Res., vol. 70, no. 13, July 1965, pp. 3217–3225.
171. GOODY, R. M.: The Atmosphere of Mars. J. Brit. Interplanetary Soc., vol. 16, 1957, pp. 69–83: or Weather, vol. 12, Jan. 1957, pp. 3–15.
172. OHRING, G.: A Theoretical Estimate of the Average Vertical Distribution of Temperature in the Martian Atmosphere. Icarus, vol. 1, no. 4, Jan. 1963, pp. 328–333.
173. ARKING, A.: Non-Gray Convective Planetary Atmospheres. Mem. Soc. Roy. Sci. Liège (5 ième Série), vol. 7, 1963, pp. 180–189.
174. SCHILLING, G. F.: Limiting Model Atmospheres of Mars. Rand Corp. Rept. R-402-JPL, Aug. 1962, 40 pp.
175. EVANS, D. C.; AND WASKO, P. E.: Model Atmospheres for the Planet Mars. Douglas Aircraft Co. Rept. No. SM-44552, Aug. 1963, 51 pp.
176. CHAMBERLAIN, J. W.: Upper Atmospheres of the Planets. Astrophys. J., vol. 136, no. 2, Sept. 1962, pp. 582–593.
177. MCELROY, M. B.; L'ECUYER, J.; AND CHAMBERLAIN, J. W.: Structure of the Martian Upper Atmosphere. Astrophys. J., vol. 141, no. 4, May 15, 1965, pp. 1523–1535.

178. JOHNSON, F. S.: Atmosphere of Mars. Science, vol. 149, no. 3702, Dec. 10, 1965, pp. 1445–1448.
179. GROSS, S. H.; MCGOVERN, W. E.; AND RASOOL, S. I.: Mars: Upper Atmosphere. Science, vol. 151, no. 3715, Mar. 11, 1966, pp. 1216–1221.
180. CHAMBERLAIN, J. W.; AND HUNTEN, D. M.: Pressure and CO_2 Content of the Martian Atmosphere: A Critical Discussion. Rev. Geophys., vol. 3, no. 2, May 1965, pp. 299–317.
181. DE VAUCOULEURS, G.: Détermination de la Pression atmosphérique sur la Planète Mars par Photométrie visuelle. Comp. Rend., Acad. Sci., vol. 220, 1945, pp. 903–904.
182. DOLLFUS, A.: Etude polarimétrique de la Lumière réfléchie par les Nuages et l'Atmosphère de la Planète Mars. Compt. Rend., Acad. Sci., vol. 227, 1948, pp. 382–384.
183. DOLLFUS, A.: Propriétés photometriques des Contrées désertiques sur la Planète Mars. Compt. Rend., Acad. Sci., vol. 244, 1957, pp. 162–164.
184. MENZEL, D. H.: The Atmosphere of Mars. Astrophys. J., vol. 63, 1926, pp. 48–59.
185. SYTINSKAYA, N. N.: The Nature of the Surface and Atmosphere of the Planet Mars According to Data of Absolute Photometry. Dokl. Akad. Nauk SSSR, vol. 43, 1944, pp. 151–154.
186. FESSENKOV, B. G.: Sur les Propriétés réfléchissantes du Sol et de l'Atmosphère de Mars. Astron. Zh., vol. 21, 1944, pp. 257–275.
187. DOLLFUS, A.: Détermination de la Pression atmosphérique sur la Planète Mars. Compt. Rend., Acad. Sci., vol. 232, 1951, pp. 1066–1068.
188. DE VAUCOULEURS, G.: Physics of the Planet Mars. Faber & Faber (London), 1954, 365 pp. See pp. 99–127.
189. DEIRMENDJIAN, D.: Note on the Surface Pressure Estimates of the Martian Atmosphere. Quart. Prog. Rept. No. 3, Rand Corp. Res. Memo. RM-2769-JPL, Apr. 28, 1961, pp. 74–76.
190. DOLLFUS, A.: Observations of Water Vapor on Mars and Venus. The Origin and Evolution of Atmospheres and Oceans, P. J. Brancazio and A. G. W. Cameron, eds., John Wiley & Sons, Inc., 1964, pp. 257–267.
191. SEKERA, Z.: Critical Remarks on the Methods Used for Determination of Surface Pressure on Mars. University of California at Los Angeles, Dept. of Meteorology, Consultant Report to Douglas Aircraft Co., Space Sciences Dept., June 1964, 6 pp.
192. HANST, P. L.: The Absorption Intensity of the 5_{ν_3} Band of Carbon Dioxide Seen on Mars—Recomputation of the Martian CO_2 Abundance and Atmospheric Pressure. Research and Advanced Development Division, Avco Corp., Wilmington, Mass., 1964, 17 pp.
193. SWAN, P. R.: CO_2 Abundance and Surface Pressure on Mars. Research and Advanced Development Div., Avco Corp., Wilmington, Mass., Nov. 20, 1964, 14 pp.
194. SHAPIRO, R.: Atmospheric Pressure at the Surface of Mars. Final Rept. on the Study of Planetary Atmosphere, Lowell Obs., Sept. 30, 1952, pp. 77–85.
195. KLIORE, A.; CAIN, D. L.; AND LEVY, G. S.: Radio Occultation Measurement of the Martian Atmosphere Over Two Regions by the Mariner IV Space Probe. Paper read at the Seventh International Space Science Symposium (COSPAR), Vienna, Austria, May 11–17, 1966, 18 pp.
196. MIYAMOTO, S.; AND MATSUI, M.: Report of Mars Observations During the

1958 Opposition. Contributions from the Institute of Astrophysics and Kwasan Obs., University of Kyoto, no. 87, 1960, pp. 1–26.

197. TANG, W.: Some Aspects of the Atmospheric Circulation on Mars. Geophysical Corp. of Am., Tech. Rept. No. 65-4-N, Mar. 1965, 43 pp.
198. TANG, W.: On the Steady Symmetrical Regime of the General Circulation of the Martian Atmosphere. Contributions to Planetary Meteorology by G. Ohring, W. Tang, F. B. House, and J. Mariano. Geophysical Corp. of Am., Tech. Rept. No. 66-8-N, Mar. 1966, pp. 1–27.
199. DOLLFUS, A.: Les Conditions Météorologiques sur la Planète Mars. La Météorologie, no. 42, 1956, pp. 81-91.
200. DOLLFUS, A.: Etude des Planètes par la Polarisation de leur Lumière, Ann. Astrophys., Supplement, no. 4, 1957, pp. 70–110.
201. DOLLFUS, A.: Planetary Studies. Proc. Lunar and Planetary Exploration Colloquium, vol. 2, no. 3, North American Aviation, Inc., Aug. 15, 1961, pp. 33–41.
202. WILSON, A. G.: Spectrographic Observations of the Blue Haze in the Atmosphere of Mars. Rand Corp. Paper No. P-1509, Oct. 6, 1958, 7 pp.
203. WILSON, A. G.: The Problems of the Martian Blue Haze. Proc. Lunar and Planetary Exploration Colloquium, vol. 1, no. 4, North American Aviation, Inc., Jan. 12, 1959.
204. GIFFORD, F. A.: A Study of Martian Yellow Clouds That Display Movement. Monthly Weather Rev., vol. 92, no. 10, Oct. 10, 1964, pp. 435–440.
205. ANTONIADI, E. M.: La Planète Mars, 1659–1929. Hermann (Paris), 1930, 239 pp.
206. RYAN, J. A.: Notes on the Martian Yellow Clouds. J. Geophys. Res., vol. 69, no. 18, Sept. 15, 1964, pp. 3759–3769.
207. GIFFORD, F. A., JR.: The Problem of the Martian Yellow Clouds. Monthly Weather Rev., vol. 91, nos. 10–12, Oct.–Dec. 1963, pp. 610–612.
208. NEWBAUER, F. M.: Thermal Correction in the Martian Atmosphere. J. Geophys. Res., vol. 71, no. 10, May 15, 1966, pp. 2419–2426.
209. ÖPIK, E. J.: Atmosphere and Surface Properties of Mars. Progress in the Astronautical Sciences, ch. 6. S. F. Singer, ed., North-Holland Publishing Co. (Amsterdam), vol. 1, 1962, pp. 261–342.
210. SAGAN, C.; HANST, P. L.; AND YOUNG, A. T.: Nitrogen Oxides on Mars. Planetary and Space Science, vol. 13, no. 1, Jan. 1965, pp. 73–88.
211. SAGAN, C.; AND KELLOGG, W. W.: The Terrestrial Planets. Vol. I of Annual Reviews of Astronomy and Astrophysics, L. Goldberg et al., eds., Annual Reviews Inc., Palo Alto, 1963, pp. 235–266.
212. SHARONOV, V. V.: On the Role of True Absorption in the Martian Atmosphere. Astron. Zh. SSSR, vol. 34, no. 4, 1956, pp. 557–567.
213. SLIPHER, E. C.: The Violet Layer and Blue Clearing. The Photographic Story of Mars, ch. 5, J. S. Hall, ed., Sky Publishing Co. (Cambridge, Mass.), 1962, pp. 37–54.
214. SAGAN, C.: Is the Martian Blue Haze produced by Solar Protons? Rand Corp. Memo. RM-2832-JPL, 1961, 9 pp.
215. SLIPHER, E. C.: An Outstanding Atmospheric Phenomenon on Mars. Publ. Astron. Soc. Pacific, vol. 49, no. 289, 1937, pp. 137–140.
216. PICKERING, W. H.: Martian Meteorology. Ann. Harvard College Obs., vol. 53, no. 8, 1905, pp. 155–172.
217. SLIPHER, V. M.: The Lowell Observatory. Publ. Astron. Soc. Pacific, vol. 39, 1927, pp. 143–154.

218. De Vaucouleurs, G.: Photographic Observations in 1956 of the Blue Clearing on Mars. Publ. Astron. Soc. Pacific, vol. 69, 1957, pp. 530–532.
219. Richardson, R. S.; and Roques, P. E.: An Example of the Blue Clearing Observed 74 Days Before Opposition. Publ. Astron. Soc. Pacific, vol. 71, 1959, pp. 321–323.
220. Focas, J. H.: Observations of Mars Made in 1961 at the Pic du Midi Observatory. JPL Tech. Rept. No. 32–151, Jan. 30, 1962, 11 pp.
221. Robinson, J. C.: Photographic Observations of Mars at New Mexico State University in 1960–1961. Icarus, vol. 2, nos. 5 and 6, Dec. 1963, pp. 403–410.
222. Martz, E. P., Jr.: Variation in Atmospheric Transparency of Mars in 1939. Publ. Astron. Soc. Pacific, vol. 66, 1954, pp. 45–51.
223. Slipher, E. C.; and Wilson, A. G.: On Blue Clearing on Mars. Leaflets Astron. Soc. Pacific, no. 301, 1954, pp. 1–8.
224. De Vaucouleurs, G.; and Young, A. T.: A Statistical Study of the Variable Opacity in the Atmosphere of Mars to Blue, 1926–1956. J. Am. Astron. Soc. Meeting, Dec. 1958.
225. Smith, B. A.: Blue Clearing During the 1960–1961 Apparition. Publ. Astron. Soc. Pacific, vol. 73, no. 435, Dec. 1961, pp. 456–459.
226. Palm, A.; and Basu, B.: The Blue Haze of Mars. Icarus, vol. 4, no. 2, May 1965, pp. 111–118.
227. Schatzmann, E.: Sur les Particles Diffusantes dans l'Atmosphère de Mars. Compt. Rend., Acad. Sci., vol. 232, 1952, pp. 692–693.
228. Urey, H. C.: The Blue Haze of Mars. Astrophys. J., vol. 128, no. 3, 1958, pp. 736–737.
229. Hess, S. L.: Blue Haze and the Vertical Structure of the Martian Atmosphere. J. Astrophys., vol. 127, 1958, pp. 743–750.
230. Kiess, C. C.; Karrer, S.; and Kiess, H. K.: A New Interpretation of Martian Phenomena. Publ. Astron. Soc. Pacific, vol. 72, 1960, pp. 256–267.
231. Warneck, J.; and Marmo, F. F.: NO_2 in the Martian Atmosphere. J. Atmospheric Sci., vol. 20, May 1963, pp. 236–240.
232. Link, F.: Couche de Poussières Meteoriques dans une Atmosphère Planètaire. Bull. Astron. Inst. Czech., vol. 2, 1950, pp. 1–16.
233. Kviz, Z.: The Blue Clearing on Mars and Its Possible Connection With the Meteor-Rainfall Hypothesis. Bull. Astro. Inst. Czech., vol. 12, no. 4, 1961, pp. 150–157.
234. Urey, H. C.; and Brewer, A. W.: Fluorescence in Planetary Atmospheres. Proc. Roy. Soc. of London, ser. A, vol. 241, 1957, pp. 37–43.
235. Dollfus, A.: Planetary Studies. J. H. Focas' results cited. Proc. Lunar and Planetary Exploration Colloquium, North American Aviation, Inc., vol. 2, no. 3, Aug. 15, 1961, pp. 17–41.
236. Dollfus, A.: Visual and Photographic Studies of Planets at the Pic du Midi. Planets and Satellites, ch. 15. Vol. III of The Solar System, G. P. Kuiper and B. M. Middlehurst, eds., University of Chicago Press, 1961, pp. 534–571.
237. De Vaucouleurs, G.: Precision Mapping of the Planet Mars. A Research Program in Planetary Astronomy at University of Texas in 1961, Fort Worth, General Dynamics, Applied Sciences Lab., Jan. 1962.
238. De Vaucouleurs, G.: Precision Mapping of Mars (La Physique des Planètes). Mem. Soc. Roy. Sci., ser. 5, vol. 7, 1963, pp. 369–385.
239. Menzel, D. H.; Young, A. T.; De Vaucouleurs, G.; Finsen, W. S.; and

LEIGHTON, W. S.: Research directed toward the Production of a Map of the Visible Features of Mars. Final Rept. Air Force Cambridge Res. Lab., Bedford, Mass., Rept. AFCRL–64–396, Apr. 1964, 51 pp.

240. DE VAUCOULEURS, G.: Charting the Martian Surface. Sky and Telescope, vol. 30, no. 4, Oct. 1965, pp. 196–201.
241. LOWELL, P. H.: Mars. Houghton Mifflin (Boston), 1896, 228 pp.
242. WILSON, A. G.: Direct Photography in the Exploration of Planetary Atmospheres. The Atmospheres of Mars and Venus, app. 1, W. Kellogg and C. Sagan, eds., National Academy of Sciences—National Research Council, Washington, D.C., Publ. 944, 1961, 151 pp. (See footnote on p. 66.)
243. TOMBAUGH, C. W.: Mars—A World for Exploration. Astronautics, vol. 4, 1959, pp. 30–31, 86–93.
244. TOMBAUGH, C. W.: Comparison of Lunar and Martian Features. Proc. Lunar and Planetary Exploration Colloquium, North American Aviation, Inc., vol. 1, no. 4, Jan. 1959, pp. 38–41.
245. LEIGHTON, R. B.; MURRAY, B. C.; SHARP, R. B.; ALLEN, J. D.; AND SLOAN, R. K.: Mariner IV Photography of Mars: Initial Results. Science, vol. 149, no. 3684, Aug. 6, 1965, pp. 627–630.
246. ÖPIK, E. J.: Mars and the Asteroids. Irish Astron. J., vol. 1, no. 1, Mar. 1950, pp. 22–24.
247. TOMBAUGH, C. W.: Martian Geology. Sky and Telescope, vol. 9, no. 11, Sept. 1950, p. 272.
248. FIELDER, G.: Photographs of Mars Taken by Mariner IV. Nature, vol. 208, no. 5004, Sept. 25, 1965, p. 1381.
249. ÖPIK, E. J.: Mariner IV and Crater on Mars. Irish Astron. J., vol. 7, nos. 2 and 3, June–Sept. 1965, pp. 92–104.
250. ANDERS, E.; AND ARNOLD, J. R.: Age of Craters on Mars. Science, vol. 149, no. 3691, Sept. 24, 1965, pp. 1494–1496.
251. WITTING, J.; NARIN, F.; AND STONE, C. A.: Mars: Age of its Craters. Science, vol. 149, Sept. 24, 1965, pp. 1496–1498.
252. BALDWIN, R. B.: Mars: An Estimate of the Age of its Surface. Science, vol. 149, Sept. 24, 1965, pp. 1498–1499.
253. KUIPER, G. P.: Visual Observations of Mars, 1956. Astrophys. J., vol. 125, 1957, pp. 307–317.
254. SHARONOV, V. V.: A Lithological Interpretation of the Photometric and Colorimetric Studies of Mars. Astron. Zh., vol. 38, no. 2, 1961, p. 267; or Soviet Astronomy-AJ, vol. 5, 1961, pp. 199–202.
255. SAGAN, C.; PHANEUF, J. P.; AND IHNAT, M.: Total Reflection Spectrophotometry and Thermogravimetric Analysis of Simulated Martian Surface Materials. Icarus, vol. 4, no. 1, Apr. 1965, pp. 43–61.
256. BINDER, A. B.; AND CRUIKSHANK, D. P.: Comparison of the Infrared Spectrum of Mars With the Spectra of Selected Terrestrial Rocks and Minerals. Commun. Lunar and Planetary Lab., vol. 2, no. 37, 1965, pp. 193–196.
257. VAN TASSEL, R. A.; AND SALISBURY, J. W.: The Composition of the Martian Surface. Icarus, vol. 2, no. 3, Sept. 1964, pp. 264–269.
258. REA, D. G.: Some Comments on the Composition of the Martian Surface. Icarus, vol. 4, no. 1, Apr. 1965, pp. 108–109.
259. SALISBURY, J. W.; AND VAN TASSEL, R. A.: Reply to Comments of D. G. Rea on The Composition of the Martian Surface. Icarus, vol. 4, no. 1, Apr. 1965, pp. 109–110.

260. FOCAS, J. H.: Seasonal Evolution of the Fine Structure of the Dark Areas of Mars. Planetary and Space Science, vol. 9, 1962, pp. 371–381.
261. DE VAUCOULEURS, G.: Sur les Variations Saisonnières Observées à la Surface de la Planète Mars en 1939 et leurs Lois de Propagation. Compt. Rend., Acad. Sci., vol. 220, 1945, pp. 388–390.
262. SLIPHER, E. C.: The Photographic Story of Mars. Sky Publishing Co. (Cambridge, Mass.), 1962, 168 pp.
263. MCLAUGHLIN, D. B.: Interpretation of Some Martian Features. Publ. Astron. Soc. Pacific, vol. 66, 1954, pp. 161–170.
264. MCLAUGHLIN, D. B.: Further Notes on Martian Features. Publ. Astron. Soc. Pacific, vol. 66, 1954, pp. 221–229.
265. MCLAUGHLIN, D. B.: New Interpretation of the Surface of Mars. Scientific Monthly, vol. 83, 1956, pp. 176–188.
266. MCLAUGHLIN, D. B.: A New Theory of the Surface of Mars. J. Roy. Astron. Soc. Canada, vol. 50, 1956, pp. 193–200.
267. MCLAUGHLIN, D. B.: The Volcanic-Aeolian Hypothesis of Martian Features. Publ. Astron. Soc. Pacific, vol. 68, 1956, pp. 211–218.
268. ARRHENIUS, S.: The Planet Mars. The Destinies of the Stars, ch. 6. (Translated from Swedish), G. P. Putnam & Sons (New York), 1918, 256 pp.
269. SALISBURY, F. B.: Martian Biology. Science, vol. 136, Apr. 1962, pp. 17–26.
270. TOMBAUGH, C. W.: Evidence That the Dark Areas on Mars Are Elevated Mountain Ranges. Nature, vol. 209, no. 5030, Mar. 26, 1966, p. 1338.
271. WELLS, R. A.: Evidence That the Dark Areas on Mars Are Elevated Mountain Ranges. Nature, vol. 207, no. 4998, Aug. 14, 1965, pp. 735–736.
272. WELLS, R. A.: Evidence That the Dark Areas on Mars Are Elevated Mountain Ranges (a reply to Tombaugh). Nature, vol. 209, no. 5030, Mar. 26, 1966, pp. 1338–1339.
273. ANTONIADI, E. M.: On a Probable Relation Between the Changes in Solar Radiation and the Melting of the Polar Snow Caps of Mars. Monthly Notices Roy. Astron. Soc., vol. 76, no. 8, 1916, pp. 643–645.
274. DE VAUCOULEURS, G.: Reconnaissance of the Nearer Planets. Air Force Office of Scientific Res. Tech. Rept. AFOSR/DRA–61–1, Nov. 1961, 141 pp.
275. TIKHOV, G. A.: L'Application des Filtres Sélecteurs a L'Étude de Mars et de Saturne. Mitteillungen der Hauptsternwarte Poulkovo, series IV, vol. 6, 1911, pp. 73–84.
276. LEIGHTON, R. B.; AND MURRAY, B. C.: The Behavior of Carbon Dioxide and Other Volatiles on Mars. Science, vol. 153, July 8, 1966, pp. 136–144.
277. SCHIAPARELLI, G. V.: II Pianeta Marte. Vallardi (Milano), 1893, 25 pp.
278. PICKERING, W. H.: Schiaparelli's Latest Views Regarding Mars. Smithsonian Inst. Ann. Rept., 1894, p. 113.
279. ROBINSON, J. C.: Ground-Based Photography of the Mariner IV Region of Mars. Icarus, vol. 5, no. 3, May 1966, pp. 245–247.
280. BURGESS, E.: There Are "Canals" on Mars. Spaceflight, vol. 8, no. 2, Feb. 1966, pp. 46–47 and 74.
281. DOLLFUS, A.: Observation de la Structure des "Canaux," de la Planète Mars. Compt. Rend., Acad. Sci., vol. 226, 1948, pp. 996–997.

282. DOLLFUS, A.: Étude Visuelle de la Surface de la Planète Mars Avec Un Pouvoir Séparateur O" 2. L'Astronomie, vol. 67, 1953, pp. 85–106.
283. LOWELL, P. H.: Mars and Its Canals. The Macmillan Co., 1908, 393 pp.
284. KATTERFELD, G. N.: On the Question of the Tectonic Origin of the Linear Formations on Mars. Vsesoiuznoe Geograficheskoe Obshchestvo (Leningrad), Izvestiya, vol. 91, no. 3, 1959, pp. 272–283.
285. GIFFORD, F. A., JR.: The Martian Canals According to Pure Aeolian Hypothesis. Icarus, vol. 3, no. 2, July 1964, pp. 130–135.
286. LEIGHTON, R. B.: The Photographs From Mariner IV. Sci. Am., vol. 214, no. 4, Apr. 1966, pp. 54–68.
287. SHARONOV, V. V.: Mars. Izdatelstvo, Akad. Nauk SSSR, Moscow-Leningrad, 1947, 180 pp.
288. HESS, S. L.: Color Changes on Mars, The Project for the Study of Planetary Atmospheres. Lowell Obs. Ann. Rept. 1950, 1951, pp. 34–38.
289. SINTON, W. M.: Letter in: Science, vol. 134, no. 3478, Aug. 25, 1961, p. 529.
290. SINTON, W. M.: Spectroscopic Evidence for Vegetation on Mars. Astrophys. J., vol. 126, 1957, pp. 214–239.
291. COLTHUP, N. B.: Identification of Aldehyde in Mars Vegetation Regions. Science, vol. 134, no. 3478, Aug. 25, 1961, p. 529.
292. REA, D. G.; BELSKY, T.; AND CALVIN, M.: Interpretation of the 3- to 4-Micron Infrared Spectrum of Mars. Science, vol. 141, no. 3584, Sept. 6, 1963, pp. 923–927.
293. REA, D. G.; BELSKY, T.; AND CALVIN, M.: Reflection Spectra of Bio-organic Materials in the 2.5–4μ Region and Interpretation of the Infrared Spectrum of Mars. Life Sciences and Space Research II, pt. II, M. Florkin and A. Dollfus, eds., North-Holland Publishing Co. (Amsterdam), 1964, pp. 86–100.
294. SHIRK, J. S.; HASELTINE, W. A.; AND PIMENTEL, G. C.: Sinton Bonds: Evidence for Deuterated Water on Mars. Science, vol. 147, no. 3653, Jan. 1, 1965, pp. 48–49.
295. REA, D. G.; O'LEARY, B. T.; AND SINTON, W. M.: The Origin of the 3.58 and 3.69-Micron Minima in the Infrared Spectra. Science, vol. 147, no. 3663, Mar. 12, 1965, pp. 1286–1288.
296. FULTON, J. D.: Survival of Terrestrial Microorganisms Under Simulated Martian Conditions. Physics and Medicine of the Atmosphere and Space, ch. 40, O. Benson and H. Strughold, eds., John Wiley & Sons, Inc., 1960, pp. 606–613.
297. KOOISTRA, J., JR.; MITCHELL, R. B.; AND STRUGHOLD, H.: The Behavior of Microorganisms Under Simulated Martian Environmental Conditions. Publ. Astron. Soc. Pacific, vol. 70, 1958, pp. 64–68.
298. HAWRYLEWICZ, E.; GOWDY, B.; AND EHRLICH, R.: Microorganisms Under a Simulated Martian Environment. Nature, vol. 193, 1962, p. 497.
299. PACKER, E.; SCHER, S.; AND SAGAN, C.: Biological Contamination of Mars, II: Cold and Aridity as Constraints on the Survival of Terrestrial Microorganisms in Simulated Martian Environments. Icarus, vol. 2, no. 4, Nov. 1963, pp. 293–316.
300. YOUNG, R. S.; DEAL, P. H.; BELL, J.; AND ALLEN, J. L.: Bacteria Under Simulated Martian Conditions. Life Sciences and Space Research II, pt. II.4, M. Florkin and A. Dollfus, eds., North-Holland Publishing Co. (Amsterdam), 1964, pp. 105–111.

301. LEDERBERG, J.; AND SAGAN, C.: Microenvironments for Life on Mars. Proc. of the Nat. Acad. of Sci., vol. 48, no. 9, Sept. 1962, pp. 1473–1475.
302. TIKHOV, G. A.: Is Life Possible on Other Planets? J. Brit. Astron. Assoc., vol. 65, 1955, pp. 193–204.
303. PIMENTEL, G. C.; ATWOOD, K. C.; GRAFTON, H.; HARTLINE, H. K.; JUKES, T. H.; POLLARD, E. C.; AND SAGAN, C.: Exotic Biochemistry in Exobiology. Biology and the Exploration of Mars, ch. 12, C. S. Pittendrigh, W. Vishmae, and J. P. T. Pearman, eds., National Academy of Sciences—National Research Council, Washington, D.C. Publ. 1296, 1966, 516 pp., pp. 243–251.
304. KILSTON, S. D.; DRUMMOND, R. R.; AND SAGAN, C.: A Search for Life on Earth at Kilometer Resolution. Icarus, vol. 5, no. 1, Jan. 1966, pp. 79–98.
305. HALL, A.: The Satellites of Mars. Appendix to Washington Observations, 1875, 1878.
306. STRUVE, H.: Beobachtungen der Marstrabanten in Washington, Pulkowa, und Lick Observatory. Mem. Acad. Impériale Sci. St. Pétersbourg, ser. 8, vol. 8, 1898, pp. 64–65.
307. STRUVE, H.: Über die Lage der Marsachse und die Konstanten im Marssystem. Sitzungsberichte der königlich preussischen Akademie der Wissenschaften, Sitzung der physikalisch-mathematischen Klass vom 30 Nov. 1911, Stuck 48, 1911, pp. 1056–1083.
308. BURTON, H. E.: Elements of the Orbits of the Satellites of Mars. Astron. J., vol. 39, no. 19, 1929, pp. 155–164.
309. SHARPLESS, B. P.: Secular Accelerations in the Longitudes of the Satellites of Mars. Astron. J., vol. 51, 1945, pp. 185–186.
310. KERR, F. J.; AND WHIPPLE, F. L.: On the Secular Accelerations of Phobos and Jupiter V. Astron. J., vol. 59, 1954, pp. 124–127.
311. SHKLOVSKIY, I. S.: Artificial Satellites of Mars, and Riddle of the Martian Satellites. From Komsomol'skaya, Pravda, May 1 and 31, 1959, in Truth of the Young Communist League (selected articles), FTD–TT–62–488/1, Translation Services Branch, Wright-Patterson AFB, Ohio, May 18, 1962.
312. REDMOND, J. C.; AND FISH, F. F.: The Luni-Tidal Interval in Mars and the Secular Acceleration of Phobos. Icarus, vol. 3, no. 2, July 1964, pp. 87–91.
313. SCHILLING, G. F.: On Exospheric Drag as the Cause of the Supposed Secular Acceleration of Phobos. J. Geophys. Res., vol. 69, no. 9, May 1, 1964, pp. 1825–1829.
314. KUIPER, G. P.: Limits of Completeness. Planets and Satellites, ch. 18. Vol. III of The Solar System, G. P. Kuiper and B. M. Middlehurst, eds., University of Chicago Press, 1961, pp. 575–591.

Glossary

Adiabatic process—A thermodynamic change of state of a system in which there is no transfer of heat or mass across the system's boundaries.

Albedo—The ratio of electromagnetic radiation reflected by a body to that incident upon it.

Anticyclone—An area of relatively high pressure from which the wind blows spirally outward in a clockwise direction in the northern hemisphere and counterclockwise in the southern hemisphere.

Aphelion—The point on a heliocentric elliptical orbit farthest from the sun.

Areocentric—Mars centered (term derived from the Greek word for the god of war, the Roman equivalent of which is Mars).

Areocentric latitude—That angle formed by a line from the center of Mars to a given point and the Martian equatorial plane.

Areographical latitude—That angle formed by the rotation axis of Mars and the plane tangent to the Mars surface at a given point.

Ascending node (of an orbit)—That point on an orbit at which a body (planet or satellite) crosses from south to north the reference plane (e.g., the ecliptic for the planets) on the celestial sphere. The opposite point, separated by 180° of longitude, is the descending node.

Astronomical Unit (A.U.)—A fundamental unit of length used in astronomy. Originally, the astronomical unit was defined as the mean distance of Earth from the Sun. In celestial mechanics, it is defined as the radius of an idealized circular and unperturbed orbit of Earth around the Sun. The recent radar determination of Mühleman (1964) is astronomical unit= 149 598 900 ±600 kilometers.

Bond albedo (or Russell-Bond albedo)—The ratio of the total flux, reflected in all directions by a sphere (planet), to the total flux incident in parallel rays from a distant source (Sun) and expressed as the product, $A=p\cdot q$, of a full-phase albedo factor p (geometrical albedo) and a phase-varying factor q (phase integral).

Brilliancy (of a disk)—A geometrical measure of disk brightness, independent of albedo, that is determined only by phase k, the apparent semidiameter s, and solar distance r according to the defining formula: $L=K\frac{s^2}{r^2}$.

Conjunction—The configuration of the Sun, a planet, and Earth when the heliocentric longitudes of the latter two are equal. The three bodies then lie most nearly in a straight line. When the planet is between the Sun and Earth, the planet is said to be in inferior conjunction; when the Sun is between Earth and the planet, the planet is said to be in superior conjunction.

Cyclone—An area of relatively low atmospheric pressure around which the wind blows spirally inward: counterclockwise in the northern hemisphere, clockwise in the southern.

Day (ephemeris)—Average value of the mean solar day taken over the last three centuries.

Day (sidereal)—Time interval between two successive transits of the vernal equinox over the same meridian.

Day (solar)—Time interval between two consecutive transits of the Sun over a meridian. Since this time interval varies with Earth's orbital motion, a mean solar day was chosen, based on a mean annual motion of Earth (assuming an equivalent circular orbit) or a fictitious mean Sun.

Declination (of a celestial point)—The angle between a point and the celestial equator, measured along the hour circle through the point and counted as north (+) or south (—) of the equator.

Disk—The flattened appearance of a celestial body as it is observed, or the projection on the celestial sphere of that portion of the observed body which is visible.

Dry adiabatic lapse-rate—The rate of decrease of temperature with height of a parcel of dry air lifted adiabatically through an atmosphere in hydrostatic equilibrium.

Ecliptic—The annual, apparent path of the Sun's center on the celestial sphere, as seen from Earth, or the intersection of Earth's orbital plane with the celestial sphere.

Elongation (of a planet)—The angle between the Sun and a planet and Earth with the vertex at the center of Earth. Elongation is measured east or west of the Sun.

Emissivity—The ratio of the total flux of radiation at all wavelengths emitted by a surface to that emitted by a perfect radiator (the ideal blackbody) at the same temperature and conditions.

Ephemeris (fundamental)—An astronomical table predicting the positions of celestial bodies at regular intervals of time (also called almanac).

Ephemeris time—Uniform or Newtonian time based on the mean rotation of Earth during the year 1900.

Epoch—An arbitrary instance of time at which positions are measured or calculated.

Geometrical albedo—The ratio of the actual brightness of a reflecting body (planet or satellite) at full solar phase to that of a self-luminous body of the same size and position and radiating a flux of light equal to that incident on the first body.

Graybody—A hypothetical body that absorbs, independently of wavelength, some constant fraction between zero and one of all electromagnetic radiation incident upon that body.

Greatest defect of illumination—The midpoint of the dark limb of a planetary disk. Its position angle Q is reckoned eastward from the north point of the disk. The angular amount q of the greatest defect of illumination is given by the formula: $q=2s\ (1-k)$, where $2s$ is the angular diameter of the disk and k the phase.

Greenhouse effect—The heating of the lower atmosphere by certain gases (e.g., water vapor or carbon dioxide) which transmit shortwave solar radiation to the surface, yet absorb and reemit portions of the planetary longwave (infrared) radiation back to the surface; thus, a downward counterradiation is produced.

Gregorian date—A date on the official calendar in use throughout the Christian world. The Gregorian calendar was instituted in 1582 by Pope Gregory XIII to correct errors accumulating in the Julian calendar.

Heliocentric—Sun centered; term derived from helios, the Greek word for sun.

Isostasy—The theory of gravitational equilibrium in a planet's crust whereby

a compensation in weight exists between adjacent major topographical features (i.e., mountains, seas, glaciers, large ore deposits, etc.).

Julian date—The number of mean solar days that have elapsed since the adopted epoch of Greenwich mean noon on January 1, 4713 B.C.

Kepler's laws—Three laws of undisturbed planetary motion formulated by Kepler:

1st law: The orbits of the planets are ellipses with the Sun at one focus.

2nd law: The radius vector Sun-to-planet sweeps equal areas in equal times.

3rd law: The squares of the planets' periods of revolution are proportional to the cubes of their mean solar distances (semimajor axes of ellipses).

Laplacian plane (or proper plane)—A plane that is fixed relative to the planet's equator, and upon which the precessing orbital plane of a satellite maintains a nearly constant inclination. The plane's position is determined by the balance of the orthogonal components of the disturbing forces (e.g., from the planet's oblateness or the Sun's attraction).

Limb—Edge of the illuminated part of a disk.

Line of apsides—A straight line infinitely extending the major axis of an elliptical orbit. This line passes through those points closest (periapsis) and farthest (apoapsis) from the dynamical center.

Line of nodes—A straight line that joins the intersection points (nodes) of the two great celestial circles that determine the orbital plane and the reference plane used to describe the motion of a planet or satellite.

Magnitude (stellar)—An inverse logarithmic measure of the brightness of a celestial body such that an increase of five magnitudes represents a hundredfold decrease in the body's brightness.

Martian date—The date in a Martian calendar patterned after the terrestrial (Gregorian) calendar, stretched over one Martian year (687 terres, days) such that, at the same dates on each planet, the geocentric and areocentric longitudes of the Sun are equal. Usually, the equivalent Martian calendar is constructed with the Southern Hemisphere vernal equinox occurring on March 21.

Mie scattering—That scattering of radiation which is produced by spherical particles of any size (for comparison see "Rayleigh scattering").

Mixing ratio—The ratio of the mass of the gas considered to that of the remaining gases in a given atmospheric mass.

North celestial pole—The northern point of intersection of Earth's rotation axis with the celestial sphere.

Opposition—The configuration of the Sun, Earth, and planet when the heliocentric longitudes of the latter two are equal. The three bodies, with Earth in the middle, are then most nearly in a straight line.

Periareon—That point on an areocentric elliptical orbit which is closest to Mars.

Pericenter (or, perifocus)—That point on an orbit which is closest to the attracting center.

Perihelion—That point on a heliocentric elliptical orbit which is closest to the Sun.

Phase—The illuminated fraction of the disk area.

Phase angle—The angle between the Sun and Earth, as observed from a planet whose center is the vertex.

Phase curve or law—The plot or mathematical law of the phase function $\phi(\alpha)$ of a planet versus phase angle α.

Phase function—The ratio of the brightness of a planet at any phase angle

α to that at full phase ($\alpha=0$), assuming the planet at unit distances from the Sun and Earth.

Phase integral—The phase varying factor that modifies the geometrical albedo (or, full-phase factor) that enters into the definition of the Bond albedo of a planet. It is expressed as the integral:

$$q=\int_0^{2\pi}\phi(\alpha)\ \sin\alpha\ d\alpha$$

of the phase function $\phi(\alpha)$.

Polarization, amount or degree of—The proportion of polarized light to total light; it is defined by:

$$P=\frac{I_1-I_2}{I_1+I_2}$$

where I_1 is the component of intensity perpendicular to the plane of vision (defined by directions of illumination and observation) and I_2 is the intensity component contained in this plane.

Polarization curve—The plot of degree of polarization versus phase angle of a planet.

Precession—The very slow (long period) motion (26 000 years for Earth) of a planet's rotation axis about the north pole of the ecliptic, caused by the action of the Sun and any large satellite upon the planet's equatorial bulge; resembles the motion of a spinning top.

Precipitable water—The total mass of atmospheric water vapor contained in a vertical column of unit cross-section extending between any two specified levels (usually the total atmospheric height).

Quadrature—The configuration of the Sun, Earth, and a planet when the geocentric longitudes of the Sun and the planet are 90° apart. The three bodies then most nearly form a right angle.

Rayleigh scattering—That scattering or radiation which is produced by spherical particles of radii smaller than about one-tenth the wavelength of the radiation (Rayleigh limit). Also called "molecular scattering."

Retrograde sense—The opposite of direct sense of rotation; that is, clockwise.

Right ascension—The angular arc measured along the celestial equator from the vernal equinox eastward (i.e., counterclockwise) to the intersection with the hour circle of the point (semigreat circle passing through the north celestial pole and the point).

Rotational lines—Spectral lines caused by rotational energy changes in a molecule.

Scale height (of an atmosphere)—The distance in which an isothermal atmosphere decreases in density from 1 to $1/e$.

Scintillation—Rapid fluctuations in brightness, color, and position of an observed luminous body (star or planet in astronomical scintillation) resulting from atmospheric inhomogeneities and fluctuations.

Synodic period of revolution (of two planets of satellites)—The time interval between consecutive oppositions or conjunctions of two bodies revolving around the same center.

Terminator—The line separating the illuminated from the non-illuminated portions of a planet or satellite; one observes a morning or evening terminator on the disk.

Twilight arc—The planetocentric angular arc that measures the displacement, resulting from atmospheric scattering of light on the planet, of the actual terminator from the theoretical terminator.

Vernal equinox—The point at which the Sun in its annual apparent path around Earth appears to cross the celestial equator from south to north at a certain time of the year (presently on Mar. 21), or the ascending node of the ecliptic on the equator.

Year, Julian—The mean length of the year on the Julian calendar; it is equal to 365.25 mean solar days, or $365^{d}6^{h}$ exactly.

Year, sidereal—The time interval between two successive returns of the Sun to a fixed celestial point (fixed star); it is the true period of revolution of Earth and is equal to 365.25636 mean solar days, or $365^{d}6^{h}9^{m}10^{s}$.

Year, tropical—The time interval between two successive returns of the Sun to the vernal equinox. Because of precession, it is shorter than the sidereal or true year. It is equal to 365.24220 mean solar days, or $365^{d}5^{h}48^{m}46^{s}$.

☆ U S. GOVERNMENT PRINTING OFFICE: 1967—O 255-979

"The aeronautical and space activities of the United States shall be conducted so as to contribute . . . to the expansion of human knowledge of phenomena in the atmosphere and space. The Administration shall provide for the widest practicable and appropriate dissemination of information concerning its activities and the results thereof."

—NATIONAL AERONAUTICS AND SPACE ACT OF 1958

NASA SCIENTIFIC AND TECHNICAL PUBLICATIONS

TECHNICAL REPORTS: Scientific and technical information considered important, complete, and a lasting contribution to existing knowledge.

TECHNICAL NOTES: Information less broad in scope but nevertheless of importance as a contribution to existing knowledge.

TECHNICAL MEMORANDUMS: Information receiving limited distribution because of preliminary data, security classification, or other reasons.

CONTRACTOR REPORTS: Scientific and technical information generated under a NASA contract or grant and considered an important contribution to existing knowledge.

TECHNICAL TRANSLATIONS: Information published in a foreign language considered to merit NASA distribution in English.

SPECIAL PUBLICATIONS: Information derived from or of value to NASA activities. Publications include conference proceedings, monographs, data compilations, handbooks, sourcebooks, and special bibliographies.

TECHNOLOGY UTILIZATION PUBLICATIONS: Information on technology used by NASA that may be of particular interest in commercial and other non-aerospace applications. Publications include Tech Briefs, Technology Utilization Reports and Notes, and Technology Surveys.

Details on the availability of these publications may be obtained from:

SCIENTIFIC AND TECHNICAL INFORMATION DIVISION

NATIONAL AERONAUTICS AND SPACE ADMINISTRATION

Washington, D.C. 20546